Proton Transport Mechanisms of Phosphoric Acid and Related Phosphorus Oxoacid Systems: A First Principles Molecular Dynamics Study

Von der Fakultät Chemie der Universität Stuttgart
zur Erlangung der Würde eines
Doktors der Naturwissenschaften (Dr. rer. nat.)
genehmigte Abhandlung

Vorgelegt von
Linas Vilčiauskas
aus Joniškis, Litauen

Hauptberichter:	Prof. Dr. Joachim Maier
Mitberichter:	Jun. Prof. Dr. Johannes Kästner
Prüfungsvorsitzender:	Prof. Dr. Emil Roduner

Tag der mündlichen Prüfung: 06.02.2012

Max-Planck-Institut für Festkörperforschung
Universität Stuttgart
2012

To my parents, all of my mentors and the memory of a fellow countryman C. J. D. Theodor von Grotthuß – pioneer of physical chemistry

Mano tėvams, visiems mokytojams ir kraštiečio, fizikinės chemijos pradininko – C. J. D. Theodor'o von Grotthuss'o atminimui

Das ewig Unbegreifliche an der Welt ist ihre Begreiflichkeit.

Albert Einstein (1879-1955)
'Physik und Realität'
Journal of the Franklin Institute **1936**, *122*, 315.

Erklärung

Die vorliegende Doktorarbeit wurde vom Autor selbst in der Abteilung von Prof. Maier und in der Max-Planck-Forschergruppe *Theorie von Halbleiternanostrukturen* am Max-Planck-Institut für Festkörperforschung, im Zeitraum von Januar 2008 bis November 2011 angefertigt. Der Inhalt ist die eigene Arbeit des Autors, Ausnahmen sind gekennzeichnet, und wurde noch nicht zur Erlangung einer Qualifizierung oder eines Titels an einer akademischen Institution eingereicht.

Stuttgart, den 16. Dezember 2011 Linas Vilčiauskas

Declaration

The work described in this thesis was carried out by the author in the Department of Prof. Maier and in the Max Planck Research Group *Theory of Semiconductor Nanostructures* at the Max Planck Institute for Solid State Research from January 2008 to November 2011. The contents are the original work of the author except where indicated otherwise and have not been previously submitted for any other degree or qualification at any academic institution.

Stuttgart, 16 December 2011 Linas Vilčiauskas

Acknowledgements

I would like express the utmost gratitude to my supervisor Dr. Klaus-Dieter Kreuer. First of all, for offering this topic for my PhD thesis and introducing me to the field of proton conductors. Secondly, for providing me the excellent funding opportunities and, certainly, for the infinite supply of ideas during the execution of this project. It was an enormous pleasure to be guided through this field by one of the leading experts. I am sure that our lengthy discussions during lunch, coffee and 'post-coffee' breaks on subjects ranging from *protons in phosphoric acid* to politics, religion or philosophy had a strong impact on my scientific and personal development.

The support, freedom and trust provided by the head of the department Prof. Dr. Joachim Maier for this project must be greatly acknowledged. In addition, I would also like to thank him and the other members of the examination committee: Prof. Dr. E. Roduner and JProf. Dr. J. Kästner for agreeing to take the responsibility of the final doctoral examination.

I sincerely appreciate the help and support provided by my co-supervisor Dr. Gabriel Bester, without whom this project, most probably, would have not even been born. In spite of likely being the most friendly and open person I have ever met, he also eagerly agreed to collaborate on this work and provided invaluable guidance and immense computer resources throughout. I certainly learned a lot from him and truly benefited from our discussions on the computational science, density functional theory and many other aspects of physics and 'daily' life.

I would like to express my greatest thanks to one of my 'key mentors' – Prof. Mark E. Tuckerman (New York University) for keenly agreeing to collaborate on this project right from the first minute and providing an invaluable help and advice on basically every single aspect of this work. In addition to being one of the world's leading experts on *ab initio* molecular dynamics and proton transport, Mark proved to be an extremely friendly and approachable person. His comments and ideas were key for this project in reaching its final shape and success.

My warm thanks go to Prof. Stephen J. Paddison (University of Tennessee, Knoxville), a ‘long-time’ collaborator of mine, for his fruitful contribution to this project, right from the ‘start line’. His comments and critique were always a valuable source of information for improving many aspects of this work.

I would kindly like to thank Dr. Bernhard Frick (Institut Laue-Langevin, Grenoble) for introducing me to the fascinating world of neutrons. I really enjoyed the fruitful work and discussions with Bernhard on quasi-elastic neutron scattering and its use for studying proton dynamics and transport during my several visits to Grenoble.

I am thankful to Dr. Carla C. de Araujo for the nice time, fruitful collaboration and discussions as well as providing important experimental input for the work on pure phosphinic acid.

I am also indebted to all the people at the FKF-EDV group (A. Schuhmacher, U. Traub, A. Burkhardt, K. Rößmann) for the very nice working environment and help with technical difficulties. Rechenzentrum Garching der Max-Planck-Gesellschaft is also greatly acknowledged for their support and opportunity to use the *VIP* machine.

I appreciate all of my friends and colleagues who provided a nice atmosphere in and outside of the Max Planck Institute during the time of my PhD studies. My thanks for the nice time spent together go to the *Lithuanian*, *Anglo-Saxon*, *Russian* communities and many other individuals: S. C. White, J. M. Law, P. M. R. Brydon, V. Alexandrov, D. Gryaznov, Y. Mastrikov, I. Pentin, I. Pentegov, D. Zagorac, J. Bauer, C. Schön, L. Kriščiūnaitė, M. Lipschis, E. Stašaitis, J. Kaiser and many others. I would also like to thank my good friends and colleagues since my time in Vilnius, with whom I kept a lot of contacts and had some wonderful time while not doing my research: A. Bambalas (Vilnius), L. Zakrys (Glasgow), V. Lapienė (Dortmund), G. Gasiūnas (Vilnius), V. Navickas (Tübingen/Ludwigshafen), K. Klemkaitė (Vilnius), G. Muižis (Vilnius) and others.

Most importantly, I’d like to thank my parents and my sister Jurgita for their continual support and belief in my feat and success.

I would also like to acknowledge those thousands of individuals who have contributed to all the open source projects, including the main ‘workhorses’ `CPMD`, `CP2K` and `VMD` as well as LaTeX, used for typesetting this thesis.

Abstract

Fundamental understanding of proton transport in hydrogen bonded systems on the molecular level remains a key problem in many areas of science ranging from electrochemical energy conversion to biological systems. Despite the enormous advances in the research of these processes, the ostensibly simplest case, proton transport in homogeneous bulk media at thermodynamic equilibrium, proved to be one of the most challenging and elusive. The large number of nontrivially coupled reaction coordinates involved in the formation and transport of protonic defects render the task of extracting the molecular level mechanisms a formidable one. It is only through enormous theoretical and experimental efforts that clear mechanistic pictures of the transport of excess protonic charge defects (H_3O^+ and OH^-) in water have emerged. However, water has negligible *intrinsic* proton conductivity. By contrast, the class of compounds known as phosphorus oxoacids have some of the highest reported proton conductivities. In this work, the molecular level proton transport mechanisms in this family of proton conductors (H_3PO_4, H_3PO_3 and H_3PO_2) and some closely related systems (H_3PO_4 - H_2O mixtures) are investigated with the help of *ab initio* molecular dynamics simulations. In fact, neat liquid phosphoric acid has the highest intrinsic proton conductivity of any known substance. Apart from playing a central role in the structure and function of biological systems (e.g. ATP, DNA, lipid membranes), systems containing phosphates/phosphonates (e.g. PBI/H_3PO_4) are attracting an increasing interest as high-temperature electrolytes for emerging fuel cell applications.

For the first time, the microscopic mechanisms of the proton transport phenomenon in these systems are revealed with an appropriate spatial and temporal resolution. The results show that strong, mutually polarizable hydrogen bonds

give rise to coupled proton motion and a pronounced protic dielectric response of the medium. This allows for the formation of *extended*, polarized hydrogen bonded (Grotthuss) chains, never truly observed in bulk hydrogen bonded systems. The results show that, in phosphoric acid, the central system of this study, such chains containing up to five consecutive hydrogen bonds can form. It is the interplay between these chains and a *frustrated* (there are more proton donor than acceptor sites) hydrogen bond network, which is found to lead to extremely high proton conductivity in phosphoric acid. This strongly contrasts to water, wherein the anomalously high rate of excess charge transport occurs not through *extended* chains but rather through *local* hydrogen bond rearrangements that drive individual proton transfer reactions. The mechanism proposed in this work, suggests that strong hydrogen bonding does not necessarily lead to protonic ordering and slow dynamics of the system, demonstrating that weak solvent coupling and sufficient degree of configurational disorder can lead to fast proton transport.

Although, phosphonic and phosphinic acids possess even stronger hydrogen bonds, the stronger dipolar and dynamic backgrounds tend to oppose the formation of extended Grotthuss chains. Moreover, these systems do not have the same intrinsically *frustrated* hydrogen bond network (there are more proton acceptor than donor sites), thus hindering the solvent reorganization (depolarization). Nevertheless, the results show that the weak hydrogen bonded configurations, although not an intrinsic property of the hydrogen bond network, are still forming in a dynamical sense due to liquid disorder. The latter, together with the formation of polarized chains explain the high charge carrier concentrations and conductivities reported in these materials, especially in H_3PO_3, where they are only slightly lower than in the case of H_3PO_4.

Apparently, proton transport in phosphoric acid is extremely susceptible to nearly all types of chemical perturbations. Apart from the severe conductivity reduction caused by the addition of bases, even the addition of acids leads to some decrease in conductivity. The only *dopant* that increases the conductivity of H_3PO_4 is water which, together with some condensation products (e.g. $H_4P_2O_7$, $H_5P_3O_{10}$) is already present even in a nominally dry acid under the conditions of thermodynamic equilibrium. In fact, the severe increase in the conductivity of phosphoric acid upon dilution cannot be explained by simple hydrodynamic diffusion of hydronium ion, indicating that proton structural diffusion plays a major role in these systems as well. The results show that very similar molecular mechanisms are at play in phosphoric acid – water system as in neat oxoacid systems. The properties of hydrogen bonds even in 1:1 $H_3PO_4 - H_2O$ mixture are virtually identical to those of pure H_3PO_4, generally, showing no resemblance to liquid H_2O. It is due to the strong and polarizable acid-water hydrogen bonds, that some degree of cooperativity can still be observed in the proton transport mechanism, although the solvent coupling in this case is much stronger due to the significantly different dielectric nature of the water phase. In addition to some vehicular contribution to proton conductivity, water also has some *plasticizing* effect, increasing the configurational disorder in the hydrogen bond network, therefore resulting in significantly higher conductivities observed in these systems.

Zusammenfassung

Das grundlegende Verständnis der Protonen-Transport-Mechanismen in Wasserstoffbrücken gebundenen Medien auf molekularer Ebene bleibt eine der zentralen Fragen in vielen Bereichen der Wissenschaft, angefangen von elektrochemischer Energieumwandlung bis hin zu Prozessen in biologischen Systemen. Trotz der starken Fortschritte in der Erforschung dieser Prozesse, erwies sich der vermeintlich einfachste Fall – Protonentransport in homogenen Bulk-Medien im thermodynamischen Gleichgewicht – als einer der herausforderndsten und am schwersten fassbaren. Die große Zahl der nichttrivial gekoppelten Reaktionskoordinaten, die an der Bildung und der Wanderung der Protonen-Defekte beteiligt sind, machen das Herausarbeiten der molekularen Details dieser Mechanismen zu einer sehr schwierigen Aufgabe. Nur durch enorme theoretische und experimentelle Anstrengungen war es möglich, eine klare mechanistische Darstellung des Transports von protononischen Defekten (H_3O^+ und OH^- Ionen) in Wasser zu entwickeln. Wasser hat jedoch eine geringe intrinsische Protonenleitfähigkeit. Im Gegensatz dazu hat eine Klasse von Verbindungen, die unter dem Namen Phosphor-Oxosäuren bekannt ist, einige der höchsten bekannten Protonenleitfähigkeiten. In dieser Arbeit werden die Protonen-Transport -Mechanismen dieser Familie von Protonenleitern (H_3PO_4, H_3PO_3 and H_3PO_2) und einigen eng verwandten Systemen (H_3PO_4 - H_2O Mischungen) mit Hilfe von *ab initio* Molekulardynamik-Simulationen auf molekularer Ebene untersucht. Reine flüssige Phosphorsäure hat die höchste intrinsische Protonenleitfähigkeit aller bekannten Substanzen. Abgesehen davon, dass Phosphate eine zentrale Rolle in der Struktur und Funktion von biologischen Systemen (z. B. ATP, DNA, Lipid-Membranen) spielen, sind Systeme, die Phosphsate/Phosphonate enthalten (z. B. PBI/H_3PO_4), von zunehmendem Interesse als Hochtemperatur-Elektrolyte in Brennstoffzellen.

Die vorliegende Arbeit gibt ertsmalig Einblicke in die mikroskopischen Details der Protonen-Ttransport-Mechanismen in diesen Systemen mit einer geeigneten räumlichen und zeitlichen Auflösung. Die Ergebnisse zeigen, dass starke, polarisierbare Wasserstoffbrücken an einer gekoppelten Protonenbewegung und ausgeprägten protonischen dielektrischen Antwort des Mediums beteiligt sind. Dies erlaubt die Bildung *ausgedehnter*, polarisierter Wasserstoffbrücken gebundener (Grotthuss-) Ketten, die zuvor noch nie in einem Bulk-System beobachtet wurden. Die Ergebnisse zeigen, dass sich in Phosphorsäure, dem zentralen System der vorliegenden Arbeit, solche Ketten von bis zu fünf aufeinander folgenden Wasserstoffbrücken bilden können. Es ist das Zusammenspiel dieser Ketten mit einem frustrierten Wasserstoffbrücken-Netzwerk (es gibt mehr Protonen-Akzeptor- als Donorstellen), das, wie herausgefunden wurde, zu der bekannten extrem hohen Protonenleitfähigkeit in Phosphorsäure führt. Der beobachtete Mechsnismus unterscheidet sich wesentlich von dem wässriger Medien, in denen die hohe Beweglichkeit protonischer Ladungsträger nicht durch die Dynamik langer Ketten, sondern durch *lokale* Umlagerungen der Wasserstoffbrücken, die die einzelnen Protonen-Übertragungs-Reaktionen auslösen, hervorgerufen wird. Der in dieser Arbeit vorgeschlagene Mechanismus legt nahe, dass starke Wasserstoffbrückenbindungen nicht gezwungenermaßen zu Protonen-Ordnung und langsamer Dynamik des Systems führen müssen, sondern zeigt, dass schwache Lösungsmitteleffekte und ein ausreichender Grad der Konfigurations-Fehlordnungung zu schnellem Protonen-Transport führen können.

Obwohl, die Phosphon- und Phosphinsäuren noch stärkere Wasserstoffbindungen aufweisen, ist die Bildung von Grotthuss-Ketten durch den stärker dipolaren Charakter des Solvents und wegen der ausgeprägteren lokalen Dynamik (die Wasserstoffbrückendichte ist niedriger als in Phosphorsäure) auf kürzere Kettenlängen begrenzt. Hinzu kommt, dass die Wasserstoffbrücken-Netzwerke dieser Systeme lediglich dynamisch frustriert sind, wodurch auch die Rate der Depolarizationsreaktionen reduziert ist. Die thermisch aktivierte Konzetration nicht über Wasserstoffbrücken gebundener OH Gruppen ist jedoch noch so hoch, dass polarisierte, wenn auch kurze, Grotthuss-Ketten, hinreichend schnell depolarisiert werden können. Dies erklärt insbesondere die Leitfähigkeit von H_3PO_3, die nur geringfügig niedriger als die von H_3PO_4 ist.

Der Protonentransport in Phosphorsäure ist offensichtlich extrem anfällig für chemische Störungen fast aller Arten. Abgesehen von der starken Leitfähigkeitsminderung durch die Zugabe von Basen, führt aber auch die Zugabe von Säuren zu einer gewissen Erniedrigung der Leitfähigkeit. Der einzige Zusatz, der die Leitfähigkeit von H_3PO_4 erhöht ist Wasser, das zusammen mit einigen Kondensationsprodukten (z. B. $H_4P_2O_7$, $H_5P_3O_{10}$) bereits in nominell trockener Säure im thermodynamischen Gleichgewicht vorliegt. Tatsächlich kann die starke Erhöhung der Leitfähigkeit nach Verdünnung von Phosphorsäure nicht durch einfache hydrodynamische Diffusion von Hydronium-Ionen erklärt werden, was darauf hindeutet, dass auch die Protonen-Strukturdiffusion eine wichtige Rolle in diesen Systemen spielt. Die vorliegenden Ergebnisse zeigen, dass sich der Protononenleitmechanismus durch Zugabe von Wasser zunächst kaum ändert. Die Eigenschaften von Wasserstoffbrückenbindung in einer 1:1 H_3PO_4-H_2O Mischung, sind praktisch identisch mit denen der reinen H_3PO_4 und zeigen keine Ähnlichkeit mit denen in flüssigem H_2O. Es sind die starken und polarisierbaren Säure-Wasser-Wasserstoffbrückenbindungen, die in diesen Systemen noch einen gewisser Grad an Kooperativiät im Mechanismus des Protonen-Transports zulassen. Neben einem gewissen *Vehikel*-Beitrag zur Protonenleitfähigkeit hat Wasser auch eine weichmachende Wirkung, die die Konfigurations-Fehlordnung im Wasserstoffbrücken-Netzwerk erhöht und so zu den deutlich höheren Leitfähigkeiten dieser Systeme beiträgt.

Contents

Abstract **ix**

Zusammenfassung **xiii**

List of Figures **xxi**

List of Tables **xxvii**

1 Introduction **1**

1.1 Proton Transport 1

1.1.1 Proton Transport in Water 5

1.1.2 Phosphorus Oxoacids 9

1.1.3 PEMFC Materials based on Phosphorus Oxoacids 16

1.2 *Ab Initio* Molecular Dynamics 18

1.2.1 Density Functional Theory 20

1.2.2 Born-Oppenheimer Molecular Dynamics 23

1.2.3 Car-Parrinello Molecular Dynamics 24

1.2.4 Evaluation of forces in AIMD 26

1.2.5 Basis Sets 27

1.2.6 Pseudopotentials 31

1.2.7 Beyond Microcanonics: Thermostatting 33

1.2.8 Equilibrium Time Correlation Functions 34

2 Aims of the project **37**

3 Computational methods and setup **39**

4 Phosphoric acid **43**
4.1 Structural Properties 43
4.2 Dynamical Properties 45
4.3 Rotational Dynamics 48
4.4 Proton Transfer Kinetics 50
4.5 Proton Transfer Energetics 52
4.6 The Structure and Energetics of Charged Species 54
4.7 On the Degree of Protonation 56
4.8 Interprotonic Coupling 58
4.9 Formation of Grotthuss Chains 62
4.10 On the Proton Transport Mechanism 65

5 Phosphonic and phosphinic acids **69**
5.1 Structural Properties 69
5.2 Dynamical Properties 73
5.3 Vibrational spectra 79
5.4 Proton Transfer Kinetics 81
5.5 Proton Transfer Energetics 83
5.6 The Structure and Energetics of Charged Species 84
5.7 On the Degree of Protonation 87
5.8 Interprotonic Coupling 89
5.9 On the Formation of Grotthuss Chains and Proton Conduction Mechanisms 91

6 Phosphoric acid and water mixtures **97**
6.1 Structural Properties 98
6.2 Dynamical Properties 102
6.3 Proton Transfer Energetics and the State of Charged Species . . . 104
6.4 Interprotonic Coupling 107
6.5 On the Formation of Grotthuss Chains and Proton Transport Mechanism 109

7 Conclusions **115**

References **119**

Lebenslauf **127**

List of Figures

1.1 Temperature dependent conductivities of the various classes of proton conducting materials. 4

1.2 Excess proton *structural diffusion* in water. The hydrogen bonds around the excess charge are contracted, favoring the PT and the hydrogen-bond breaking and forming processes occur in the more loosely bound outer hydration shells. The proton potentials show the adiabatic transfer of the central proton.[2,3,6] 7

1.3 Structure of phosphoric (left), phosphonic (middle) and phosphinic (right) acid molecules. Different coloring correspond to different atoms: phosphorus (purple), oxygen (red) and hydrogen (white). . 10

1.4 Mechanism of proton conduction in phosphoric acid based on PFG-NMR and conductivity data.[68]. 12

1.5 Temperature dependence of ^1H and ^{31}P diffusion coefficients.[68]. . 13

1.6 H/D isotope effect for the diffusion of ^1H and $^2H(D)$ in mixtures of H_3PO_4 and D_3PO_4.[80] 14

3.1 Variation of the total energy (conserved quantity), electronic kinetic energy (Car-Parrinello) and temperature (classical kinetic energy of the nuclei) during the `CPMD` simulation. 41

3.2 Variation of the total energy (conserved quantity) and temperature (clasical energy of the nuclei) during the `CP2K` simulation. 42

4.1 A snapshot of a typical configuration from an equilibrated simulation box containing 54 H_3PO_4 molecules. 44

4.2 Radial pair distribution functions of liquid phosphoric acid. The results of two simulations are compared to the neutron scattering study.[156] The g_{HX} and g_{XX} are defined in the same way as in the experimental work: ($g_{HX}(r) = 0.823 g_{HO}(r) + 0.182 g_{HP}(r)$; $g_{XX}(r) = 0.673 g_{OO}(r) + 0.298 g_{OP}(r) + 0.033 g_{PP}(r)$). 46

4.3 Average mean square displacements and corresponding diffusion constants as obtained from the Einstein relation for hydrogen and phosphorus atoms in H_3PO_4 at 383 K. 48

4.4 The average angular displacement of the P–O bond with respect to time and the corresponding rotational diffusion constant. . . . 50

4.5 Orientational correlation functions C_n for the $\mathbf{u}_{P-O}$ bond. $n = 1,2,3$ are shown. 51

4.6 Proton transfer population correlation functions (including and excluding proton rattling) and their triexponential fits. 53

4.7 $P(R_{OO}, \delta)$ probability distribution 54

4.8 Free energy profile $A(\delta)$ along the proton transfer coordinate δ. . 54

4.9 RDFs g_{OO} and running coordination numbers (n_{OO}) of oxygen atoms for phosphoric acid in its various states of protonation. . . 56

4.10 Free energy profiles $A(\delta)$ along the proton transfer coordinate δ for H_3PO_4, $H_4PO_4^+$ and $H_2PO_4^-$. 57

4.11 The probability distribution of oxygen protonation states defined as the sum of individual bond-orders due to surrounding protons ($\sum n_i$). 58

4.12 Absolute magnitude of a purely electrostatic force $F(t)$ acting on a transferring proton ($\delta \to 0$; time = 0 ps) due to all other protons in the system.[171] 60

4.13 $g_{HH}(H_3PO_4)$ radial distribution function resolved in r and δ, containing information about the spatial distribution of protons with respect to δ (δ_{eq} is the equilibrium value in the simulation).[171] . . 60

4.14 g_{PP} RDF resolved in r and δ. 61

4.15 The running coordination numbers $n_{OO}(r,\delta)$ resolved in δ and r for donating and accepting oxygen atoms. 61

4.16 Proton coupling correlation function $C_{pc}(n)$ as a function of connectivity n. Specific values include $n = 0$, (single H-bond), 1 (adjacent H-bonds), and 6 (longest non-cyclic path in the H-bond network). Only the H-bonds with $\delta \leq 0.1$ Å (only $\sim 1.5\%$ of the total number) are considered as undergoing PT. The time increment τ_{res} sets the finite relay time for the system to respond to correlated PTs.[171] 64

4.17 Snapshots of the elementary steps of the proton structural diffusion mechanism in H_3PO_4. This sample event shows five molecules extracted from the simulation box, which participate in the correlated PTs over four neighboring H-bonds and in the formation of a Grotthuss chain. The schemes below the molecular structures show the ions and the interchain dipoles, with the remaining solvent molecules represented by a generalized coordinate $\vec{S}$. The arrows denote the PTs and molecular reorientations for the important steps in the mechanism: (a) and (b) correlated PTs and formation of a Grotthuss chain; (c) and (d) reorientation of the solvent H_3PO_4 molecule induced by the formation and breaking of the 'frustrated' H-bond; (e) and (f) formation and breaking of the second 'frustrated' H-bond.[171] 68

5.1 Snapshots representing the typical configurations from an equilibrated simulation boxes containing (a) 54 H_3PO_3 and (b) 54 H_3PO_2 molecules. 70

5.2 The full simulated radial pair distribution function g_{XX} (where X = P, O and H) and g_{XX} from the neutron scattering study.[95] . . . 71

5.3 Radial pair distribution functions for the liquid H_3PO_4, H_3PO_3 and H_3PO_2. (top) $g_{H_OH_O}$ only for the acidic protons (excluding the hydrogens covalently bonded to phosphorus). (middle) g_{OH_O} for the acidic protons and oxygen atoms, the first peak comes form the covalent O–H bond and the second due to the H-bonding (H$\cdots$O). (bottom) g_{XX}, where X = P or O, shows the different heavy atom pair contributions. 72

5.4 H-bond geometries for H_3PO_4 (black), H_3PO_3 (red) and H_3PO_2 (green): probability distributions for (left) $R_{O...O}$ distances, and $\alpha_{O-H...O}$ angles. 73

5.5 Proton and molecular diffusion coefficients determined by the PFG-NMR with respect to temperature.[66] 77

5.6 Conductivities and the respective contributions due to structural diffusion in H_3PO_4, H_3PO_3 and H_3PO_2.[66] 78

5.7 The average angular displacement of the P–O bond with respect to time and the corresponding rotational diffusion constants for H_3PO_4, H_3PO_3 and H_3PO_2 at 383 K. 80

5.8 Average mean square displacements and corresponding diffusion constants as obtained from the Einstein relation for hydrogen and phosphorus atoms in H_3PO_4 at 383 K. 81

5.9 Comparison of the vibrational power spectra for H_3PO_4, H_3PO_3 and H_3PO_2. 82

5.10 Proton transfer population correlation functions (including and excluding proton rattling) and their triexponential fits for H_3PO_3. . 83

5.11 Proton transfer population correlation functions (including and excluding proton rattling) and their triexponential fits for H_3PO_2. . 84

5.12 Free energy profiles $A(\delta)$ along the proton transfer coordinate δ for H_3PO_4, H_3PO_3 and H_3PO_2. 85

5.13 g_{OO} and running coordination numbers (n_{OO}) of oxygen atoms for H_3PO_3 in its various states of protonation. 87

5.14 g_{OO} and running coordination numbers (n_{OO}) of oxygen atoms for H_3PO_2 in its various states of protonation. 88

5.15 Free energy profiles $A(\delta)$ along the proton transfer coordinate δ for H_3PO_3, $H_4PO_3^+$ and $H_2PO_3^-$. 89

5.16 Free energy profiles $A(\delta)$ along the proton transfer coordinate δ for H_3PO_2, $H_4PO_2^+$ and $H_2PO_2^-$. 90

5.17 The probability distribution of various oxygen protonation states defined as the sum of individual bond-orders due to surrounding protons ($\sum n_i$). 91

5.18 $g_{\mathrm{HH}}(r, \delta; H_3PO_3)$ radial distribution function resolved in r and δ, containing information about the spatial distribution of protons with respect to δ (δ_{eq} is the equilibrium value in the simulation). . 92

5.19 $g_{\mathrm{HH}}(r, \delta; H_3PO_2)$ radial distribution function resolved in r and δ, containing information about the spatial distribution of protons with respect to δ (δ_{eq} is the equilibrium value in the simulation). . 93

5.20 Proton coupling correlation function $C_{pc}(n)$ as a function of connectivity n. Only the H-bonds with $\delta \leq 0.1$ Å ($\sim 2.0\%$ of the total number for H_3PO_3 and $\sim 3.5\%$ for H_3PO_2) are considered as undergoing PT. The time increment τ_{res} sets the finite relay time for the system to respond to correlated PTs ($\tau_{res} = 50$ fs). 94

5.21 Snapshots of the elementary the proton structural diffusion steps in H_3PO_2. The schemes bellow the molecular structures show the ions and interchain dipole orientations, with the solvent being represented by a generalized coordinate $\vec{S}$. The charged ion pair is indicated with (+) and (-), the partial charges on the oxygen atoms are marked by $+\delta$ and $-\delta$. The arrows denote the proton hops and molecular reorientations. 96

6.1 A snapshot of a typical configuration from an equilibrated simulation box containing 36 H_3PO_4 and 36 H_2O molecules. 98

6.2 The total simulated radial pair distribution function g_{XX} (black) (where X = P, O and H) and g_{XX} (red) from the neutron scattering study of Kameda et al.[189] 99

6.3 Radial pair distribution functions of the H_3PO_4 water solutions. The structure of neat H_3PO_4 and H_2O are given for comparison. (top) g_{HH} for System II, H_3PO_4 and H_2O. (middle) g_{OH} for for System I, System II, H_3PO_4 and H_2O; the first peak comes form the covalent O–H bond and the second due to the H-bonding (H. . . O). (bottom) g_{XX}, where X = P or O, shows the different contributions from heavy atom pairs to the total RDF. 101

6.4 Average mean square displacements and corresponding diffusion constants as obtained from the Einstein relation for hydrogen, oxygen and phosphorus atoms in System II at 383 K. 104

6.5 Vibrational spectrum for System II (H_3PO_4 + H_2O (1:1)) (blue) and H_3PO_4 (black). 105

6.6 Free energy profiles $\Delta A(\delta)$ along the proton transfer coordinate δ for PT between phosphoric acid and water for System I. 107

6.7 Free energy profiles $\Delta A(\delta)$ along the proton transfer coordinate δ for all protons and different proton donor/acceptor pairs in System II. 108

6.8 $g_{\mathrm{HH}}(SystemII)$ radial distribution function resolved in r and δ, containing information about the spatial distribution of protons with respect to δ (δ_{eq} is the equilibrium value in the simulation). . 109

6.9 Proton coupling correlation function $C_{pc}(n)$ as a function of connectivity n for pure H_3PO_4 and System II. $\delta_{cut} \leq 0.1$ Å and $\tau_{res} =$ 0 and 50 fs. 111

6.10 Snapshots of the elementary proton structural diffusion steps in System II. The charged ion pair is indicated with (+) and (-). The arrows denote the proton hops and molecular reorientations. . . . 113

List of Tables

5.1 Calculated and experimental diffusion coefficients at 383 K for phosphonic and phosphinic acids. 79

5.2 Calculated fractions of molecules with uncompensated protonic charge (having excess or deficient protons) for H_3PO_4, H_3PO_3 and H_3PO_2 systems and different proton assignment criteria $\delta_{\text{cut-off}}$. . . 86

6.1 Calculated fractions of water and phosphoric acid molecules in their different states of protonation in System II, with different proton assignment criterion $\delta_{\text{cut-off}}$. 106

1

Introduction

1.1 Proton Transport

The molecular understanding of proton transport is one of the long-standing problems in many areas of science ranging from electrochemical energy conversion to biological systems.[1–5] Despite the vast advances in the understanding of these processes, the apparently simplest case of proton transport in bulk media under the conditions of thermodynamic equilibrium, appears to be the most challenging.[3,6] The complication arises due the high number of solvent coordinates and a nontrivial coupling between the coordinates of the solvent and those of the protonic defects. In large part thanks to *ab initio* molecular dynamics (AIMD) simulations, water became the first and remains the only extended H-bonded system for which a molecular picture of protonic defect transport has been envisioned in great detail.[7–25]

A big part of the motivation for this work stems not just from the fundamental interest in proton transport processes in H-bonded media, but also from the practical interest in the development of new proton conducting electrolytes for Polymer Electrolyte Membrane Fuel Cells (PEMFC). The search for new energy sources and energy management systems is the vital feat facing human society in the coming years. Fuel cells have the potential to become important energy conversion devices, able to directly convert the chemical energy stored in the fuel to electric power, at very high conversion efficiencies and zero CO_2 emissions.

PEMFC is a type of fuel cell, where hydrogen gas is used as a fuel and which typically operates at low or intermediate temperatures, with a main practical use in portable and automotive applications. Certainly, the car industry shows the highest interest due to the potential of PEMFCs to replace the internal combustion engine. Unfortunately, the development and industrialization of PEMFCs have been experiencing severe issues. One of them is the lack of suitable electrolyte materials for the separator membranes, capable of functioning at higher temperatures. Generally, these materials have to fulfill a number of requirements: show good proton conductivities, no parasitic transport of other species, and have operating temperatures not limited by the boiling point of water.[2,26] Therefore, the increase of the PEMFC operating temperatures is one of the key issues in the present-day fuel cell research, aimed at not just raising the electrolyte proton conductivities, but also facilitating the function of precious catalysts, necessary for the fuel oxidation. Most of the PEMFC systems currently in use, still rely on Nafion or Nafion-like materials, based on the polymeric perfluorinated hydrocarbon backbone with sulfonic groups attached to the side-chains.[27] These materials still require water in order to ionize the acidic groups and produce mobile protonic charge carriers, which in turn limits the operating temperatures to approximately the boiling point of water. Therefore, systems able to function under low-humidity[28] or even anhydrous conditions[29–33] are attracting a lot of interest. Further progress in this field is virtually impossible without the detailed, molecular understanding of the proton conduction processes in these materials.

This work mainly deals with the proton conduction processes in bulk media under standard electrochemical conditions. It is important to stress that, the thermally activated, random motion of particles is responsible for the appearance of protonic as well as any other kind of ionic conduction in the electrochemical environments. The electric fields applied typically are well within the linear response regime and the resulting gradients of the electrochemical potentials are small in comparison to the internal potentials existing in condensed matter. The Nernst-Einstein relation between the diffusion and mobility is therefore usually fully valid. Hence, only the aspects of proton transport under the conditions of thermodynamic equilibrium are addressed in this thesis and topics such as proton transport in high electrochemical potential gradients, biological systems functioning far from the thermodynamical equilibrium, or excited state proton transfer are omitted from the discussion.

Traditionally, it is viewed that short and strong hydrogen bonds (H-bonds), involving the electronegative species (usually O, N or F) are necessary for any kind of proton transfer (PT) reactions to appear. The complete description of the long-range proton transport process must essentially involve several necessary steps of charge carrier dynamics: (1) formation, (2) solvation and separation, (3) migration and (4) subsequent neutralization, all accompanied by the appropriate solvent reorganization. Therefore, proton transport requires the solvent relaxation along the proton migration path, which is achieved through the breaking and forming of H-bonds within the solvation shells of the protonic defect. In this way, good protonic conductors represent a special class of dynamical H-bonded networks, with H-bonds being strong enough to allow for the PT and a mechanism for the breaking of these bonds enabling the solvent reorganization.

In principle, all of the possible systems able to solvate and transport protonic defects can be grouped into several classes. The most relevant in this context are aqueous systems (acidic and basic aqueous solutions, hydrated ionomers etc.), oxoacids and their salts (H_3PO_4, H_3PO_3, $CsHSO_4$ etc.), metal oxides at high-temperature ($BaCeO_3$, $BaZrO_3$ etc.), and heterocycles (imidazole, pyrazole, benzimidazole etc.). Moreover, only a few of these systems are also able to intrinsically generate protonic charge carriers. Phosphorus oxoacids are among the materials with not only good proton solvating properties but also high intrinsic charge carrier concentrations, due to the high degree of self-dissociation. In a neat liquid state, phosphoric acid (H_3PO_4), the central compound of this work, has the highest known intrinsic protonic conductivity of any material (Fig. 1.1). These observations undoubtedly make phosphorus oxoacid based systems of great potential for the development of new non-aqueous PEMFC electrolyte materials and an interesting class of compounds for the fundamental understanding of proton transport processes in H-bonded media as well as the due to the role phosphates play in the acid-base chemistry of biological systems.[34]

There are two major *modes* of protonic charge transport. The simplest case scenario involves a translational motion of protons attached to some bigger species (*vehicle mechanism*).[35] The proton diffuses together with a vehicle (e.g. H_3O^+,

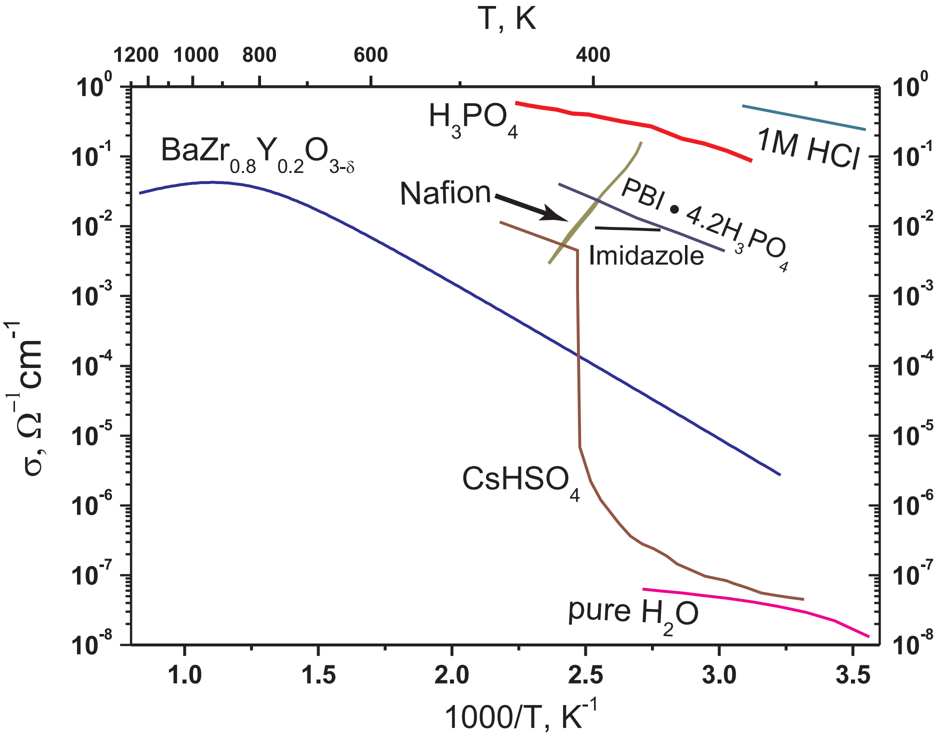

Figure 1.1: Temperature dependent conductivities of the various classes of proton conducting materials.

NH_4^+) carrying the protonic current and the observed conductivities, in this case, are entirely determined by the rate of the vehicle's (molecular) diffusion, which in turn depends on the hydrodynamic or Stokesian properties of the medium. The other *mode* of proton transport involves proton transfers (essentially a chemical reaction) from one vehicle to another, without pronounced translational dynamics of the vehicles themselves. Normally, these transfers are accompanied by an additional reorganization of the proton solvating environment resulting in an uninterrupted pathway for the migrating proton and the relevant rates of the transport are determined by the proton transfer and the solvent reorganization. This process is usually called the *structure* or *structural diffusion*, or in the case of proton transport in water – Grotthuss mechanism. The latter coinage of the term, though widely used in various sources, neither reflects the original ideas of von Grotthuss[36] nor the current understanding of this process in aqueous media.[3,6,7]

1.1.1 Proton Transport in Water

Since water is the most vital and ubiquitous substance on the planet, its various properties have been under the utmost scrutiny for centuries. This also pertains to its proton conducting properties. The first rigorous theory of aqueous electrolysis and essentially proton transport was proposed more than two centuries ago by von Grotthuss.[36] On the basis of the experiments with Volta pile and its effects on various solutions, he anticipated the structure of water as circles of positively (H) and negatively (O) charged, constantly exchanging, ionic species. Furthermore, he thought that under the applied current, these circles (water was still believed to be HO at the time) open up and form wires, wherein a collective exchange of hydrogen and oxygen species account for the conductivity and evolution of gases in aqueous electrolysis.[36] For a long time, various modified theories comprising this extremely appealing idea were considered to explain the high mobility of excess and missing protons in aqueous acidic and basic solutions. The 'big leap' in the understanding of proton conduction in water was the establishment of the fact that, the proton cannot exist as a free particle in, a condensed medium, but must be embedded into the electronic density of a more electronegative species (H_3O^+).[37] It was not until the beginning of the 20th century that the mobilities of excess and missing protons in aqueous acidic and basic solutions exceeding those of other ions were recognized (H^+: ∼9 times higher than Li^+ or ∼5 times higher than K^+).[38–40] The first mathematically rigorous theory was attempted by Hückel,[41] where he already realized the importance of the PT and tried to calculate the water dipole reorientation rates into positions favoring PT between the neighboring water molecules. Later, Bernal and Fowler improved the existing theories by presenting the first quantum mechanical treatment of the PT process, with the molecular rotation treated completely isotropically.[42] An almost analogous, just slightly more rigorous treatment was independently presented by Wannier.[43] Both of these theories indicated proton tunneling as the rate limiting step, however the experimental kinetic isotope effect was surprisingly absent. The next model of Gierer and Wirtz described the process by a single temperature-dependent activation step, but still featured structureless liquid water.[44] The next question raised was: what is the rate-limiting step: the proton transfer or the molecular rotation? The historical works of Conway, Bockris and Linton[45] as well as Eigen and de Mayer[46] agreed that classical proton transfer must be slow, with the proton tunneling being much faster and the rotation of the H-bonded water molecules near the central, particularly stable, H_3O^+ ion, limiting the reaction rate. The later contributions by Halle and Karlström[47] and Hertz[48] included the importance of the solvent's dielectric response (polarizability) as well as refined the description of the 'Grotthuss mechanism' by suggesting that the protonic charge transport (conductivity) must be reflected in a corresponding displacement of the protonic mass diffusion and its trajectory.

Many controversies were principally solved with the advent of computer simulations[3,9–19,49–53] and ultrafast infrared spectroscopy measuements.[21,24,25,54,55] Despite the pervasive use of the term 'Grotthuss mechanism' and pictures stemming from the original notion, the current understanding of bulk proton transport has considerably evolved. First of all, the concerted proton hopping between the H-bonded molecules (in such a highly polar medium as water) would result in, an energetically prohibitive, polarized situation. Hence, the protons can be only displaced over a very short distance without an accompanying solvent reorganization and must be strongly coupled to the solvent. The modern view of the elementary step favors the 'presolvation' (in the spirit of Marcus theory of electron transfer[56,57]) picture: the proton receiving species must assume the same coordination pattern as the species into which it is going to be transformed upon the PT.[7–11,18,19,58] In this way, many bonds and particles are involved in shifting a proton by a small distance, with the PT occurring in the tightly bound charged complex (Zundel ($H_5O_2^+$)[59] and Eigen ($H_9O_4^+$)[46] ions) and solvent reorientation (H-bond bond breaking and forming) taking place in the more loosely bound outer solvation shells (Fig. 1.2). The excess protonic defect propagates as a topological defect through the H-bond network via interconversion of its two limiting forms (Eigen and Zundel ions). The H-bonds around the excess proton are significantly contracted ($\mathrm{r}_{\mathrm{OO}}^{average} \approx 2.85$ Å versus $\mathrm{r}_{\mathrm{OO}}^{defects} \approx 2.55$ Å), thus providing a way for an almost barrierless proton transfer close to the adiabatic limit (no pronounced tunneling). In this way, the net displacement of the center of excess charge upon the proton transfer is very small – of the order of one water molecule, discarding the possible existence of extremely mobile protons in aqueous acidic solutions. This is manifested in only a slight increase in proton tracer diffusion coefficient compared to that of oxygen, due to the structural diffusion.[60] Moreover, as a result of water's high molecular diffusion coefficient, the simple hydrodynamic diffusion of protonic defects makes a substantial contribution to the total proton conductivity, e.g for acidic solutions ∼22% (assuming the same diffusion coefficients for H_2O and H_3O^+). The contributions due to the structural and molecular diffusion in water are certainly strongly dependent on temperature, pressure and acid concentration. In general, the increasing temperature and excess proton (acid) concentration diminish the structural diffusion,[60] while the increasing pressure raises it (up to ∼0.6 GPa).

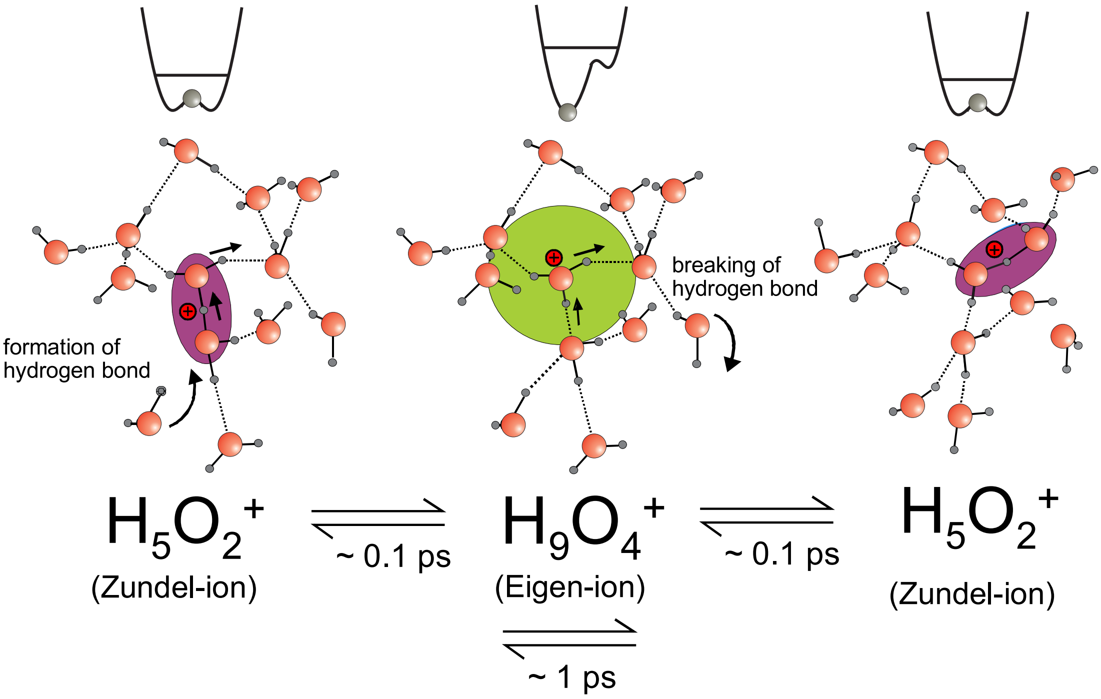

Figure 1.2: Excess proton *structural diffusion* in water. The hydrogen bonds around the excess charge are contracted, favoring the PT and the hydrogen-bond breaking and forming processes occur in the more loosely bound outer hydration shells. The proton potentials show the adiabatic transfer of the central proton.[2,3,6]

Another important question concerning the transport of protonic charges is: are the mechanisms of excess proton and proton hole identical? This issue still remains controversial. Traditionally, the mechanism of OH^- transport in aqueous media was explained by simply invoking symmetry arguments leading to the concept of the 'mirror mechanism': H_3O^+ is a water molecule with an extra proton, whereas OH^- is a water molecule missing a proton (having a *protonic hole*) and the structural diffusion mechanism has the same mechanism with just the H-bond polarities and directions of proton transfers being reversed. The modern understanding suggests that this might not be the case for the negatively charged protonic defects in water. Path integral AIMD simulations found that the preferred solvation shell of OH^- in water is not composed of three accepted and one donated hydrogen bonds (suggested by a standard Lewis picture of an isolated OH^-).[11,19] The hydrated hydroxide ion is rather 'hypercoordinated': it can accept four H-bonds and form a square-planar configuration and transiently donate one H-bond.[19,20,22,23,25] The physical origin of this effect is traditionally explained by the delocalization of the oxygen lone pairs forming a uniform electron pair density with toroidal symmetry. Once the number of accepted H-bonds in the first OH^- solvation shell is reduced from four to three and one H-bond is fully donated, leading to a typical water-like tetrahedral solvation, a proton can be transferred forming a new properly solvated water molecule. A larger structural rearrangement is necessary in the case of OH^- which could account for a slightly lower mobility of hydroxide, as compared to the case of an excess proton.[19] Due to the very low degree of self-dissociation of water, the aqueous protonic defects can only be studied upon extrinsic doping (both theoretically and experimentally). This could possibly lead to an artificial bias or even a symmetry breaking of the 'mirror image' mechanism.

It always remains instructive to ask whether long-range correlated proton motion via extended 'Grotthuss chains' is possible in any system. One way to observe a concerted 'Grotthuss mechanism' in for example water is to imagine a situation without a polarizable solvent, for instance a chain of water molecules confined in a carbon nanotube[61–63] or arguably some biological 'proton wires'.[5,64] Up to now, the details of a similar process in the case of bulk polar media have not yet been revealed.

1.1.2 Phosphorus Oxoacids

Phosphorus oxoacids are a fundamentally interesting family of proton conductors (Fig. 1.3). This work focuses on the phosphorus oxoacids, three of which can been isolated in their pure form. Formally, they differ in their phosphorus oxidation state: phosphoric or orthophosphoric acid (P^{+5}) H_3PO_4, phosphonic or phosphorous acid (P^{+3}) H_3PO_3 and phosphinic or hypophosphorous acid (P^{+1}) H_3PO_2. It is probably the only class of H-bonded proton conducting liquids where one can systematically observe how the changes in the dimensionality and topology of the H-bond network affect the proton transport properties. Among the three of them, phosphoric acid has the highest proton density, a very peculiar proton donor versus acceptor site ratio (3:2 – 3 OH proton donor and one unprotonated oxygen acceptor site) and the highest reported conductivity. As will be shown later, many of the physical properties show very interesting changes when moving from H_3PO_4 to H_3PO_3 (proton donor–acceptor site ratio 2:2) and finally to H_3PO_2 (donor–acceptor sites ratio 1:2). It is only recently that the proton conducting properties (conductivity, diffusion) of pure phosphonic and phosphinic acids were studied experimentally.[65,66] Moreover, the systematic relation between the transport properties and the topology of the H-bond network have not yet been addressed for any system. This work is probably the first attempt to investigate these questions at the molecular level, trying to fundamentally relate the details of the proton dynamics to those of the macroscopic transport. The systematic experimental and theoretical studies of this class of materials could provide a fundamental underpinning for the questions addressed by the PEMFC community as well as fundamental research in H-bonded systems. In the following sections, some of the available experimental and theoretical results on phosphorus oxoacids and related systems are shortly reviewed.

1.1.2.1 Phosophoric Acid

Phosphoric acid H_3PO_4 is the emphasis of this work. In a neat liquid state, it is the best intrinsic proton conductor among the various classes of materials ($\sigma \approx$ 0.15 S/cm at 50° C; Fig. 1.1). The intrinsic nature of protonic conductivity in this system makes it distinct from water, which shows significant protonic con-

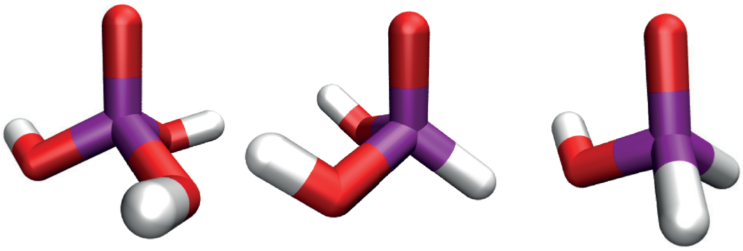

Figure 1.3: Structure of phosphoric (left), phosphonic (middle) and phosphinic (right) acid molecules. Different coloring correspond to different atoms: phosphorus (purple), oxygen (red) and hydrogen (white).

ductivity only when ‘doped’ with acids or bases. The pronounced amphoteric character of phosphoric acid (it both donates and accepts protons and has high K_a and K_b values) leads to a high degree of self-dissociation ($\sim$7%[67] compared to $\sim 10^{-5}$% in water). Moreover, the mobility of protonic charge carriers in H_3PO_4 is comparable only to that of aqueous systems.[60,68] This is surprising, considering that H_3PO_4 has a viscosity two orders of magnitude higher ($\sim$100 cP)[69] than that of water. The proton transport number of $t_{H^+} \approx 98\%$ makes phosphoric acid an almost exclusively protonic conductor with only the remaining 2% of the current carried by the Stokesian (vehicular) diffusion of phosphorus species.[68] These observations make phosphoric acid not only an interesting system for the fundamental understanding of proton dynamics and transport in H-bonded systems, but also for the development of high-temperature anhydrous polymer electrolytes (for e.g. fuel cell membranes).

When it comes to the topology of the hydrogen bond network, the imbalance in the numbers of potential proton donor and acceptor sites (three O–H donors compared to only one non-protonated oxygen) is anticipated to lead to a high degree of configurational *frustration* (local formation of high energy sites). In water, and even more clearly in hexagonal ice, each water molecule contributes equally to approximately four hydrogen bonds: two as a donor and the other two as an acceptor. Crystalline H_3PO_4[70] possesses three types of hydrogen bonds: one formed by an oxygen which is a donor only and an oxygen which is an acceptor only ($r_{O\cdots H}$ = 1.55 Å), the second which is formed by an acceptor-only oxygen and an oxygen that both donates an accepts a hydrogen bond ($r_{O\cdots H}$ = 1.59 Å), and the third, which is the longest and most distorted, formed by a donor-only oxygen and an oxygen that is both a donor and an acceptor ($r_{O\cdots H}$ = 1.97 Å; $\angle_{O-H\cdots O}$ = 152°). It is obvious that due to the high density of protons and these structural peculiarities, which we term *frustration* of the hydrogen bond network, the system tends to act against the protonic ordering and the entropy reduction. Experimentally, this is also clearly manifest in the lower melting point of H_3PO_4 compared to the other two phosphorus oxoacids. Despite the higher number of hydrogen bonds, phosphoric acid has a melting point of $T_m(H_3PO_4)$ = 42 °C, which is lower than that of phosphonic acid ($T_m(H_3PO_3)$ = 73 °C) and only slightly higher than that of phosphinic acid ($T_m(H_3PO_2)$ = 26 °C). The same trend can be seen in the symmetry lowering of the space group of solid phosphoric acid (P 2_1/c (No. 14))[70] as compared to that of phosphonic acid (P na2_1 (No. 33))[71] and that of phosphinic acid (P $2_1 2_1$2 (No. 18)).[72] It is, therefore, very likely that the intrinsic disorder and frustration of the hydrogen bonds are closely linked to the stability and mobility of protonic charge carriers and hence the protonic conductivity of H_3PO_4.

To date, the molecular proton transport mechanisms in phosphoric acid have certainly received far less attention[73,74] than those in aqueous systems. Nevertheless, some type of 'proton relay' or 'proton switch' mechanism for the proton transport in neat H_3PO_4 acid was hypothesized, as early as late sixties, on the basis of conductivity measurements on pure and *doped* acid.[75–78] The relation between the structural diffusion and high conductivity in phosphoric acid for varying concentration range was later confirmed by the spin-echo Pulsed Field Gradient NMR (PFG-NMR).[68,79] The experimentally measured ratio between proton and phosphorus diffusion coefficients is as high as ∼4.5, and decreases slightly with increasing temperature (Fig. 1.5).[68] The magnitude of this ratio suggests that proton diffusion is virtually decoupled from the diffusion of phosphorus species. The Haven ratio, defined as the ratio between the proton self-diffusion coefficients, as obtained from the PFG-NMR, and those directly calculated from the conductivity via the Nernst-Einstein relation (assuming that all the protons in H_3PO_4 contribute to conductivity), shows a deviation from unity in H_3PO_4 (1.54 at 315 K).[68] This suggests that some of the fast proton motion is correlated (protonic defects pair or cluster), and does not lead to real charge separation and conduction (Fig. 1.4). Finally, it must be stressed that the isotope effects (Fig. 1.6) on the proton transfer are very small, suggesting that similarly to the case of water, the proton transfer is close to the adiabatic limit (taking place without barrier and no pronounced tunneling) and completely driven by solvent fluctuations.[1,80]

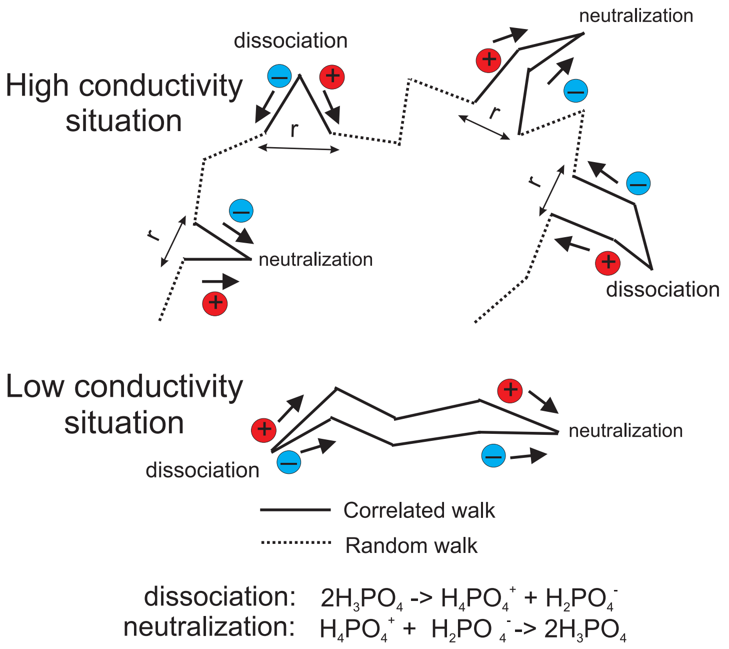
High conductivity situation
dissociation
r
neutralization
r
neutralization
r
r
dissociation
Low conductivity situation
dissociation
neutralization
Correlated walk
Random walk
dissociation: $2H_3PO_4$ -> $H_4PO_4^+$ + $H_2PO_4^-$
neutralization: $H_4PO_4^+$ + $H_2PO_4^-$ -> $2H_3PO_4$

Figure 1.4: Mechanism of proton conduction in phosphoric acid based on PFG-NMR and conductivity data.[68].

The very short intermolecular hydrogen bonds ($r_{OO} \approx 2.6$ Å compared to about $r_{OO} \approx 2.8$ Å in water) are commonly associated with flat H-bond potentials and a pronounced protonic polarizability, also known as 'Zundel polarizability'.[81] Moreover, their mutual polarizability could allow for a correlated proton motion within extended chains of H-bonded molecules, as was also inferred from IR studies.[82]

Another important observation comes from the fact that proton conductivity in phosphoric acid is extremely susceptible to nearly all types of *chemical perturbations*. Apart from the severe conductivity reduction caused by the addition of bases[78] (e.g. imidazole[83]), even the addition of acids leads to some decrease in conductivity.[78] The only *dopant* that increases the conductivity of H_3PO_4 is water,[69,78,79] which together with some condensation products (e.g. $H_4P_2O_7$,

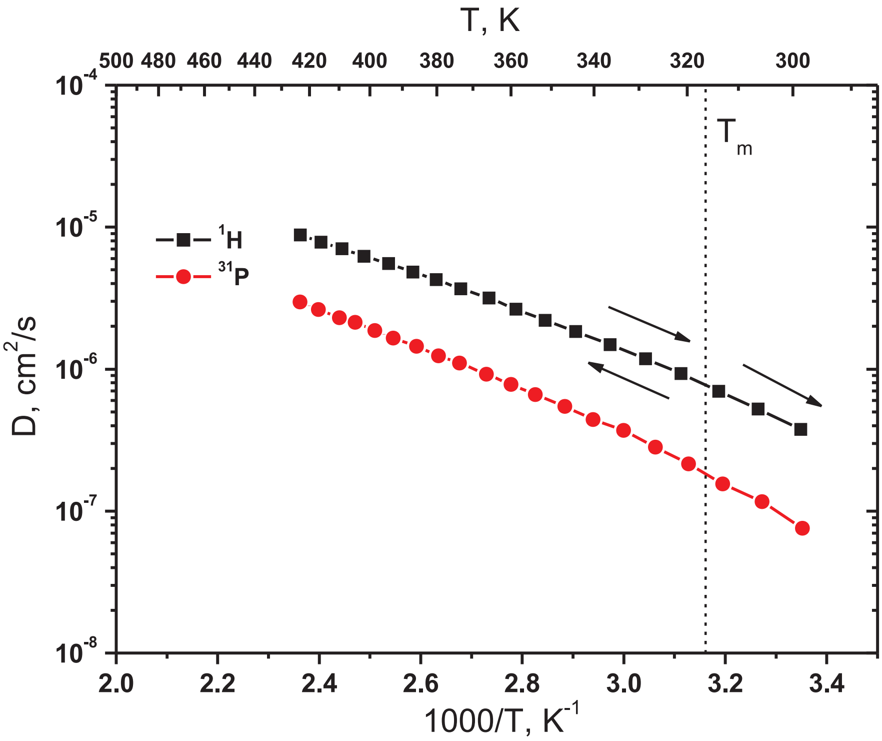

Figure 1.5: Temperature dependence of ^{1}H and ^{31}P diffusion coefficients.[68].

$H_5P_3O_{10}$) is already present even in a nominally dry acid under the conditions of thermodynamic equilibrium.[67,84] Whether the excess water simply accelerates the intrinsic proton conduction process operating in H_3PO_4, or the entire proton conduction mechanism changes, is not clear as of yet and is therefore, addressed in this work (Chap. 6).

As was previously mentioned, the molecular details of the proton transfer and transport dynamics in H_3PO_4 have not been investigated at the same level of detail as in the other proton conducting systems: water, imidazole[85–88] or metal oxides.[89–93] Up to this point, not much is known about the molecular details of elementary reactions governing proton conductivity in phosphoric acid, neither in terms of complex sizes nor in terms of the time scales involved. The only available data hinting at the critical length and duration of the elementary proton transfer reaction was estimated from Quasielastic Neutron Scattering (QENS) by fitting the dynamic structure factors to the jump diffusion model.[68,94] Apart from

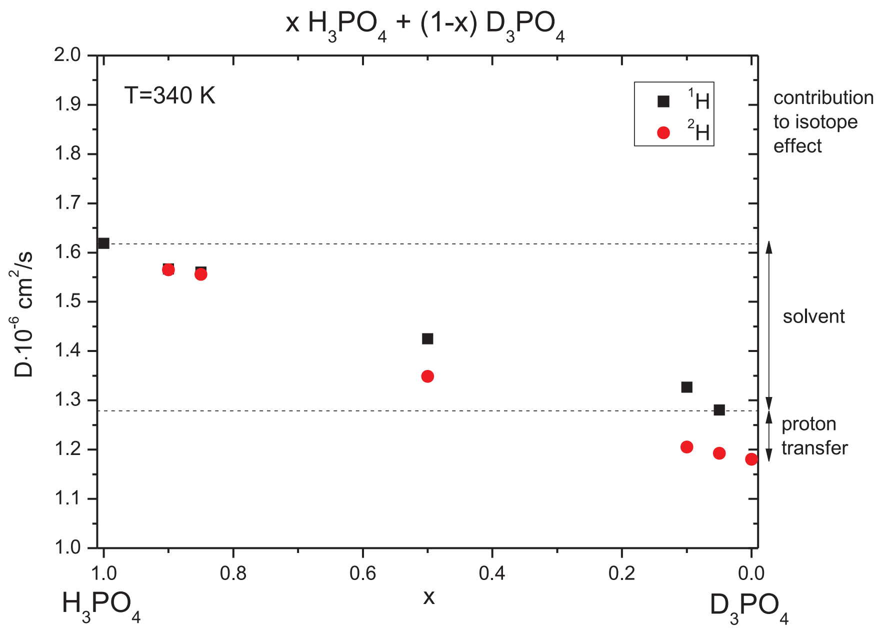

Figure 1.6: H/D isotope effect for the diffusion of ^{1}H and ^{2}H(D) in mixtures of H_3PO_4 and D_3PO_4.[80]

QENS, the first theoretical attempt to acquire information about the important length scales of the elementary proton transfer step was based on static full-electron quantum chemical calculations.[74] These calculations indicated a strong effect on the proton transfer energetics in phosphoric acid clusters having up to six molecules, suggesting that ensembles containing at least six molecules should be studied in order to capture the details of elementary proton transfer reaction.[74]

1.1.2.2 Phosphonic Acid

Technologically, phosphonic acid (H_3PO_3) is no less important than phosphoric acid. The presence of a P–H bond allows the chemical modification or tethering of $POHO_2$ groups via the introduction of a P–C bond and opening new possibilities for producing new materials. The recent study by Schuster et al. established the most important aspects of proton conduction in a nominally dry H_3PO_3.[65] Similarly to the case of H_3PO_4, the structural diffusion of protonic defects, which are intrinsically present due to the highly pronounced self-dissociation, is mainly responsible for the conductivity of phosphonic acid. Generally, the key aspects of this process in H_3PO_3 resemble those of H_3PO_4. The even ratio between proton donor and acceptor sites (2 vs. 2) does not lead to the intrinsic frustration of the H-bond network. In the crystalline state all H-bonds are of the same length. Furthermore it is clearly manifested in the higher melting point ($T_m(H_3PO_3)$ = 73 °C vs. $T_m(H_3PO_4)$ = 42 °C) and higher space group (P $2_1 2_1 2$ (No. 18) vs. P $2_1/c$ (No. 14)) in the crystalline state, as compared to phosphoric acid.

Coming to the transport properties of phosphonic acid, the hydrodynamic background (due to the diffusion of phosphorus species) in the liquid state is obviously stronger than in the case of phosphoric acid, as can be seen from the higher H and P diffusion coefficients. Moreover it shows stronger correlations in the diffusion of protonic defects (higher Haven ratio ∼2.5 vs. ∼1.5 in H_3PO_3) resulting in lower conductivity and less pronounced proton structural diffusion (∼90 % vs. ∼98 % in H_3PO_4). Interestingly, the H-bonds in both crystalline and liquid H_3PO_3 are in average stronger than those of H_3PO_4, as was estimated by elastic neutron scattering.[71,95] This should result in an even higher protonic polarizability of the H-bonds.[82] However, the stronger dipolar response (gas phase $\mu_{H_3PO_3} \approx 1.6$ D vs. $\mu_{H_3PO_4} \approx 0.45$ D) of the solvent might in principle bias this property. In the case of phosphoric acid, due to the excess of proton donor versus acceptor sites, high configurational frustration is already an 'intrinsic' property of this system. In phosphonic and phosphinic acids, on the other hand, there are enough proton acceptor sites. Therefore, in the rest of the text, the term 'intrinsically frustrated' will be used only in the case of H_3PO_4.

The absence of intrinsic configurational frustration in phosphonic acid makes the topology of the H-bond network less complicated. However, the IR study of Zundel and Leuchs,[82] predicted that a finite concentration of more loosely bound or *free O–H* groups must exist in liquid phosphonic acid. This would suggest that, although frustrated H-bonds (formed between two proton donating O–H groups) are not an intrinsic property of the H-bond network, they are still transiently forming due to liquid disorder.

The molecular details of proton transport in phosphonic acid have been even less scrutinized than those of phosphoric acid. One of the first attempts to study these processes at the molecular level was by Joswig et al.[96]. In this work an alternative AIMD scheme was used, namely Density Functional Tight-Binding Molecular Dynamics. Although this method allows the description of bond breaking and forming processes *on-the-fly*, the suitability of this method for the description of protonic defect transport in water has been recently questioned.[97]

1.1.2.3 Phosphinic Acid

Phosphinic or hypophosphorous acid (H_3PO_2) is certainly the least investigated system. The crystal structure analysis revealed the existence of very short almost symmetrical H-bonds and the formation of one-dimensional zig-zag chains of phosphinic acid molecules.[72] The 1D character of the chains indicates the reduced dimensionality and simpler topology of the H-bond network. However, this together with the presence of very short and strong H-bonds ($r_{OO} \approx 2.5$ Å) could result in a very pronounced mutual protonic polarizability and lead to collective proton motion within the H-bonded chains.[82,98] Although, this motion could be very strongly perturbed by the much stronger dipolar nature (gas phase $\mu_{H_3PO_2} \approx 2.6$ D) of the solvent than in the case of H_3PO_4 and H_3PO_3.

Up to now, the proton transporting properties of neat H_3PO_2 have not been studied. However, the PEMFC electrolytes containing phosphinic acid in various forms have already attracted some interest.[33,99–102] Therefore, the first molecular simulation study described in this thesis was additionally supplemented by experimental work. The crystals of nominally dry phosphinic acid were isolated. The proton conductivities and PFG-NMR tracer diffusion coefficients were measured at different temperatures in the molten acid. These data and their comparison to the AIMD results will be presented in Chap. 5.

1.1.3 PEMFC Materials based on Phosphorus Oxoacids

For many years, phosphoric acid has been used as an electrolyte in phosphoric acid fuel cells (PAFC).[103] PAFCs, with the operating temperatures in the range of 150–200 °C, are still mainly used for stationary and residential applications. PAFCs have not gained a widespread use in other fields, mainly because of their bulkiness and the problems related to the handling of hot, highly corrosive liquid phosphoric acid electrolyte. A much more viable solution is expected to come from PEMFCs where the phosphorus oxoacid is immobilized in the form of composites with polymeric matrices or chemically tethered (phosphonic acid) to the polymer backbone via spacers.[104–106] However, the main problem with most of these materials are the strong immobilization and/or chemical interaction effects on the proton conducting properties. The observed conductivities show dramatic decreases upon the reduction in the acid volume fraction.[29,31] In most of the cases, this cannot be explained by the simple excluded volume (geometric confinement) effects on the diffusion of protonic defects, indicating the presence of strong chemical interactions between the charge carrier species and the backbone. The most severe effects certainly come from the presence of basic species.[78,83] A short review of the two sample strategies for preparing phosphorus oxoacid based proton conducting electrolytes is given the following sections.

1.1.3.1 PBI/PA system

The idea of blending phosphoric acid with some basic polymers dates back to Lassegues.[107] Certainly the most relevant and best studied is a mixture with poly(benzimidazole) (PBI/PA).[29,31,108] The system features a strong hydrogen bonded complex between the benzimidazolinium cation and the dihydrogen phosphate anion. However, this system shows a dramatic drop in the conductivity values upon decreasing acid concentration (*doping level*). Moreover, a certain level of relative humidity has to be kept at higher temperatures to prevent the acid from condensing.[2] It is important to note that these observations cannot be explained simply by reducing the existing volume, which is not accessible to proton conduction, and indicate the presence of strong chemical interactions between the basic (benzimidazole) polymer backbone and phosphoric acid. It has been experimentally shown that structural diffusion is still responsible for the good protonic conductivity in these systems, indicating that the principal *mode* of the protonic transport does not change. Moreover PBI/PA shows quite low gas permeabilities and almost no water electro-osmotic drag, even at higher relative humidities.[2]

1.1.3.2 Phosphonated Polymers

The other strategy for using phosphorus oxoacids as a protogenic groups in real electrolytes, is to chemically bind them to the polymer backbone via the formation of direct P–C bond. Knowing the deficiencies of the PBI/PA system, in order to allow reasonable intrinsic protonic conductivities the main requirements for these materials are clear: the concentration of phosphonic acid groups must be as high as possible and their aggregation has to be as unconstrained as possible. Unfortunately, many of these materials such as poly(vynilphosphonic acid) (PVPA)[32,109] do not satisfy the principal goal. They only show reasonable proton conductivities in the presence of water and even this residual conductivity could be a result of intrinsic water due to the polycondensation of phosphonic acid groups.[32] However, for a hydration number of $\lambda([H_2O]/[R{-}PO_3H_2]) \approx 0.8$, a moderate conductivity ranging from ~10^{-4} S/cm at room temperature to ~10^{-2} S/cm at 100 °C was reported.[32] At the same time, the hydration number of $\lambda \approx 0.8$ can only be kept at a high water pressure (p_{H_2O} = 1 atm at 120 °C). Moreover, since this conductivity is very close to the conductivity of the ion exchanged K^+-form, it most likely stems from the mobility of hydronium (H_3O^+) ions.[32] The future prospects for this type of materials strongly rely on the advances in the fundamental understanding of the elementary processes governing the charge transport.

1.2 *Ab Initio* Molecular Dynamics

Many experimental techniques were widely applied to investigate the proton transfer and long-range transport in various media, among them dielectric spectroscopy, nuclear magnetic resonance, quasielastic neutron scattering, ultrafast infrared spectroscopy etc. Despite the fact that many of these techniques can bridge a wide range of length and time scales, only a handful can provide certain information with *molecular resolution*. At the atomic scale, the molecular modeling becomes indispensable. Molecular dynamics is one of the most widely used techniques to sample the phase space of a given system and provide the necessary information about the structure and dynamical processes within materials. The *traditional* way of doing molecular dynamics is by pre-determining the interaction potentials in advance. Normally, they are split up into contributions arising from 1,2. . . n-body interactions, long-range and short-range terms, etc..., which must be represented by well-defined analytical functional forms. However, the inherent chemical nature of the proton transfer reaction, where the bonds are broken and newly formed, renders the standard force field based molecular dynamics approaches of little use. A number of reactive force field schemes,[110,111] where some sort of prior knowledge about the process being studied is necessary in order to design a working scheme, have been proposed and proven to be successful for describing aqueous proton transfer processes.[12–17,112–114] Another way to overcome this limitation is to directly calculate the electronic structure of the system at each time step, calculate the forces on the atoms and propagate the dynamical equations of motion. Various flavors of these methods usually come under the name of *ab initio* molecular dynamics (AIMD). The main advantage of AIMD is that, in principle, no prior knowledge is necessary about the important configurations in order for the process to be simulated, and the approximation is shifted from the design of a suitable form of the potential to selecting a proper scheme for solving the Schrödinger equation.[115] which allows for the dynamical treatment of bond breaking and forming as well inclusion of polarization. Unfortunately, the lift of these limitations does not come at free cost – the time and length scales being sampled are significantly reduced. Therefore one has to be very careful about the statistical significance of the results coming from the AIMD simulations. Nevertheless, density functional theory (DFT)[116,117] coupled to molecular dynamics[118] was proven to be extremely successful for describing proton transfer and transport in diverse media: water,[9–11,18,19,49–51] methanol,[119,120] imidazole,[85–87] ammonia,[121,122] liquid HF,[123,124] solid proton conductors[125,126] and many others. To the best of our knowledge, the only AIMD simulation of H_3PO_4 was performed by Tsuchida.[73] Unfortunately, this work was not aimed at studying the proton transport mechanisms and the limited time scales involved were insufficient to properly sample long-range proton transfer events.

1.2.1 Density Functional Theory

In principle, *ab initio* molecular dynamics can be used in conjunction with any quantum mechanical method for computing electronic structure, which in turn will govern the quality of the AIMD results.[115] At the moment, the method of choice for the absolute majority of simulations is the Hohenberg–Kohn–Sham[116,117] density functional theory.[127–131] This formulation was exclusively used in this work as well. It still provides one of the best trade-offs in terms of computational cost and accuracy. The electronically 'uncomplicated' chemical bonds and their dynamics (absence of van der Waals forces (dispersion), excited states with charge transfer, complicated transition states, strong electron correlations) are usually well described within the standard framework of DFT.[115]

The basic idea behind the DFT, is the mapping of the original interacting electron system onto an auxiliary non-interacting one, having the same density. In this part, only the general aspects of density functional theory, directly related to the use of AIMD, are presented.

The total ground state energy of a system of electrons, interacting with classical nuclei at positions $\{R_I\}$, is variationally expressed as the minimum of the Kohn–Sham (KS) energy in the basis of single-particle orbitals $\{\phi_i\}$:

$$E_{tot} = \underset{\Psi_0}{min} \left\{ \langle \Psi_0 \left| \mathcal{H}_e \right| \Psi_0 \rangle \right\} = \underset{\{\phi_i\}}{min} \; E^{KS} \left[\{\phi_i\} \right]. \tag{1.1}$$

This introduces a substantial simplification, since the many-body wavefunction Ψ_0 is replaced by a set of orthonormal ($\langle \phi_i | \phi_j \rangle = \delta_{ij}$) single-particle KS orbitals. The KS energy then has a form:

$$E^{KS} \left[\{\phi_i\} \right] = T_S \left[\{\phi_i\} \right] + \int V_{ext}(\mathbf{r}) \; n(\mathbf{r}) \; d\mathbf{r} \; + \; \frac{1}{2} \int V_H(\mathbf{r}) \; n(\mathbf{r}) \; d\mathbf{r} \; + \; E_{XC} \left[n(\mathbf{r}) \right] \tag{1.2}$$

where the electronic density $n(\mathbf{r})$ is evaluated from a Slater determinant obtained by including the occupied orbitals (f_i are the integer occupation numbers):

$$n(\mathbf{r}) = \sum_{i}^{occupied} f_i \left| \phi_i(\mathbf{r}) \right|^2 \tag{1.3}$$

and the first term T_S is the electron kinetic energy term of a non-interacting system:

$$T_S\left[\{\phi_i\}\right] = \sum_{i}^{occupied} f_i \left\langle \phi_i \left| -\frac{1}{2}\nabla^2 \right| \phi_j \right\rangle \tag{1.4}$$

just experiencing the same external potential (V_{ext}) on the electron density as the fully interacting system. The external potential in which the electrons move, comprises the electron-nuclei and nuclei-nuclei Coulomb interaction terms:

$$V_{ext}(\mathbf{r}) = -\sum_{I} \frac{Z_I}{|\mathbf{R_I} - \mathbf{r}|} + \sum_{I<J} \frac{Z_I Z_J}{|\mathbf{R_I} - \mathbf{R_J}|}. \tag{1.5}$$

The third term in Eq. 1.2 is the classical electrostatic energy between the two electronic densities also known as the Hartree term. The Hartree potential is equal to:

$$V_H(\mathbf{r}) = \int \frac{n(\mathbf{r}')}{|\mathbf{r} - \mathbf{r}'|} d\mathbf{r}'. \tag{1.6}$$

which in turn is related to electronic density via Poisson's equation:

$$\nabla^2 V_H(\mathbf{r}) = -4\pi n(\mathbf{r}). \tag{1.7}$$

The last term (E_{XC}) in Eq. 1.2 is called the exchange-correlation functional, which is the difference between the exact and the KS Hamiltonian and comprises electronic exchange and correlation effects. The KS functional is minimized by self-consistently varying this functional with respect to the electronic density or orbitals (including the orthonormality constraint) leading to KS SCF equations:

$$\left\{ -\frac{1}{2}\nabla^2 + V_{ext}(\mathbf{r}) + V_H(\mathbf{r}) + \frac{\delta E_{XC}[n]}{\delta n(\mathbf{r})} \right\} \phi_i(\mathbf{r}) = \sum_j \Lambda_{ij} \phi_j(\mathbf{r}) \tag{1.8}$$

$$H^e_{KS} \phi_i(\mathbf{r}) = \sum_j \Lambda_{ij} \phi_j(\mathbf{r}) \tag{1.9}$$

where Λ_{ij} are the Lagrange multipliers for ensuring the orthonormality constraints. Although, these equations, only involve the effective *one-particle* Hamiltonian H_e^{KS}, they still include the *many-body* effects through the exchange-correlation (XC) potential:

$$\frac{\delta E_{XC}[n]}{\delta n(\mathbf{r})} = V_{XC}(\mathbf{r}) \tag{1.10}$$

The approximation for this unknown term is a crucial ingredient for any application of the DFT. The most popular flavor of exchange–correlation functionals, which were also exclusively used in this work, belong to the class of the *Generalized Gradient Approximation (GGA)* XC functionals. They are based on an assumption that the functional is an integral over a function, which is only depending on the density and its gradient at a given point in space:

$$E^{XC}_{GGA}[n] = \int n(\mathbf{r'})\varepsilon^{XC}_{GGA}\left(n(\mathbf{r'}), \nabla n(\mathbf{r'})\right) d\mathbf{r'} \tag{1.11}$$

This function is usually split into two terms: the exchange ε_X and the correlation ε_C. The simplest approximations to these comes from the exchange and correlation energy of an interacting homogeneous electron gas $\varepsilon^{LDA}_{XC}(n)$, which only depends on the *local* density $n(\mathbf{r})$ at space point r in the inhomogeneous system. This is known as the *Local Density Approximation (LDA)* and a number of different parameterizations for $\varepsilon^{LDA}_{XC}(n)$ exist in the literature. A significant improvement in the accuracy of DFT is introduced by including the gradient of the density (Eq. 1.11).

An even a more sophisticated type of approximation to the functionals proven to be very successful was the introduction of *hybrid functionals.*[132,133] In addition to the standard GGA terms, they include some of the Hartree–Fock or full *exact* exchange via a fixed mixing parameter. A significant improvement for many material properties such as: bond energies, lattice parameters, band-gaps etc. was reported for some systems. Liquid water has already been investigated using several of the hybrid functionals within AIMD.[134–136]

Even more complicated schemes for improving the GGAs already exist, for instance including the higher-order density gradients or the local kinetic energy density.[137] Unfortunately, most of the implementations are still too expensive to be applied in AIMD. The field of development of new parameterizations and concepts for DFT continues to be a very active area of research with new ideas constantly appearing in the community.[115]

1.2.2 Born-Oppenheimer Molecular Dynamics

The simplest approach to couple the electronic structure and molecular dynamics simulations is by straightforward solving of the static electronic structure problem at each time step with respect to the set of fixed nuclear positions at that instant of time.[115] In this way, the electronic structure part is reduced to solving a time-independent quantum problem and the nuclei are propagated according to Newtonian equation of motion (EOM) using the forces coming from the electronic structure calculation. Basically, the time dependence of the electronic structure is imposed through its parametric dependence on the classical motion of the nuclei. This approach, usually called Born–Oppenheimer molecular dynamics (BOMD), can be simply expressed in a form of a Newtonian EOM:[115]

$$M_I \ddot{\mathbf{R}}_I(t) = -\nabla_I \underset{\Psi_0}{min} \left\{ \langle \Psi_0 \left| \mathcal{H}_e \right| \Psi_0 \rangle \right\} \tag{1.12}$$

$$E_0 \Psi_0 = \mathcal{H}_e \Psi_0 \tag{1.13}$$

where the forces come directly from the solution of a stationary Schrödinger equation via the Hellmann-Feynman theorem.

In contrast to the inherently time-dependent schemes (e.g. Ehrenfest or Car-Parrinello),[115] in BOMD the wavefunction has to be optimized at each time step, for instance by diagonalizing the KS Hamiltonian. The corresponding constrained minimization (one-particle wave functions (orbitals) ϕ_i are orthonormal, i.e. $\langle \phi_i | \phi_j \rangle = \delta_{ij}$) of the total energy with respect to the orbitals is expressed by:

$$\underset{\{\phi_i\}}{min} \left\{ \langle \Psi_0 \left| \mathcal{H}_e \right| \Psi_e \rangle \right\} |_{\{\langle \phi_i | \phi_j \rangle = \delta_{ij}\}} \tag{1.14}$$

This can in turn be expressed by the following Lagrangian:

$$\mathcal{L} = -\langle \Psi_0 \left| \mathcal{H}_e \right| \Psi_0 \rangle + \sum_{i,j} \Lambda_{ij} \left(\langle \phi_i | \phi_j \rangle - \delta_{ij} \right) \tag{1.15}$$

where Λ_{ij} are the Lagrange multipliers, imposing the orthonormality constraint on the orbitals. Variation of the Lagrangian with respect to the orbitals leads to the BOMD EOMs, which within the Kohn–Sham DFT are:

$$M_I \ddot{\mathbf{R}}_I(t) = -\nabla_I \underset{\{\phi_i\}}{min} \left\{ \left\langle \Psi_0 \left| H_e^{KS} \right| \Psi_0 \right\rangle \right\} \tag{1.16}$$

$$0 = -H_e^{KS} \phi_i \ + \sum_j \Lambda_{ij} \phi_j \tag{1.17}$$

where the second equation is just the previously described KS equation with an effective one-particle KS Hamiltonian (H_e^{KS}). It is normally either directly diagonalized, or minimized using the nonlinear optimization techniques.[115]

1.2.3 Car-Parrinello Molecular Dynamics

An ingenuous solution, which revolutionized the field of AIMD was proposed by R. Car and M. Parrinello in 1985.[118] It substantially reduces the computational cost by avoiding the full wavefunction optimization at each time step. (In fact, nowadays, the best minimizers and new initialization and pre-conditioning schemes make BOMD as efficient as Car-Parrinello Molecular Dynamics (CPMD)). In general, the method includes the electrons as active dynamical degrees of freedom and combines the advantages of both: explicitly electronic time-dependent schemes (e.g. Ehrenfest) and those of BOMD.[115] In the latter approach, there is no explicit electron dynamics whatsoever and the electronic problem is treated within the time-independent Schrödinger equation. Therefore, the time step for integrating the EOM is nevertheless governed by the nuclear dynamics, whereas in Ehrenfest dynamics it must be much smaller in order to allow for the proper integration of the EOM of the much faster electronic dynamics. Basically, the ideal scheme should allow the integration of the EOM on the time scale dictated by the nuclear dynamics, but nevertheless effectively take the smooth time evolution of the dynamically evolving electronic subsystem into account.[115] The latter aspect allows one to circumvent the explicit diagonalization or minimization procedure to solve the electronic structure problem, before the molecular dynamics can be propagating to the next time step. The Car-Parrinello algorithm in principle combines these aspects in a very efficient fashion. The basic idea behind it, is to take advantage of the adiabatic separation between the nuclear and electronic dynamics, due to their intrinsically very different time scales. This can be achieved by transforming the quantum-mechanical dynamical system into a fictitious classical-mechanical one.[115] Certainly, this comes at the expense of loosing the correct time-dynamical information of the electronic dynamics, since the transformed system becomes purely classical. The forces on the nuclei can be obtained by differentiating the corresponding Lagrangian with respect to the nuclear positions. Moreover, one can already imply that the differentiation with respect to the orbitals could give the correct forces on the nuclei.[115] The Lagrangian proposed by Car and Parrinello can be expressed in the following form:

$$\mathcal{L}_{CP} = \sum_{I}^{N} \frac{1}{2} M_I \dot{R}_I^2 + \sum_{i}^{n} \frac{1}{2} \mu_i \left\langle \dot{\phi}_i | \dot{\phi}_i \right\rangle - \langle \Psi_0 | \mathcal{H}_e | \Psi_0 \rangle + \sum_{i,j} \left[\Lambda_{ij} \left(\langle \phi_i | \phi_j \rangle - \delta_{ij} \right) \right] . \tag{1.18}$$

A set of equations of motion for the electrons and nuclei can be obtained from this Lagrangian by applying the associated Euler-Lagrange equations:

$$M_I \ddot{\mathbf{R}}_I = -\nabla_I \langle \Psi_0 | \mathcal{H}_e | \Psi_0 \rangle \tag{1.19}$$

$$\mu \left| \ddot{\phi}_i \right\rangle = -\frac{\partial}{\partial \langle \phi_i |} \langle \Psi_0 | \mathcal{H}_e | \Psi_0 \rangle + \sum_j \Lambda_{ij} | \phi_j \rangle \tag{1.20}$$

where μ is one of the important parameters with no real quantum or classical analogue. It is known as fictitious mass and represents the inertial parameter assigned to the orbital degrees of freedom. In principle, the magnitude of this parameter decides the adiabatic separation between the electronic and nuclear subsystems. In Eq. 1.20, Λ_{ij} are the Lagrangian multipliers ensuring the orbital orthonormality.

From the EOMs, it comes out that the nuclei evolve in time at a certain physical temperature $\propto \sum_I M_I \dot{\mathbf{R}}_I^2$, and the electrons have some much *colder*, physical, fictitious temperature $\propto \sum_i \mu \langle \dot{\phi}_i | \dot{\phi}_i \rangle$. *Low electronic temperature* basically means that the electronic subsystem is close to its instantaneous energy minimum, i.e. close to the Born–Oppenheimer surface.[115] Therefore, if the electronic temperature is sufficiently low,the optimized wave function of the starting nuclear configuration must also stay close to the Born–Oppenheimer surface during the time evolution. The adiabatic decoupling of the two subsystems is only possible if the power spectra of the vibrational density of states for these systems do not overlap. This is the main reason why the original formulation of the Car-Parrinello algorithm had problems in dealing with metallic systems.

1.2.4 Evaluation of forces in AIMD

A key step in any molecular dynamics method is the calculation of forces acting on the nuclei. Generally this corresponds to a derivative:

$$\mathbf{F} = -\nabla_I \left\langle \Psi_0 \left| \mathcal{H}_e \right| \Psi_0 \right\rangle \tag{1.21}$$

which is analytically equal to:

$$\nabla_I \left\langle \Psi_0 \left| \mathcal{H}_e \right| \Psi_0 \right\rangle = \left\langle \Psi_0 \left| \nabla_I \mathcal{H}_e \right| \Psi_0 \right\rangle + \left\langle \nabla_I \Psi_0 \left| \mathcal{H}_e \right| \Psi_0 \right\rangle + \left\langle \Psi_0 \left| \mathcal{H}_e \right| \nabla_I \Psi_0 \right\rangle . \tag{1.22}$$

If the wave function is an exact eigenfunction of the Hamiltonian $\mathcal{H}_e$, then the above expression assumes the well-known Hellmann-Feynman form, which is valid for any variational wave function (under the assumption of a complete, non-atom centered basis set):

$$\mathbf{F}^{HFT} = - \left\langle \Psi_0 \left| \nabla_I \mathcal{H}_e \right| \Psi_0 \right\rangle . \tag{1.23}$$

If the basis functions explicitly depend on the atom positions and if the effective one-particle Hamiltonian is not perfectly self-consistent, two other sorts of forces are expected additionally to the Hellmann-Feynamn force:[115]

$$\mathbf{F} = \mathbf{F}^{HFT} + \mathbf{F}^{IBS} + \mathbf{F}^{NCS}. \tag{1.24}$$

The second term comes under various names: *incomplete basis set correction*, *wave function force* or *Pulay force*. It basically can be included through the gradients of basis functions with respect to the positions of atom centers. This force term is canceling out if one expands the wave functions in non-nuclei-centered basis functions such as plane waves. The third term is known as *non-self consistency correction* and represents the difference between the exact – fully self-consistent, and approximate – non-self-consistent Hamiltonians. The latter term is usually assumed to be vanishingly small, though this is never a case in numerical computations.[115]

Although, it is obvious that the Hellmann-Feynman theorem is of little use for numerical electronic structure calculations, it turns out that in the case of Car-Parrinello scheme using the plane wave basis, the resulting force can be assumed to be equal to the Hellmann-Feynman expression. This comes from the fact, that the non-self-consistency is counterbalanced by the finite non-zero and oscillating orbital acceleration term ($\mu\ddot{\phi}_i(t)$).

1.2.5 Basis Sets

At the core of any electronic structure method is the choice of functions for representing the orbitals ϕ_i and in turn the complete wave function. Generally, a linear combination of these functions will be used, which in the limit of complete set can represent any function:

$$\phi_i(\mathbf{r}) = \sum_\nu c_{i\nu} f_\nu(\mathbf{r}; \{\mathbf{R}_I\}). \tag{1.25}$$

In quantum chemistry and electronic structure calculations, the prevalent choices of the basis functions are: Slater ($\propto \exp(-\alpha|\mathbf{r}|)$), Gaussian ($\propto \exp(-\alpha r^2)$) and plane waves. In addition to these, a number of less widely distributed expansions have been efficiently implemented: numerical basis sets, discrete variable representations, wavelets, non-orthogonal generalized Wannier functions etc. In the following sections, the plane wave and Gaussian basis sets, mainly used in this work are discussed in more detail.

1.2.5.1 Plane Waves

The use of plane waves (PW) for describing electrons stems from solid state theory. The inherent periodicity of a lattice, results in a periodic potential, imposing the same periodicity on the wave functions and electronic density (Bloch's theorem). Therefore, plane waves come up as a natural expansion for the periodic orbitals:

$$\phi_{\mathbf{G}}^{PW}(\mathbf{r}) = 1/\sqrt{\Omega}\exp[i\mathbf{G}\mathbf{r}] \tag{1.26}$$

where Ω is the periodic cell volume and $\mathbf{G}$ is the reciprocal lattice vector. In principal, plane waves produce a complete and orthonormal set of basis functions and can be directly used in the Eq. 1.25, with the summation over ν replaced by the integral over the G-space. With these definitions the wave functions for the different eigenstates j can be expressed as:

$$\varphi_j^{(\mathbf{k})}(\mathbf{r}) = \exp[i\mathbf{k}\mathbf{r}]\sum_G C_{j\mathbf{k}}(\mathbf{G})\phi_{\mathbf{G}}(\mathbf{r}) \tag{1.27}$$

with $\mathbf{k}$ vectors in the phase factor, lying in the first Brillouin zone and the wave functions $\varphi_j^{(\mathbf{k})}$ corresponding to separate Schrödinger equations, but *interacting* among each other via the self-consistency procedure.

In principle, an infinite number of $\mathbf{G}$ vectors are needed in the PW expansion to represent the wave functions with perfect accuracy. However, the Fourier coefficients $C_{j\mathbf{k}}(\mathbf{G})$ decrease with increasing $|\mathbf{k}+\mathbf{G}|$, so that the expansion can be reasonably truncated at some energy cutoff E_{cut}:

$$\frac{\hbar^2}{2m}|\mathbf{k}+\mathbf{G}|^2 < E_{cut}. \tag{1.28}$$

For simulations of disordered/liquid systems investigated in this work an expansion around the Γ-point ($\mathbf{k} = 0$) usually suffices. Then, the expression in Eq. 1.28 defines a sphere of radius G_{cut} in the space of wave vectors:

$$|\mathbf{G}| < G_{cut} = \sqrt{\frac{2mE_{cut}}{\hbar^2}}. \tag{1.29}$$

As mentioned before, the advantages of plane waves include the fact that they are atom position independent, therefore canceling the Pulay forces and simplifying the force calculations – an essential step for AIMD. Secondly, they are not localized on any particular point in space, making them very suitable for systems with delocalized electrons. Moreover, the quality of a calculation can be improved through the increase of only one parameter – E_{cut}, allowing a systematic approach to the complete basis set limit. Lastly, there is a number of algorithmic advantages of PWs: the kinetic term in the one-particle Hamiltonian is diagonal in reciprocal space. Therefore, the calculations can be significantly speeded up, because the density and wave functions can be very efficiently transformed between real and reciprocal spaces through the use of Fast Fourier Transforms (FFT).

1.2.5.2 Gaussian and Plane Waves Approach

Unfortunately, there cannot be only advantages of the PWs compared to the other types of basis sets. First of all, the true wave functions of the core states have strong and rapid oscillations close to the nuclei, meaning that increasingly large Fourier components are necessary to resolve these features in real space. This is why the pseudopotential approximation is inherent to the PW approaches. The strongly varying core electronic states must be represented by smooth and nodeless effective potentials (pseudopotentials). The second drawback of the PWs is mostly relevant for heterogenous systems or interfaces. The fact that PWs are unbiased functions and makes no way to increase their number in regions which are more chemically relevant or to reduce their number in the regions with vacuum or lighter atoms.

The advantages of localized basis functions, for which Gaussian-type orbitals are the most popular in the electronic structure theory, are: they much more naturally representing the electrons in atoms and molecules, the increase in their number rapidly improves the accuracy of a calculation in a systematic way, still maintaining the compact description of the wavefunctions. The latter allows for an efficient solution of SCF equations and utilization of sparsity of the Kohn-Sham and overlap matrices for systems with increasing sizes.

The method, which aims at taking the best of both worlds, is implemented in the `CP2K` package and is known as the Gaussian-plane wave (GPW) approach.[138–140] The scheme employs Gaussian-type basis to describe the wave functions and, in addition, an auxiliary plane wave basis to represent the density. With density expanded in PWs, the efficiency of FFTs can be exploited to solve the Poisson equation and to obtain the electrostatic Hartree energy in a time that scales linearly with the system size.

The first representation of the density in the GPW is expanded in atom-centered, contracted Gaussian functions:

$$n(\mathbf{r}) = \sum_{\mu\nu} P^{\mu\nu} \varphi_\mu(\mathbf{r}) \varphi_\nu(\mathbf{r}) \tag{1.30}$$

where P is the density matrix and $\varphi_\mu(\mathbf{r}) = \sum_i d_{i\mu} g_i(\mathbf{r})$, $g_i(\mathbf{r})$ are primitive Gaussians. The second form for the density involves the expansion in PWs:

$$\tilde{n}(\mathbf{r}) = 1/\Omega \sum_{\mathbf{G}} \tilde{n}(\mathbf{G}) \exp[i\mathbf{G} \cdot \mathbf{r}] \tag{1.31}$$

With this, the Kohn–Sham energy functional is expressed as follows:

$$\begin{aligned} E^{KS}\left[n(\mathbf{r})\right] = \sum_{\nu\mu} P^{\mu\nu} \left\langle \varphi_\mu(\mathbf{r}) \left| -\frac{1}{2}\nabla^2 \right| \varphi_\mu(\mathbf{r}) \right\rangle \ + \\ + \ \sum_{\nu\mu} P^{\mu\nu} \left\langle \varphi_\mu(\mathbf{r}) \left| V_{loc}^{PP}(r) \right| \varphi_\mu(\mathbf{r}) \right\rangle \ + \\ + \ \sum_{\nu\mu} P^{\mu\nu} \left\langle \varphi_\mu(\mathbf{r}) \left| V_{nl}^{PP}(\mathbf{r}, \mathbf{r}') \right| \varphi_\mu(\mathbf{r}) \right\rangle \ + \ 2\pi\Omega \sum_{\mathbf{G}} \frac{\tilde{n}'(\mathbf{G})\tilde{n}(\mathbf{G})}{\mathbf{G}^2} \ + \\ + \ \int \tilde{n}(\mathbf{r}) \varepsilon_{GGA}^{XC}\left(\tilde{n}(\mathbf{r}), \nabla\tilde{n}(\mathbf{r})\right) d\mathbf{r} \ + \ \frac{1}{2} \sum_{I \neq J} \frac{Z_I Z_J}{|\mathbf{R}_I - \mathbf{R}_J|} \end{aligned} \tag{1.32}$$

where the first term is the kinetic energy, the second and the third describe the interaction of the valence electrons with the nuclei via an effective potential (local and non-local parts), the fourth is the Hartree electrostatic term, the fifth is the exchange-correlation functional and the last one represents the interaction between the nuclei.

1.2.6 Pseudopotentials

The replacement of chemically inert core electrons is common in all kinds of electronic structure calculations and provides a very intuitive and reasonable approximation to describe chemical bonds and reactions. As mentioned before, the use of pseudopotentials (PP) is deeply-rooted into the plane wave approach, where only smooth, nodeless functions can be properly represented on the real space grids. The core states are usually treated using angular momentum dependent PPs, where the true potential and valence orbitals outside a chosen core region coincide, but the inner part remains much smoother, and the nuclei represented as rigid non-polarizable cores. Normally, the core electronic states are weakly dependent on the chemical environment of a particular atom. Nevertheless, the PPs are usually built and optimized to be transferable from one chemical state to another. It is important to note that PPs not only reduce the number of electrons and make the real space representation of the true wavefunctions possible, but can also very effectively account for relativistic effects within the core electrons, among other things.

1.2.6.1 Norm-conserving Pseudopotentials

One of the most wide-spread types of PPs for the use within the plane wave calculations, are the norm-conserving pseudopotentials. They were mostly used in this work as well. One of the ways for constructing the norm-conserving PPs is based on the rules proposed by Hamann, Schlüter and Chiang (HSC):[141]

- The eigenvalues of a particular atomic configuration between the pseudo-wavefunction (Ψ_l) and all-electron reference wavefunction (Φ_l) should agree:

$$\epsilon_l = \tilde{\epsilon}_l \tag{1.33}$$

- The pseudo- and all-electron wavefunctions should agree beyond the core radius:

$$\Psi_l(r) = \Phi_l(r), for\ r \geq r_c \tag{1.34}$$

- The norms of the all-electron and pseudo wavefunctions should agree in the core region (norm-conservation condition):

$$\langle\Phi_l|\Phi_l\rangle_R = \langle\Psi_l|\Psi_l\rangle_R\,, for\ R \leq r_c \tag{1.35}$$

- The logarithmic derivatives of the all-electron and pseudo wavefunctions should agree for $r \geq r_c$.

In addition to these rules, HSC also proposed a recipe for generating PPs with the above defined properties. The all-electron atomic potential is initially multiplied by a smoothing short-range cutoff function, which removes the strongly attractive and varying part of the potential. Then this function is numerically parametrized to produce eigenvalues equal to the valence levels and the eigenfunctions identical to the real valence functions beyond the cutoff radius. Finally, the charge inside the core region is forced to be equal to the actual charge in that region for a particular ion.

The type of PPs used in this work within the `CPMD` scheme were of Troullier-Martins type, where the wave function in the core region has the form:

$$\Phi_l(r) = r^{l+1}\exp[p(r)] \tag{1.36}$$

where

$$p(r) = c_0 + c_2r^2 + c_4r^4 + c_6r^6 + c_8r^8 + c_{10}r^{10} + c_{12}r^{12}. \tag{1.37}$$

Basically, it suggests that the asymptotic behavior of the pseudo wave functions can be improved by setting all the odd coefficients in the polynomial Eq. 1.37 to zero, (in fact neglecting all the odd derivatives at the origin). Furthermore, usually the potentials are forced to be flat (zero-curvature) at the origin.

1.2.6.2 Separable Dual–space Gaussian Pseudopotentials

The PP scheme implemented in the `CP2K` package is that of Goedecker, Teter and Hutter.[142] They introduced a way to optimize a small set of parameters for the local and nonlocal parts of the PP that fulfills the HSC conditions and leads to highly transferable PPs. The local part has an analytical form:

$$V^{loc}(r) = \frac{-Z_{ion}}{r}\text{erf}\left[\frac{\bar{r}}{\sqrt{2}}\right] + \exp\left[-\frac{1}{2}\bar{r}^2\right]\left[c_1 + c_2\bar{r}^2 + c_3\bar{r}^4 + c_4\bar{r}^6\right] \tag{1.38}$$

where Z_{ion} is the ion charge, $\bar{r} = r/r_{loc}$, and erf is an error function. The nonlocal part takes the following form:

$$V^{nl}(\mathbf{r}, \mathbf{r}') = \sum_{i=1}^{3}\sum_{j=1}^{3}\sum_{m=-l}^{l} Y_{lm}(\omega)p_i^l(r)h_{ij}^l p_j^l(r)Y_{lm}^*(\omega') \tag{1.39}$$

where Y_{lm} are the spherical harmonics and $p_i^l(r)$ the normalized radial Gaussian projectors. The projectors are just the products of a Gaussian and a polynomial. These PPs have an analytical form in the Fourier space and offer an optimal compromise between the good convergence properties in real and Fourier spaces.

1.2.7 Beyond Microcanonics: Thermostatting

Microcanonical or *NVE* ensemble is the *natural* ensemble of molecular dynamics. For this reason, a fixed temperature, vital for any comparison of the AIMD results to experimental data, is not a conserved quantity in the Newtonian molecular dynamics. Among the number of approaches to control the kinetic energy (temperature) of the particles in MD, an approach, based on the *deterministic* extended systems dynamics by imposing a dynamical friction, is the most widely spread in the AIMD community. However, this technique, usually based on the Nosé-Hoover equations, suffers from the non-ergodicity problems for certain types of Hamiltonians (e.g. harmonic oscillator). The deficiencies of the original formulation were cured by the introduction of Nosé-Hoover chain (NHC) thermostats by Martyna et al., which is achieved by coupling one Nosé-Hoover thermostat to another one and so on.[143,144] Moreover, the use of Car-Parrinello method usually requires the thermostatting of the fictitious electron system as well. This can be efficiently done using the same approach. For the case of canonical CPMD, the conserved constant of motion (energy) can be expressed as:

$$E^{NVT}_{cons} = \sum_i^n \mu \left\langle \dot{\phi}_i \middle| \dot{\phi}_i \right\rangle + \sum_I \frac{1}{2} M_I \dot{\mathbf{R}}_I^2 + E^{KS}[\{\phi_i\}, \{\mathbf{R}_I\}] +$$
$$+ \sum_{l=1}^{L} \frac{1}{2} Q^e_l \dot{\eta}_l^2 + \sum_{l=2}^{L} \frac{\eta_l}{\beta_e} + 2T^0_e \eta_1 + \sum_{k=1}^{K} \frac{1}{2} Q^n_k \dot{\xi}_k^2 + \sum_{k=2}^{K} k_b T \xi_k + g k_b T \xi_1 \qquad (1.40)$$

where Q are the inertial parameters or *masses* of the thermostat, K and L are the lengths of thermostats for the nuclear and electronic degrees of freedom, respectively, ξ and η are the dynamical friction coefficients, which damp or accelerate the nuclei or electrons and thus cool or heat the system if the instantaneous kinetic energies are higher than target temperatures (T and T_e, with $\beta_e = 1/k_b T_e$,) and g is the number of dynamical degrees of freedom.

It has been proven that the Nosé-Hoover chains are able to produce correct canonical ensemble and conserve the total energy, despite in fact, being non-Hamiltonian. For most of the cases, as well as for this work, it is very beneficial to couple a chain of thermostats for each degree of freedom, which usually improves the expensive equilibration in the AIMD.[144]

1.2.8 Equilibrium Time Correlation Functions

The big advantage of molecular simulations is their ability to yield thermodynamic quantities, which are directly related to experimental observables. Besides, simple averages such as radial pair distribution functions, many experimental quantities can be only accessed from the time-correlation functions and their Fourier transforms. In this section, some of the properties and the way to evaluate the equilibrium time-correlation functions are reviewed.[145]

In molecular dynamics, not only coordinates but also velocities, corresponding to the desired equilibrium distribution, are generated and can be retained for subsequent calculation of the time correlation functions. Assuming an adequate sampling of the phase space probability distribution, each of the configurations obtained can be used as an initial condition for performing the averaging. This is particularly important for the applications of AIMD, since the available statistics is very limited due to the high computational cost. Therefore, the important quantities usually have to be evaluated from a single trajectory. In principle, the equivalence of time and phase space averages (ergodic condition) have to be assumed:[145]

$$C_{AB}(\tau) = \int \mathrm{dx}\ f_0(\mathcal{H}(\mathrm{x}))\ a(\mathrm{x})\ b(\mathrm{x}_r(\mathrm{x})) = \lim_{\mathcal{T}\to\infty} \frac{1}{\mathcal{T}} \int_0^{\mathcal{T}} dt\ a(\mathrm{x}_t)\ b(\mathrm{x}_{t+\tau}) \qquad (1.41)$$

where $C_{AB}(t)$ is an equilibrium time-correlation function, $f_0(\mathcal{H}(\mathrm{x}))$ is a phase space probability distribution function and x_t is a phase space vector (which contains positions and velocities). Seemingly the Eq. 1.41 contains a contradiction: it implies that each configuration, generated by solving Hamiltonian EOM is an independent sample of the phase space, however at the same time it assumes that any point $\mathrm{x}_{t+\tau}$ in the trajectory can be uniquely determined from any other point in it – x_t. This paradox can be resolved by the existence of a finite correlation time, over which the time-correlation function decays to zero, and which is much smaller that the total length of the trajectory $\mathcal{T}$.[145]

Let's assume that an MD trajectory consists of M points: $\mathrm{x}_{n\Delta t}(n = 1, \ldots, M)$. Then, it is possible to split the trajectory into segments each having K points ($K \ll M$ and $K\Delta t$ is approximately the correlation time). By segmenting the trajectory in as many ways as possible, each point in the trajectory serves both: as an independent sampling of $f_0(\mathcal{H}(\mathrm{x}))$, and as a point in the time correlation function. For a finite trajectory composed of discrete points the average can be expressed as:

$$C_{AB}(n\Delta t) = \frac{1}{M-n} \sum_{m=1}^{M-n} a(\mathrm{x}_{m\Delta t})\ b(\mathrm{x}_{(m+n)\Delta t}),\ \ n = 1, \ldots, K. \qquad (1.42)$$

2

Aims of the project

The main goal of this project is the fundamental study of molecular proton transport mechanisms in a family of phosphorus oxoacids and some closely related systems with the help of *ab initio* molecular dynamics simulations. Proton transport in this class of materials is of extreme relevance to many fields of science; chemistry (fundamental understanding of the limits of proton transport; the relation between strong bonding, disorder and charge transport), engineering (proton conducting electrolytes for fuel cells) and biophysics (proton transport at the phospholipid membrane and aqueous interfaces). Phosphoric acid is the central system of this study and all the other systems investigated in this work, in principle, represent a number of possible *perturbations* to its proton conducting properties. All of the studied systems were systematically treated at the same level of theory. The work is structured into the following chapters with respect to the system being addressed:

1. Investigation of the elementary proton transfer reactions and local dynamics in neat, liquid phosphoric acid. The key questions to be asked are: (1) How many molecules are involved in the elementary reaction steps? (2) What are the relevant time scales and energy barriers governing these reactions? (3) What are the solvent effects on the proton dynamics? (4) What is the range of this coupling? (5) How are these processes related to the long-range proton transport in phosphoric acid? (6) What do they imply for the development of new proton conducting materials with technological

applications?

2. Comparison of the important aspects of proton transport mechanism in phosphoric acid to those in phosphonic and phosphinic acid. The central questions addressed are: how does the (1) Hydrogen bond network topology (dimensionality), (2) Dynamical background and (3) Dielectric properties affect the elementary proton transport processes and (4) What are the fundamental similarities and differences in the transport mechanisms?

3. Analysis of the role played by water in the proton conduction of phosphoric acid: (1) Why is it the only *dopant*, which does not destroy the proton conducting properties? (2) Does the excess water simply accelerate the intrinsic proton conduction process or the entire mechanism changes? (3) How do the local interactions and (4) The dynamics of hydrogen bonds change under the presence of water molecules. (5) How do these properties depend on the water's concentration?

3

Computational methods and setup

The proton dynamics and mobility in phosphoric, phosphonic and phosphinic acids and phosphoric acid in mixtures with water are studied within the framework of *ab initio* molecular dynamics simulations. The system of highest interest, liquid phosphoric acid, is studied using two different methodologies in order to prove the consistency of results among different computational schemes. In all cases, cubic simulation boxes with the periodic boundary conditions are used. Boxes containing 54 molecules and having dimensions of L = 16.738 Å, 16.452 Å and 15.826 Å were respectively used for the simulation of phosphoric, phosphonic and phosphinic acids. These setups correspond to the experimental densities just above the melting point ($\rho(H_3PO_4)$=1.885 g/cm^3; $\rho(H_3PO_3)$=1.651 g/cm^3; $\rho(H_3PO_2)$=1.493 g/cm^3). Phosphoric acid-water systems with two very different ratios are studied. The first one has 50 H_3PO_4 molecules and 4 condensed H_3PO_4 molecules (2 $H_4P_2O_7$ + 2 H_2O). This setup corresponds to the experimental composition of the nominally dry phosphoric acid in thermodynamic equilibrium.[67] The second one has 36 H_3PO_4 molecules and 36 H_2O molecules, which corresponds to the 1:1 molar ratio or 85 wt.% phosphoric acid solution (typical electrolyte concentration for the PAFCs). All except the additional simulation of pure phosphoric acid, employed the Car-Parrinello *ab initio* molecular dynamics (CPMD)[118] scheme as implemented in the `CPMD` code.[146] A plane wave (PW) expansion within the Kohn–Sham formulation of Density Functional Theory[116,117] was used to represent the electronic structure. The KS orbitals were expanded at the Γ-point up to a PW kinetic energy cut-off of 100 Ry. A well known and meticulously tested generalized gradient approximation (GGA) exchange-correlation functional of Becke-Lee-Yang-Parr (BLYP)[147,148] was used in all CPMD simulations. Norm-conserving Troullier-Martins[149] pseudopotentials were used to treat the core electronic states. The fictitious electron mass was set to $\mu = 500$ a.u and the masses of deuterium were assigned to the hydrogen atoms in order to increase the adiabatic decoupling of nuclear and electronic dynamics and allow for a larger time step (4 a.u. ≈ 0.1 fs) for integrating the equations of motion (EOM). This simulation is referred as PW-BLYP in this work. In the second simulation of phosphoric acid, the methodology available in the `CP2K` code was used.[140,150] `CP2K` is based on the Born-Oppenheimer Molecular Dynamics scheme (BOMD)[115] and uses a mixed plane wave and gaussian-type atomic orbital basis set for representing the KS orbitals. The kinetic energy cut-off for the expansion of the electronic density was taken at 280 Ry and an optimized TZV2P basis set,[151] known to give reliable results for a set of different molecular systems was utilized to expand the orbitals. The self-consistent field convergence for the energy minimization at each BOMD time step was set to 10^{-6} Ha. In order to check the performance of different functionals, another popular GGA exchange-correlation functional, namely that of Perdew, Burke and Enzernhof (PBE) was selected.[152] The atomic cores were represented by the separable dual-space Goedecker-Teter-Hutter pseudopotentials.[142,153] In this simulation, the time step was set to 0.5 fs, and the true proton mass (1.0 a.u.) was used. In this work, the latter simulation is referred as GPW-PBE. The use of ^{2}H for PW-BLYP and ^{1}H for GPW-PBE allows for direct comparison to experiment on both deuterated and non-deuterated systems. Both simulations employed the same molecular dynamics protocol. The initial coordinates were first pre-equilibrated with the help of classical molecular dynamics.[154] Next, a 10 ps equilibration with AIMD in a canonical (NVT) ensemble using massive Nosé-Hoover chain thermostatting was undertaken.[143,144] The target kinetic temperatures for the equilibration were set to 383 K. Despite the fact that all the simulated systems have different phase diagrams, the same kinetic temperature was used in order to allow for better further comparison. In all cases, the kinetic temperatures of the simulations are well above the respective melting points. This also slightly speeds up the proton dynamics and avoids the formation of glassy states but does not change the physical mechanism. Subsequently, the thermostats were switched off and the systems were allowed to evolve in a microcanonical ensemble (NVE) at an average kinetic temperature of 383K. The positions and velocities of all the particles were stored at 1 fs intervals. All the simulations were performed on the *VIP* (IBM Power6) machine at the Rechenzentrum Garching der Max-Planck-Gesellschaft and the local departmental cluster of Intel Xeon nodes equipped with an Infiniband interconnect. The codes were parallelized using Message Passing Interface (MPI) and gave very favorable scalings up to hundreds of CPUs. Most of the molecular visualizations were accomplished with the help of the VMD package[155] all the data post-processing and calculation of correlation functions were performed with the home-written scripts.

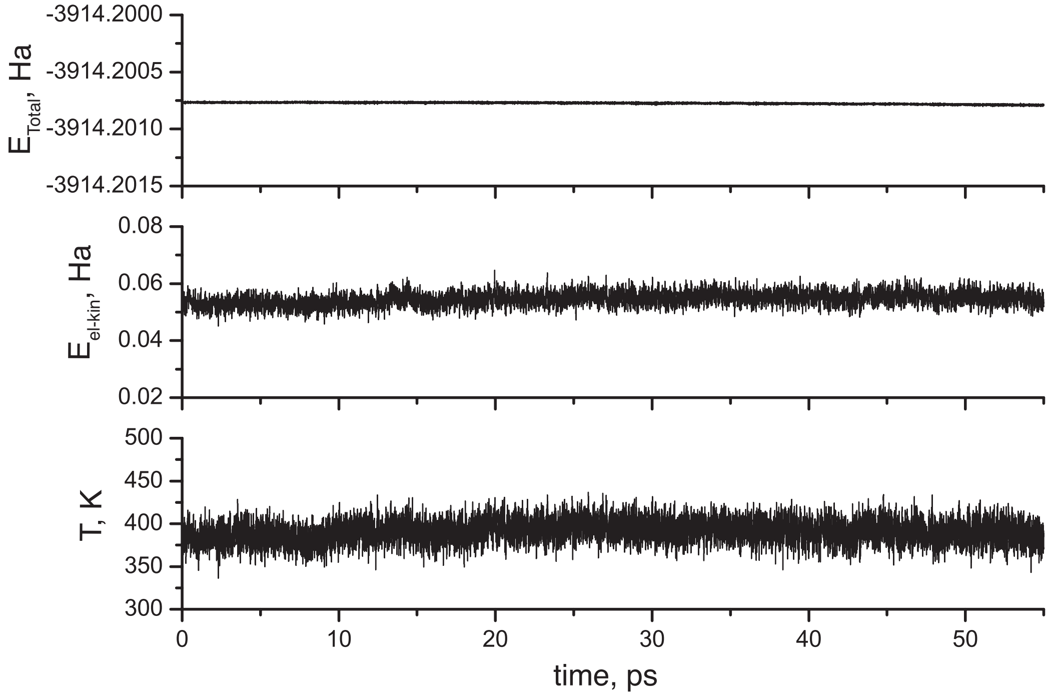

Figure 3.1: Variation of the total energy (conserved quantity), electronic kinetic energy (Car-Parrinello) and temperature (classical kinetic energy of the nuclei) during the `CPMD` simulation.

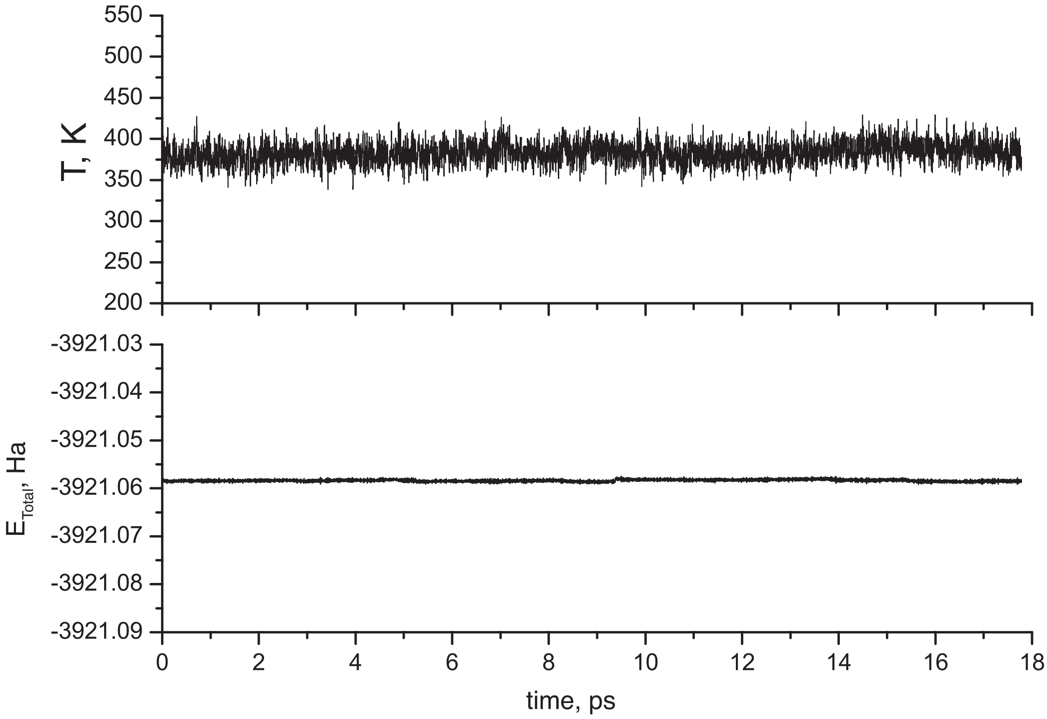

Figure 3.2: Variation of the total energy (conserved quantity) and temperature (clasical energy of the nuclei) during the `CP2K` simulation.

4

Phosphoric acid

In this chapter the results of the AIMD simulation on neat phosphoric acid are presented. Two production runs of 25 ps (GPW-PBE) and 55 ps (PW-BLYP) were obtained. The directly accessible properties such as structure or diffusivities are compared to the available experimental data. This comparison helps to benchmark the general quality of the simulations. Afterwards the attention is turned towards the discussion of the proton transport mechanism, where important concepts of Grotthuss chains in bulk polar protic medium and the solvent reorganization facilitated by the H-bond network frustration are introduced. A snapshot of a typical configuration from the simulation box is shown in Fig. 4.1.

4.1 Structural Properties

The quality of the simulations can be directly checked through the evaluation of Radial Pair Distribution Functions (RDF) (Fig. 4.2), and their straightforward comparison to neutron scattering results. The neutron diffraction study by Tromp et al. on the deuterated samples of the nominally dry H_3PO_4 provided the structure of liquid phosphoric acid at two temperatures (25 °C and 60 °C).[156] The results showed that the structure of H_3PO_4 does not significantly depend on temperature, even between the glassy supercooled (at 25 °C) and the normal liquid (at 60 °C) states. Hence, it is still appropriate to compare the experimental and simulated data sets even if the kinetic temperature in the simulation

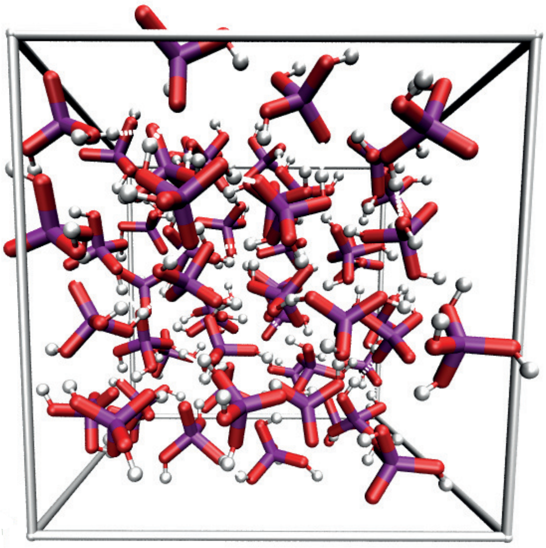

Figure 4.1: A snapshot of a typical configuration from an equilibrated simulation box containing 54 H_3PO_4 molecules.

is higher (∼110 °C). The data in Fig. 4.2 show the RDFs for different pairs of atoms without discriminating for the type of heavy atom, using the same procedure as in the experimental study:[156] $g_{HX}(r) = 0.823g_{HO}(r) + 0.182g_{HP}(r)$ and $g_{XX}(r) = 0.673g_{OO}(r) + 0.298g_{OP}(r) + 0.033g_{PP}(r)$. The simulations show reasonably good agreement with experiment. Surprisingly, different simulations give virtually identical results, despite the use of different functionals, basis sets, and propagation schemes. This indicates that the main source of discrepancy between the experiment and the simulation is likely due to the general deficiencies of the GGA and complete neglect of nuclear quantum effects. The latter is most likely the reason for the slight disagreement between the experimental and simulated g_{HH} (Fig. 4.2 (top)), which nevertheless is still generally in accord with the neutron scattering data. Nuclear quantum effects also likely influence g_{HX} (Fig. 4.2 (middle); X=P,O) as well, where the very pronounced sharpness of the first peak (covalent O–H bond) is a result of the purely classical treatment of the nuclei. Nevertheless, the hydrogen bond (the second peak in Fig. 4.2 (middle)), which is key for our study, is quite well described by both functionals: PBE slightly overestimates the hydrogen bond strength ($r_{H\cdots O}(PBE) \approx 1.54$ Å) and BLYP gives almost the exact experimental value ($r_{H\cdots O}(BLYP) \approx 1.58$ Å vs. $r_{H\cdots O}(exp) \approx$

1.59 Å). The third peak in g_{HX} (intramolecular P–H correlation) shows a correct bonding strength but is slightly overstructured compared to experiment. As one can see from the heavy atom RDFs (Fig. 4.2 (bottom)), all the peaks are relatively sharp, indicating a very rigid structure with strong, almost linear hydrogen bonds: $r_{\mathrm{O\cdots H}} + r_{\mathrm{H-O}} = 2.58$ Å vs. $r_{\mathrm{O\cdots O}} = 2.54$ Å (Fig. 5.4). For the latter, the real equilibrated samples of nominally dry H_3PO_4 always contain intrinsic water along with the condensates, which is not present in this setup. Despite these small inconsistencies, the results show that the DFT model used here can correctly describe the structure of such a tight and complex three-dimensional hydrogen bond network as bulk phosphoric acid.

4.2 Dynamical Properties

Given the structure of H_3PO_4, the next step is the elucidation of the dynamical properties. Diffusion constants are among the most important quantities easily accessible from the molecular dynamics trajectories. They are usually obtained from the linear regime of the mean square displacement (MSD) dependence over time, via the Einstein relation. Expressed as an ensemble average, it has the following form:

$$D_{\mathrm{self}} = \frac{1}{6} \lim_{t\to\infty} \frac{d}{dt} \left\langle \frac{1}{N} \sum_{i=1}^{N} |\mathbf{r}(t) - \mathbf{r}(0)|^2 \right\rangle . \tag{4.1}$$

The proton and phosphorus diffusion coefficients thus obtained can be directly compared to the PFG-NMR results. As indicated in Fig. 4.3, the PW-BLYP calculated proton diffusion constant ($D^{\mathrm{2H}}_{\mathrm{PW-BLYP}} = 4.03 \cdot 10^{-6}$ cm^2/s) is in very good agreement with the experimental value ($D^{\mathrm{2H}}_{\mathrm{exp}}$ (383 K) $= 5.4 \cdot 10^{-6}$ cm^2/s), despite very limited statistics. The GPW-PBE value shows slightly worse agreement ($D^{\mathrm{1H}}_{\mathrm{GPW-PBE}} = 2.5 \cdot 10^{-6}$ cm^2/s vs. $D^{\mathrm{1H}}_{\mathrm{exp}}$ (383 K) $= 5.08 \cdot 10^{-6}$ cm^2/s). A similar trend is observed when comparing the phosphorus diffusion coefficients: PW-BLYP shows better agreement with experiment ($D^{\mathrm{P}}_{\mathrm{PW-BLYP}} = 0.751 \cdot 10^{-6}$ cm^2/s vs. $D^{\mathrm{P}}_{\mathrm{exp}}$ (383 K) $= 1.15 \cdot 10^{-6}$ cm^2/s) than the respective GPW-PBE simulation ($D^{\mathrm{P}}_{\mathrm{GPW-PBE}} = 0.594 \cdot 10^{-6}$ cm^2/s). In any case, it is clear that AIMD simulations are capable of giving a quantitative agreement with the PFG-NMR

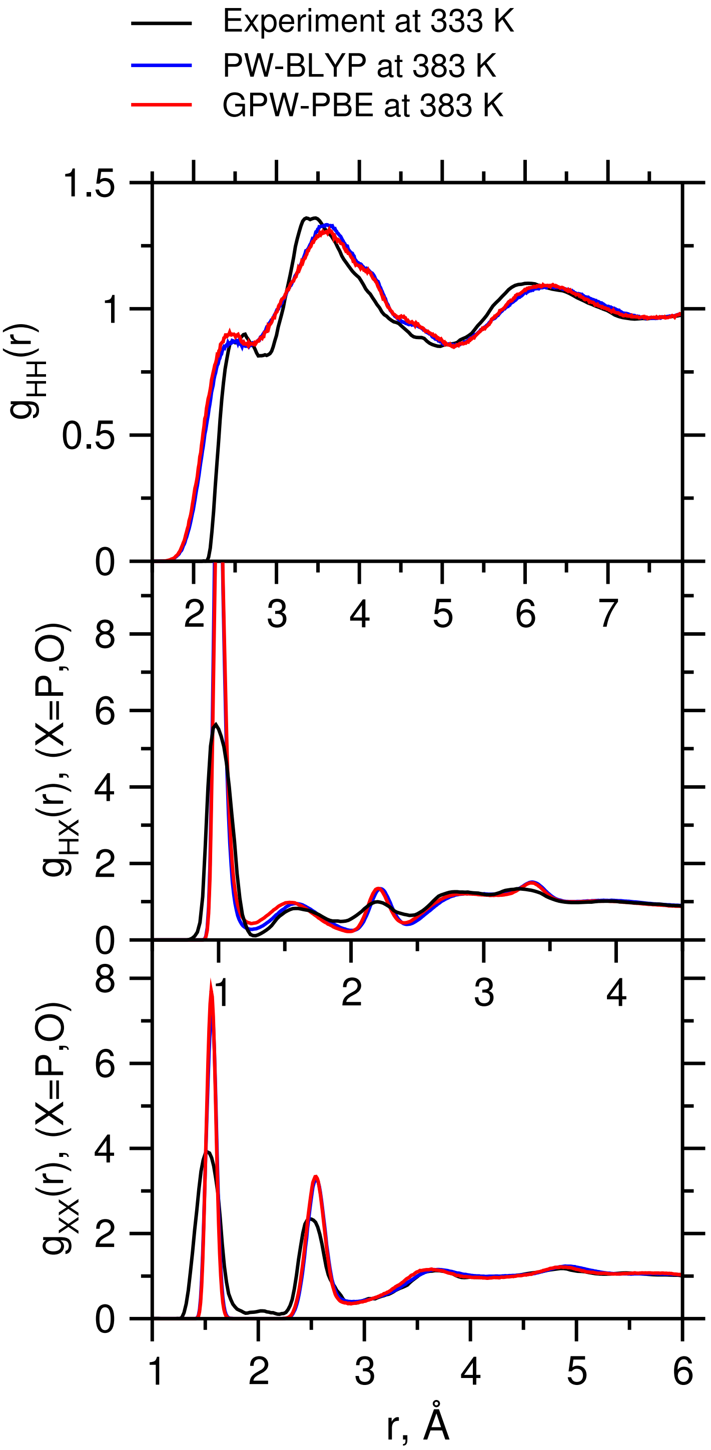

Figure 4.2: Radial pair distribution functions of liquid phosphoric acid. The results of two simulations are compared to the neutron scattering study.[156] The g_{HX} and g_{XX} are defined in the same way as in the experimental work: ($g_{HX}(r) = 0.823g_{HO}(r) + 0.182g_{HP}(r)$; $g_{XX}(r) = 0.673g_{OO}(r) + 0.298g_{OP}(r) + 0.033g_{PP}(r)$).

and, more importantly, reproducing the experimental $D^{\mathrm{H}}/D^{\mathrm{P}}$ ratio ($D^{\mathrm{H}}_{\mathrm{exp}}/D^{\mathrm{P}}_{\mathrm{exp}}$ ≈ 4.4 vs. $D^{\mathrm{^2H}}_{\mathrm{PW-BLYP}}/D^{\mathrm{P}}_{\mathrm{PW-BLYP}} \approx 5.4$ vs. $D^{\mathrm{^1H}}_{\mathrm{GPW-PBE}}/D^{\mathrm{P}}_{\mathrm{GPW-PBE}} \approx 4.2$). It is important to note that at $T = 383$ K, $D^{\mathrm{^1H}}_{\mathrm{exp}}/D^{\mathrm{^2H}}_{\mathrm{exp}} \approx 1.2$ suggesting that nuclear quantum effects on diffusion are likely rather small.

It is important to note that the calculated diffusion constants are also smaller due to finite size effects, and the application of the available hydrodynamic corrections could certainly improve them.[157,158] The most important contribution to the corrected diffusion coefficient of a periodic system is inversely proportional to the length of the simulation box (the other terms are usually small):[158]

$$D_0 = D_{PBC} + \frac{k_b T \xi}{6\pi\eta L} \tag{4.2}$$

where D_0 is the diffusion coefficient in the limit of an infinite system's size, D_{PBC} is the diffusion coefficient for a periodic system, η is the viscosity, for a cubic simulation box L is its length, and $\xi = 2.837$ is a constant. Although no shear viscosities are available from the BLYP or PBE simulations of phosphoric acid, instead one can take experimental viscosities ($\eta^{383K}_{\mathrm{H_3PO_4}} \approx 0.02\ Pa \cdot s$). This approach gives $D^{\mathrm{P}}_{\mathrm{PW-BLYP,PBC}} = 0.988 \cdot 10^{-6}$ cm^2/s and $D^{\mathrm{P}}_{\mathrm{GPW-PBE,PBC}} = 0.831 \cdot 10^{-6}$ cm^2/s, which are obviously closer to the PFG-NMR value of $D^{\mathrm{P}}_{\mathrm{exp}}$ (383 K) $= 1.15 \cdot 10^{-6}$ cm^2/s.

At this point, it is important to mention that PFG-NMR measures, in principle, the long-range particle diffusion, which is certainly beyond the range currently achievable by AIMD. However, the surprisingly good agreement for absolute values and their ratios suggests that the simulations capture the most important features as well as the correct picture of proton structural diffusion in phosphoric acid. A thorough analysis of the trajectories shows a significant number of diffusive proton transfer events in which an individual proton exchanges at least three nearest neighboring oxygens, as well as several events in which an individual proton migrates over four and five oxygens. The analysis of these events should allow the extraction of the important details of the elementary proton transfer reaction and solvent reorientation mechanism responsible for the protonic conductivity. Furthermore, since both computational schemes give virtually identical structure and diffusion coefficients, the results obtained from the longer PW-BLYP simu-

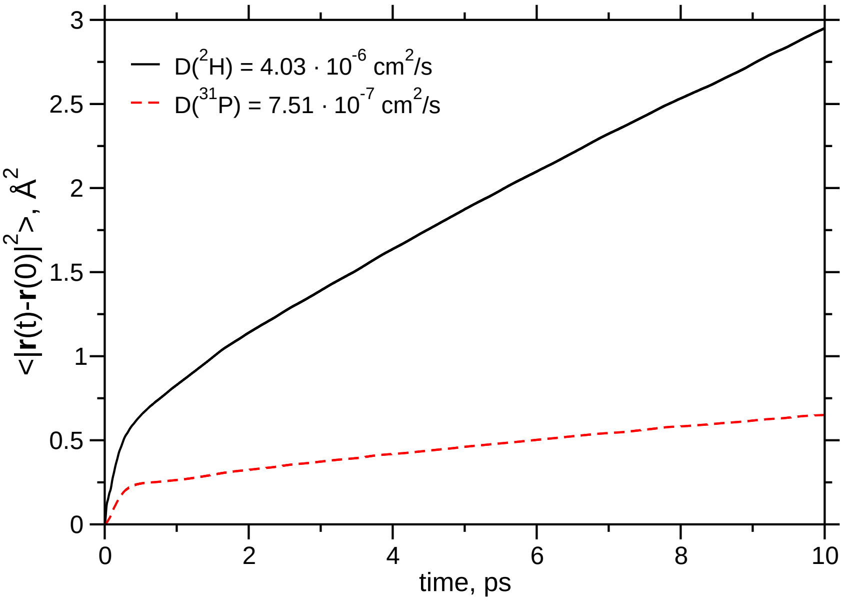

Figure 4.3: Average mean square displacements and corresponding diffusion constants as obtained from the Einstein relation for hydrogen and phosphorus atoms in H_3PO_4 at 383 K.

lation will be exclusively used for the further analysis concerning the dynamical properties and proton transfer mechanisms.

4.3 Rotational Dynamics

The classic picture of the proton conduction process suggests that rotational reorientation of the proton host species is responsible for the dielectric relaxation of the solvent and the subsequent separation of charge carriers, which are able to carry current upon the application of electric field. Therefore, we attempt here to rigorously investigate the solvent's rotational dynamics and its relation to proton transport in phosphoric acid.

As a first approximation, the rotational dynamics of the phosphate tetrahedra can be described via an isotropic angular Brownian diffusion model also known as a Debye diffusive model. Within this model, a rotational diffusion constant D_{rot}

can be evaluated from the angular mean square displacement via the relation:

$$D_{\mathrm{rot}} = \frac{1}{4} \lim_{t\to\infty} \frac{d}{dt} \left\langle \frac{1}{N_{P-O}} \sum_{i=1}^{N_{P-O}} (\Delta\theta(t))^2 \right\rangle \tag{4.3}$$

where $N_{\mathrm{P-O}}$ is the number of P–O bonds and and $\Delta\theta$ is the angular displacement between time 0 and t. The isotropic rotational diffusion constant as estimated from the trajectory (Fig. 4.4) is $D_{rot} = 0.0078$ rad^2·ps^{-1}, which, depending on the model, is almost two orders of magnitude smaller than that of water.[159,160] This correspondence is not surprising if one remembers the difference in viscosities between the two liquids (∼1 cP vs. ∼100 cP). The applicability of the isotropic free rotational diffusion model for the description of hydrogen bonded liquids with a special emphasis on water has been recently questioned.[159,161] The inconsistency of the aforementioned model in the case of phosphoric acid is equally obvious if one tries to evaluate the orientational correlation functions:

$$C_n = \langle P_n[\mathbf{u}(t) \cdot \mathbf{u}(0)] \rangle \tag{4.4}$$

where $P_n(x)$ is the rank-n Legendre polynomial ($P_0(x) = 1$; $P_1(x) = x$; $P_2(x) = 1/2(3x^2 - 1)$; $P_3(x) = 1/2(5x^3 - 3x) \ldots$) and $\mathbf{u}$ is a vector attached to the P–O bond. The calculated value for C_n are depicted in Fig. 4.5. The exponential decay constants τ_n of the C_n, corresponding to the experimentally measurable reorientation times, are directly related to D_{rot} through the following relation:

$$\tau_n = \frac{1}{n(n+1)D_{rot}}. \tag{4.5}$$

This relation indicates that the ratios of τ_n for different values of n must be ratios of integers and that $\tau_1/\tau_{n>1}$ must, itself, be an integer. In the case of water,[159] these ratios as well as the resulting, D_{rot}, show strong deviations from those obtained by evaluating the angular mean-square displacement. Our results show, that this is also definitely the case for H_3PO_4. The estimated τ_1/τ_2 is 1.6, instead of theoretical 3.0 and $\tau_1/\tau_3 = 1.9$ deviates even more from the predicted value of 6.0. The observed discrepancies are even larger than those in water and point to the fact that phosphoric acid has an even more complex hydrogen bond network with what is likely to be a more complex molecular reorientation mechanism.

Obviously, the slow and hindered rotational dynamics of the PO_4 coupled with the fact that phosphoric acid can, nevertheless, conduct protons implies that the full rotational freedom of the phosphate tetrahedra is not an essential part of the proton conduction mechanism. In other words, the solvent's rotational dynamics is basically decoupled from the dynamics of the protonic subsystem and there is a different mechanism of the dielectric relaxation behind the successful formation and migration of charge carriers.

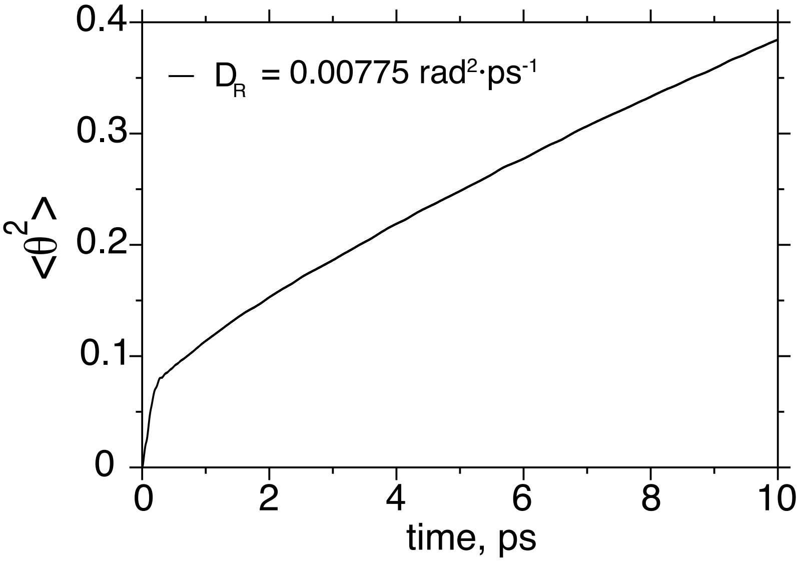

Figure 4.4: The average angular displacement of the P–O bond with respect to time and the corresponding rotational diffusion constant.

4.4 Proton Transfer Kinetics

The important time scales for proton transfer kinetics including proton hopping and solvent reorientation can be rigorously extracted with the help of the population correlation function (PCF) approach.[53,120,162–166] This method has been very successfully applied for the investigation of hydrogen bond kinetics in a number of systems, mostly for aqueous acidic and basic solutions,[53,114,166] but also for other systems such as methanol-water mixtures[120] or CsH_2PO_4.[126] The advent of

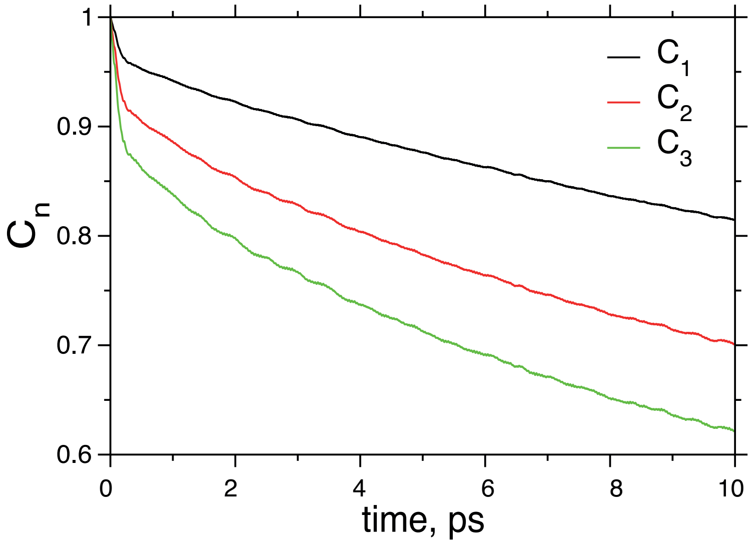

Figure 4.5: Orientational correlation functions C_n for the $\mathbf{u}_{\mathrm{P-O}}$ bond. n = 1,2,3 are shown.

ultrafast spectroscopy measurements of hydrogen bond kinetics[55] provide experimental confirmation for this approach.[21] The PCF scheme is generally formulated as follows: we assume that each proton belongs to one of the oxygen atoms in the system: O*–H $\cdots$ O, where O* refers to an oxygen atom with a covalently bound hydrogen and O indicates an oxygen with no proton. Next, an instantaneous indicator function $h(t)$ is defined such that $h(t) = 1$ if a tagged oxygen atom is O* at time t and $h(t) = 0$ otherwise. In the same way, a continuous indicator function is defined such that $H(t) = 1$ if O* retains its identity from $t = 0$ up to time t and $H(t) = 0$ otherwise. Then we define a correlation function via

$$C_c(t) = \frac{\langle h(0) \cdot H(t) \rangle}{\langle h \rangle} \tag{4.6}$$

$C_c(t)$ gives the probability of finding an O* that remains as such continuously for a total time t. For short to intermediate times, the calculated $C_c(t)$ might have several components: coming from the fast proton hopping (rattling) and the long-range proton transport processes including solvent reorganization. Thus, the decay of $C_c(t)$ can be fitted to the multi-exponential form:

$$C_c(t) = \sum_{i=0}^{n} a_i \exp\left(-t/\tau_i\right) \tag{4.7}$$

with the time constants (τ_i) corresponding to the different processes. The PT PCFs can be calculated in two ways, including rapid proton rattling events, where a chosen proton comes back to the same O* after certain time or excluding this kind of events. The obtained PCFs for both situations and their triexponential fits are shown in Fig. 4.6. For the PCF including all proton transfers, the obtained decay constants are $\tau_1 = 0.15$ ps, $\tau_2 = 1.12$ ps and $\tau_3 = 8.2$ ps. The first, fastest constant represents the fast proton rattling and is almost identical to the observed interconversion time between the Zundel and Eigen ions in the case of excess proton in water.[18,21] The slower components already describe the solvent reorganization process and will be later discussed and related to the overall proton transport mechanism. The PT PCF which excludes proton rattling shows three components of very similar magnitude: $\tau_1 = 13.6$ ps, $\tau_2 = 16.3$ ps and $\tau_3 = 19.7$ ps, probably indicating that there is only one slow process leading to this time scale and the appearance of three slightly different constants could be attributed to the lack of statistics in this simulation. It is important to note, that from Fig. 4.6 one can see that in a simulation comprising 55 ps, 95 % of all protons exchange their nearest oxygen neighbor at least once, and even 65 % of all protons undergo a complete transfer without coming back to the initial oxygen. Up to now, such dynamics of the entire protonic subsystem has never been observed in an AIMD simulation.

4.5 Proton Transfer Energetics

In order to estimate the energetics of proton transfer, the free energy profile along a chosen proton transfer coordinate was calculated. For this, an asymmetric stretch coordinate $\delta = \mathrm{r}_{\mathrm{H}\cdots\mathrm{O}} - \mathrm{r}_{\mathrm{H-O}}$, which follows the progress of the proton through hydrogen bond is defined.[10,11,19,167] The free energy barrier of the proton transfer is usually computed from the probability distribution function $P(R_{\mathrm{OO}}, \delta)$

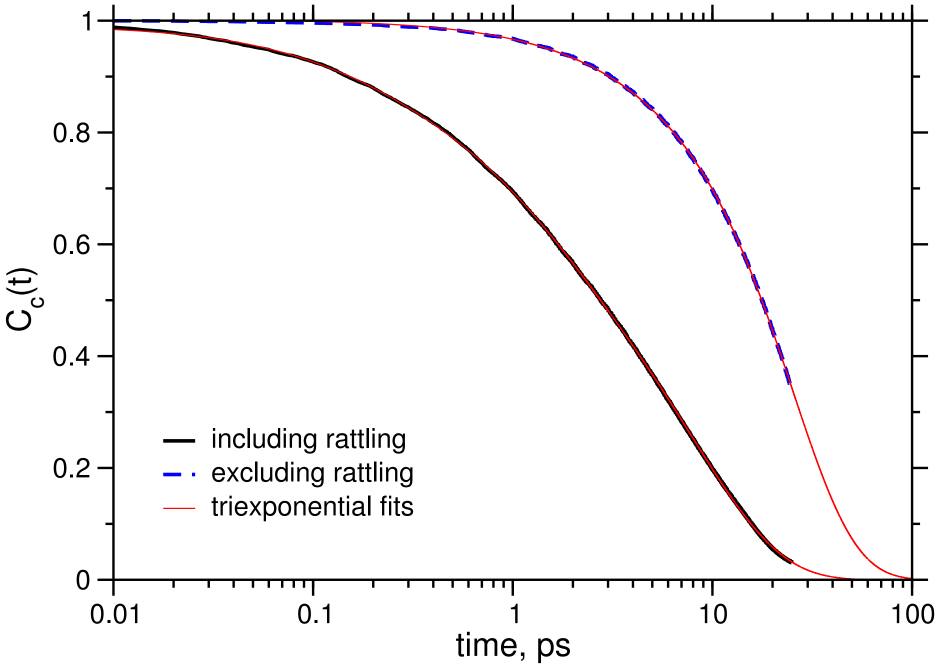

Figure 4.6: Proton transfer population correlation functions (including and excluding proton rattling) and their triexponential fits.

(Fig. 4.8 a)), where R_{OO} is a proton donor-acceptor separation, using the following relation:

$$A(\delta) = -k_B T \ln(\int P(R_{\mathrm{OO}}, \delta)\, dR_{\mathrm{OO}}) \tag{4.8}$$

The calculated free energy profiles, which show a distinct double well character, are depicted in Fig. 4.8 (b). Generally, the proton transfer barrier is strongly influenced by the donor-acceptor separation, with the predominant contribution coming from the most probable $\mathrm{O_D}-\mathrm{O_A}$ separation. The barriers tend to increase with increasing temperature, due to the increasing average $\mathrm{r_{O_D \cdots O_A}}$ separation. In our case, the two simulations show slightly different barriers, despite an almost identical $\mathrm{r_{O_D \cdots O_A}}$. The estimated proton transfer barrier from the GPW-PBE simulation is ~60 meV, which is approximately 20 meV lower than that obtained from the PW-BLYP. Both values roughly correspond to twice the average thermal kinetic energy of our simulations (~34 meV) and the difference between the two schemes is likely due to differences in the functionals, basis sets, and sampling. Nuclear quantum effects might lower these barriers slightly, but as already noted, the effects are expected to be small. It is important to mention that, in contrast to most of the studies of intrinsic protonic defects (e.g water, imidazole), all the protons and H-bonds can be treated at the same footing for evaluating the free energy barriers. The discussion of how the proton energetics change around the charge species is presented in the next section. In any case, the calculated barriers are very low, and cannot account for the activation energies obtained from conductivity, proton diffusion or spin-lattice relaxation time measurements. In essence, this indicates that the fast local proton transfer cannot be the rate limiting step behind the long-range proton transport.

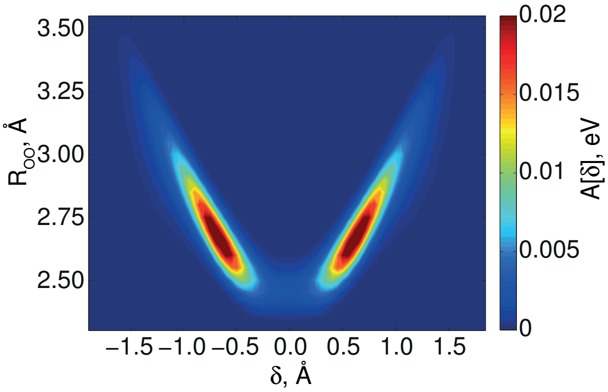

Figure 4.7: $P(R_{OO}, \delta)$ probability distribution

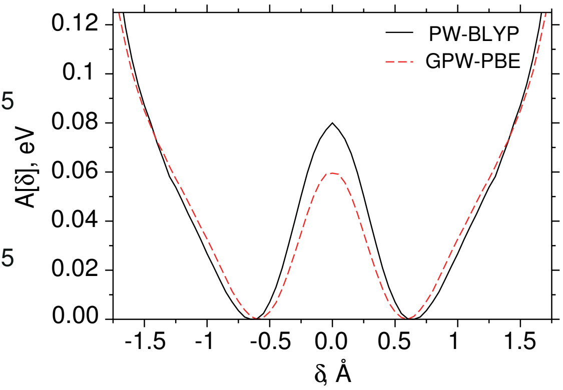

Figure 4.8: Free energy profile $A(\delta)$ along the proton transfer coordinate δ.

4.6 The Structure and Energetics of Charged Species

Another important aspect concerning the structure and dynamics of protonic defects is, how do the local H-bond structure and proton dynamics change around the regions carrying excess of deficient protonic charges. The formal definition of what is a protonic defect in the case of structural diffusion is certainly nontrivial. Even though, one can formally treat the phosphoric acid molecules carrying an excess proton (positively charged species $H_4PO_4^+$) and missing a proton (negatively charged species $H_2PO_4^-$) as charged defects. The analyses described in this section are based on the assignment of every proton to its nearest neighbor oxygen atom and a simple counting of all these oxygens belong to a particular PO_4 unit. In this way, the resulting degree of self-dissociation (including all transient and incomplete PTs without solvent relaxation) is ∼25%, which is significantly higher than the experimental one (∼7.4 %). Nevertheless, the physical agreement is probably very close and the difference must be attributed to the simplicity of the way the charges are counted. The experimental degree of self-dissociation represents the concentration of fully separated charge carriers, whereas in the aforementioned procedure all rattling PT events are included.

The structural diffusion of protonic charge in water can be characterized as a motion of *topological defects*, having significantly different solvation structures than the bulk molecules. This usually includes a significant contraction of the H-bond network and an integer change of coordination numbers around the charged region. In the case of phosphoric acid, a similar, just not as severe contraction of the H-bond network in the vicinity of the charged species is observed: $\mathrm{r_{OO}(H_4PO_4^+)} \approx 2.52$ Å $< \mathrm{r_{OO}(H_2PO_4^-)} \approx 2.55$ Å $< \mathrm{r_{OO}(H_3PO_4)} \approx 2.58$ Å (Fig. 4.9). Moreover, the solvation patterns of these species are not identical either; the running coordination numbers of the first solvation shell of each molecule are: $\mathrm{n_{OO}(H_4PO_4^+)} \approx 4.4 < \mathrm{n_{OO}(H_2PO_4^-)} \approx 6.0 < \mathrm{r_{OO}(H_3PO_4)} \approx 7.2$ (Fig. 4.9; the value of $\mathrm{n_{OO}}$ is taken at the first minimum in $\mathrm{r_{OO}}$ and multiplied by four). This situation is reminiscent of hydronium and hydroxide ion solvation in water, where the positive species assume an undercoordinated, and the negatively charged ones an overcoordinated solvation patterns.

The energetics of PT around the $H_4PO_4^+$ and $H_2PO_4^-$ shows some interesting features as compared to the remaining protons as well. The PT free energy profiles, as estimated from Eq. 4.8, for only those protons located around the charged defects are shown in the Fig. 4.10. One can clearly see that the PT barrier around a positively charged defect is significantly lower if compared to the overall barrier. A barrier of this height (43 meV) is almost completely filled by the thermal energy (35 meV), suggesting that the PT involving a positively charged species is virtually barrierless. The PT barrier around the negative species is slightly higher (52 meV), indicating that these species are slightly less mobile than the positive ones. This asymmetry is reminiscent of that for hydronium

(H_3O^+) and hydroxide (OH^-) ions in water, confirming the concept that even for intrinsic protonic defects in H-bonded systems, one cannot expect a 'mirror image' scenario for the solvation and dynamics of oppositely charged defects.

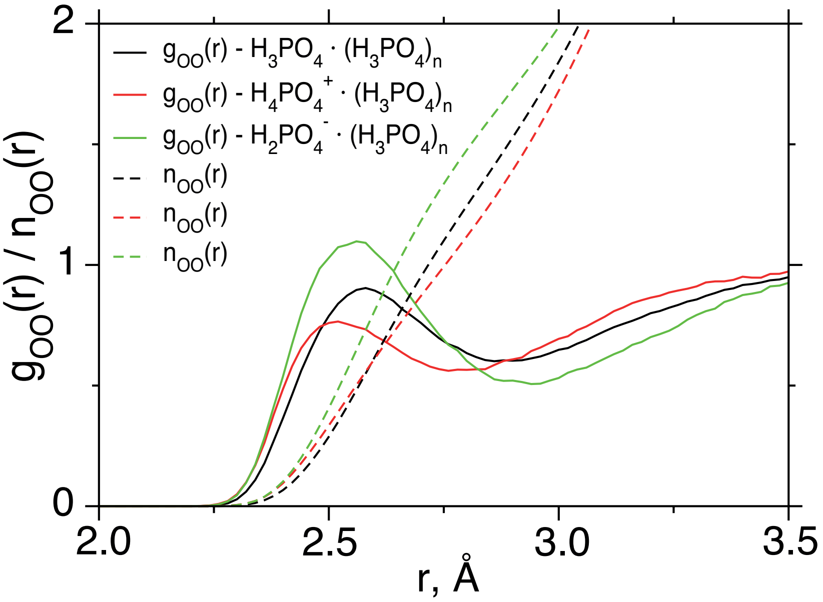

Figure 4.9: RDFs g_{OO} and running coordination numbers (n_{OO}) of oxygen atoms for phosphoric acid in its various states of protonation.

4.7 On the Degree of Protonation

As was already mentioned, the H-bond network in phosphoric acid is very peculiar. The *frustration* of the H-bond network, where an H-bond is formed by a proton donor and an already protonated oxygen (acceptor), results in local formation of sites with higher energy. As will be discussed further, these configurations are extremely important for the proton transport mechanism because they allow for efficient solvent reorientation. In the g_{OH} and g_{OO} RDFs (Fig. 4.2), the H-bond peaks show a significant asymmetry, but no evidence of splitting. This implies that, on a time average, all oxygens form a continuous population of various H-bond configurations. The existence of slightly different, weaker, H-bonds in liquid phosphoric acid was observed in the IR spectra.[82] Therefore, an attempt for a more rigorous characterization of the oxygen protonation states and

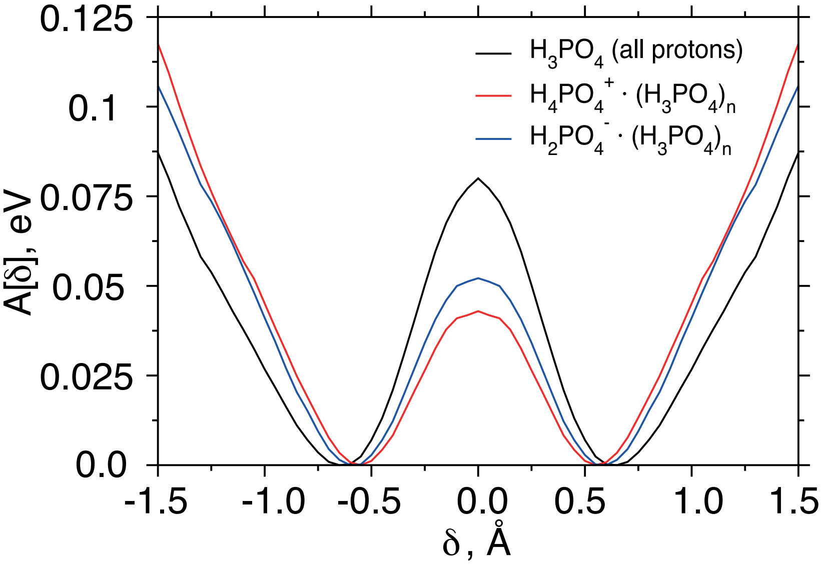

Figure 4.10: Free energy profiles $A(\delta)$ along the proton transfer coordinate δ for H_3PO_4, $H_4PO_4^+$ and $H_2PO_4^-$.

the predominant H-bond configurations is made. For this, an approach based on the original Pauling's idea of bond-orders is used.[168] Various bond-order analyses have already been successfully applied for describing the protonic defects in water.[169,170] For the case of phosphoric acid, we use Pauling's empirical bond-order definition:

$$n_i = \exp\left[-\frac{(r_i - r_s)}{a}\right] \tag{4.9}$$

where r_i is an $\mathrm{r_{O-H}}$ separation from the simulation, r_s is an equilibrium O–H bond length in the gas phase ($n = 1$) and a is an empirical parameter, parametrized to reproduce $n = 0.5$ (when a proton is equally shared by two oxygens). Both of the parameters are fine-tuned to reproduce the overall average protonation of 0.75 (3 protons per 4 oxygens). The resulting distribution is depicted in Fig. 4.11, which represents the probability for an oxygen atom to be in a certain protonation state defined as a sum of bond-orders (n_i) of an oxygen atom due to the neighboring protons. Although, it is obvious that even this type of analysis cannot unambiguously show the different populations of oxygen protonation states (Fig. 4.11), it still carries much more information than, for example a radial distribution function. The first peak at $\sum_i n_i \approx 0.2$ corresponds to oxygens that only accept H-bonds (only proton acceptors), whereas the second peak is composed of two populations: one representing only donating oxygens and a second, representing oxygens that are simultaneously donors and acceptors. Obviously, the latter configurations with $\sum_i n_i \geq 1.0$, correspond to frustrated H-bonds and indicate no "quasi-water" molecules ($\sum_i n_i \approx 2.0$) forming in the simulation.

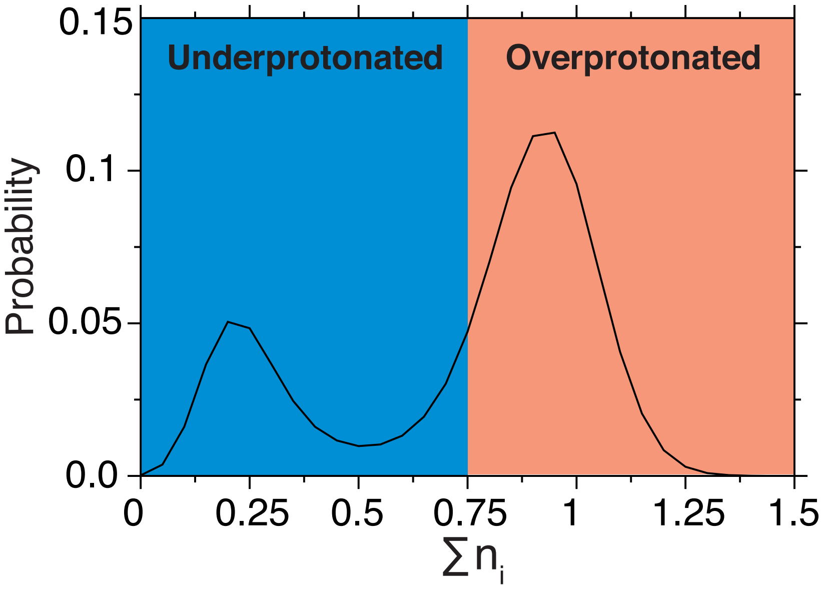

Figure 4.11: The probability distribution of oxygen protonation states defined as the sum of individual bond-orders due to surrounding protons ($\sum n_i$).

4.8 Interprotonic Coupling

The predominant proton dynamics observed in the simulations can be characterized by frequent crossings of the PT barrier at the center of the H-bond (proton rattling).[171] Although the average equilibrium dynamics of neighboring protons does not show any pronounced correlations, there are special configurations acting as nucleation points for the formation of extended Grotthuss chains via the proton-proton interaction. Such configurations occasionally form by a PT between two neutral molecules resulting in a contact ion pair ($H_4PO_4^+/H_2PO_4^-$). The main driving force for such events, which preferentially take place in transiently short H-bonds, is most likely the direct electrostatic proton-proton coupling. The possibility of collective, highly coupled proton motion in H_3PO_4 was already predicted by Zundel, using IR spectroscopy.[82] The first attempt to investigate the interprotonic interactions and their relation to the proton transport, is based on an assumption of a purely electrostatic coupling between protons and its correlation to PT events. For this, a force acting on each proton due to all the other protons in the system is defined. As a first approximation, it is assumed that this interaction is of a bare Coulombic form, with the protons being positive point charges (+e). The summation over particles is carried out in real space only, with a cut-off radius equal to half of the simulation box length (8.37 Å). All proton transfer events (including rattling) are mapped onto the same time scale and the time origin is exactly the instant when the proton changes its nearest neighboring oxygen. In order to show the time variation of the averaged force, 1 ps trajectory segments are taken prior to and after a PT event. The resulting force is averaged over all transfer events, and the results are depicted in Fig. 4.12, which shows the trace of the absolute magnitude of this force ($F(t)$) versus time.[171] As seen in Fig. 4.12, the force, originating from the electrostatic repulsion due to all protons in the environment, shows a distinct maximum for the PT transition state ($\delta = 0$, where $\delta = \mathrm{r}_{\mathrm{H}\cdots\mathrm{O}} - \mathrm{r}_{\mathrm{H-O}}$). Certainly, this approximation is very crude and can only provide a rough impression of the coupling between the protons. It completely neglects the dynamical screening and charge redistribution (polarization). One way to improve this force would be for example to take the charges on the hydrogen atoms directly from the DFT calculation (e.g. Mulliken or electrostatic potential derived charges).

The electrostatic driving force for the correlated PTs has a major contribution from the repulsion of a single, most likely, the incoming proton.[171] This is clearly indicated in the δ-resolved HH radial distribution function $\mathrm{g}_{\mathrm{HH}}(r, \delta)$ depicted in Fig. 4.13, which shows an increase in the height of the main peak at $r \approx 3.5$ Å and $\delta \approx 0$.[171] This essentially confirms the previous conclusion obtained from the Coulombic force calculation, that the proton transfer process is strongly correlated to the dynamics of surrounding protons.

At this point, it is important to stress, that the strong interprotonic coupling and the resulting concerted motion are only possible in very few systems, specifi-

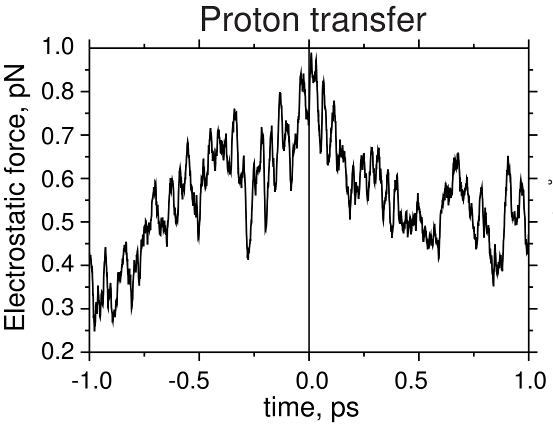

Figure 4.12: Absolute magnitude of a purely electrostatic force $F(t)$ acting on a transferring proton ($\delta \to 0$; time = 0 ps) due to all other protons in the system.[171]

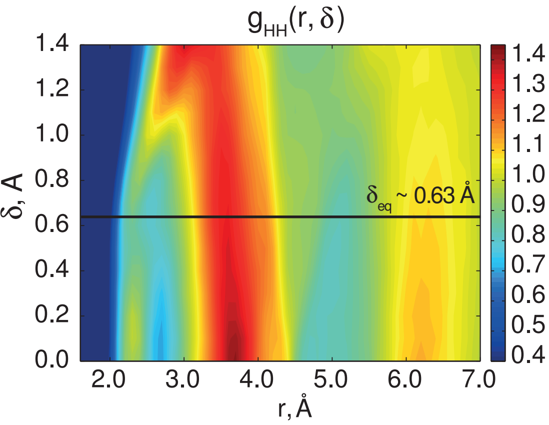

Figure 4.13: $g_{\mathrm{HH}}(H_3PO_4)$ radial distribution function resolved in r and δ, containing information about the spatial distribution of protons with respect to δ (δ_{eq} is the equilibrium value in the simulation).[171]

cally those in which the solvent is only weakly coupled to proton transfer. In the case of H_3PO_4, this effect is probably a consequence of short hydrogen bonds with high protonic polarizability and the weak dipolar response of the solvent. Nevertheless, the coupled proton hopping probably only affects the initial steps of the proton conduction process (formation of the charge carriers) and has little or even no effect on the solvent relaxation processes leading to the successful separation and migration of charge carriers. The relation between the interprotonic coupling and long-range proton transport mechanism will be thoroughly discussed in the following sections.

In order to search for a possible *presolvation* picture, similar to that used to describe the transport of H^+ and OH^- in water,[9,11] the RDFs resolved with respect to δ for other types of atoms were also analyzed. For example, $g_{\mathrm{PP}}(r, \delta)$ did not show any change in the local coordination (the first and second solvation shells) of phosphate with respect to δ (Fig. 4.14), confirming the initial hypothesis that the dynamics of phosphate tetrahedra are not directly coupled to the PT process. The more interesting correlations are those for the donating ($g_{\mathrm{O_DO}}(r, \delta)$) and accepting oxygens $g_{\mathrm{O_AO}}(r, \delta)$. The results (Fig. 4.15) show slightly different solvation patterns for proton accepting and donating oxygens, although not a full integer change of the local coordination number, during a proton transfer event. This contrasts with the case of an excess proton in water, where the proton receiving water molecule must lose one acceptor hydrogen bond prior to the proton transfer event.

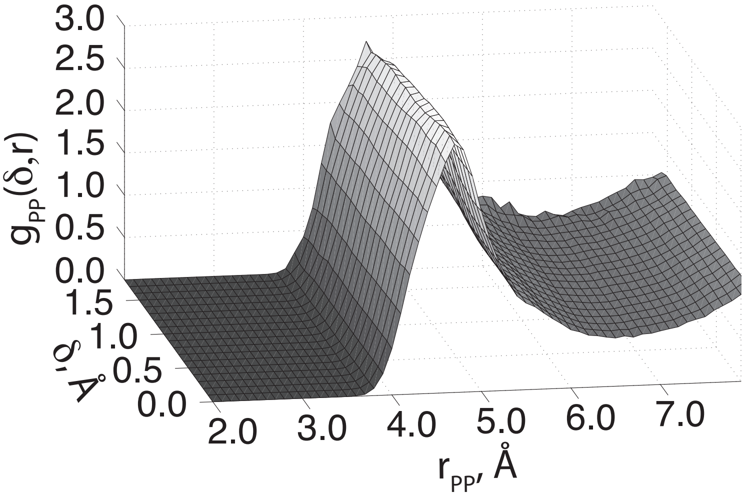

Figure 4.14: g_{PP} RDF resolved in r and δ.

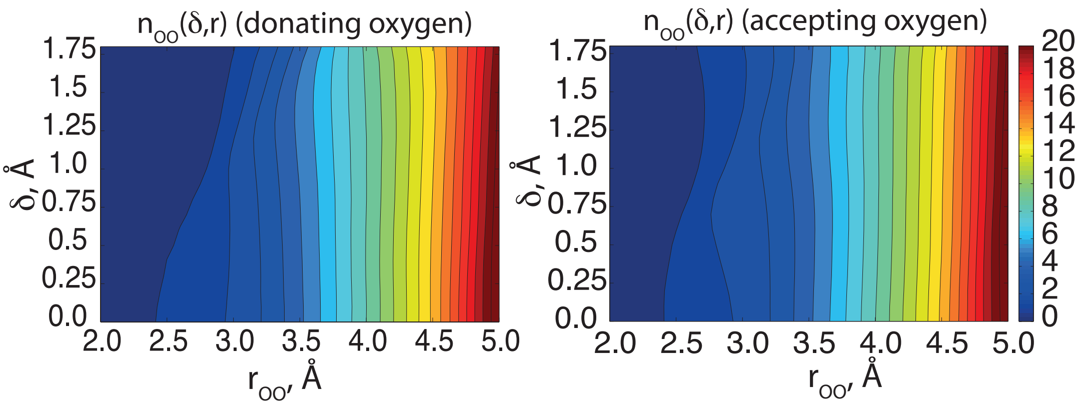

Figure 4.15: The running coordination numbers $n_{OO}(r,\delta)$ resolved in δ and r for donating and accepting oxygen atoms.

4.9 Formation of Grotthuss Chains

Once the importance of interprotonic coupling for the PT process is recognized, the following question immediately arises: what is the correlation length, or how many hydrogen bonds does this correlated motion involve?[171] On a more quantitative level, the AIMD calculations allow us to determine two important quantities, specifically, the average length of an extended Grotthuss chain and the average time interval for each step in the chain formation. In order to extract these, we employ a correlation function, designed using a graph-theoretic approach. Similarly to previous approaches,[125,172] we view the phosphate tetrahedra and H-bonds as the nodes and edges of an undirected graph, and from this, we construct a δ-restricted adjacency matrix D_{ij} that connects vertices i and j only if $\delta < 0.1$ Å (there is a transferring proton in the i, j bond). We then use D_{ij} to develop a correlation function $C_{pc}(n)$ that specifies the probability of two PT events, n H-bonds away from each other being correlated within a certain response time increment τ_{res}, which must be short compared to the average PT time for any given H-bond:[171]

$$\begin{aligned} C_{pc}(n) = \Bigg\langle \sum_{i=1}^{N} \sum_{\substack{j=1 \\ j\neq\forall\mathbf{X}}}^{N} \int_{T} [\delta(1 - D_{ij}(t))]dt \\ \Bigg\{ \sum_{\substack{k_1=1 \\ k_1\neq\forall\mathbf{X}}}^{N} \cdots \sum_{\substack{k_{n-1}=1 \\ k_{n-1}\neq\forall\mathbf{X}}}^{N} \sum_{\substack{k_n=1 \\ k_n\neq\forall\mathbf{X}}}^{N} \int_{t_0-\tau_{res}}^{t_0+\tau_{res}} [\delta(1 - D_{jk_1}(t')]\ dt' \\ \cdot \int_{t_1-\tau_{res}}^{t_1+\tau_{res}} [\delta(1 - D_{k_1k_2}(t'')]\ dt'' \cdot \ldots \\ \ldots \cdot \int_{t_{n-1}-\tau_{res}}^{t_{n-1}+\tau_{res}} [\delta(1 - D_{k_{n-1}k_n}(t' \ldots '))]\ dt' \ldots ' \Bigg\} \Bigg\rangle_{t_0\cdots t_n} \end{aligned} \qquad (4.10)$$

where n is the separation between the H-bonds (connectivity) and varies from 1 (adjacent H-bonds) to the longest non-cyclic path in the H-bond network. N is the number of PO_4 tetrahedra. In this equation $\delta(x)$ is the Dirac delta function. t_0

is a first instance in the trajectory at which $D_{ij}(t) = 1$ and $\int[\delta(1-D_{ij}(t))]dt = 1$; in the same way, t_1 is the first instance in the trajectory range from $t_0 - \tau_{res}$ to $t_0 + \tau_{res}$ for which $\int[\delta(1 - D_{jk_1}(t'))]dt' = 1$. This moment in the trajectory, together with the H-bond network, seeds the build up of a Grotthuss chain. The same procedure is repeated until the last t_n is found for which $\int[\delta(1 - D_{k_{n-1}k_n}(t' \ldots '))]\, dt' \ldots ' = 1$. The notation $\langle \cdots \rangle_{t_0 \cdots t_n}$ indicates an ensemble average that depends on the identification of the times $t_0, ..., t_n$. The use of this procedure allows the more distantly separated PTs to have longer response times than the ones in the adjacent H-bonds. $\mathbf{X}$ is a subset containing the running indices ($\mathbf{X} = \{i, j, k_1 \ldots k_n\}$), which accrues an increasing number of index members with increasing n.

In principle, the expression in Eq. 4.10 describes the probability of finding H-bonds having a certain δ value with respect to the separation of these H-bonds in the network of H-bonds. It is calculated by a simple algorithm: First, an H-bond with $D_{ij}(t_0) = 1$ is found, and assuming this to be the start of a chain of correlated PT events $C(0)$, a search, explicitly including τ_{res}, for the neighboring H-bond with protons undergoing transfer ($D_{jk_1}(t') = 1$) is performed. If there is such an element, it is included in $C(1)$. The search of correlated proton hops within the more distant H-bonds is continued by checking for $D_{k_1k_2}(t'') = 1$ and adding it to $C(2)$. This procedure is continued until the maximum n is reached. The resulting function is then averaged over the entire trajectory ($\forall t_0 \in T$) and PO_4 units. At this point, it is important to mention that τ_{res} and the δ cut-off parameters can be slightly varied in order to include fewer or more PT events ($D = 1$) into $C_{pc}(n)$. However, the number of included events cannot be too large, because the correlation function $C_{pc}(n)$ will simply start probing the average distribution of all protons in the H-bond network. Finally, the correlation function is normalized to unity by taking the probability of finding a single PT ($D_{ij} = 1$), which gives to the value of $C(0)$.

When $\tau_{\text{res}} = 0$, quasi-coherent PT dynamics is probed, and the probability of PTs within the two subsequent H-bonds is as high as ~8%, as shown in Fig. 4.16. This is roughly three orders of magnitude larger than would be expected for completely uncorrelated events ($\delta \leq 0.1$ Å for only $\sim 1.5\%$ of the total number of H-bonds). The probability of forming more extended Grotthuss chains increases with time; for an increment of $\tau_{res} \approx 50$ fs, Fig. 4.16 indicates a ∼10% probability for forming a Grotthuss chain of five phosphate species connected by four H-bonds (see also Fig. 4.17 (a)).[171] Fig. 4.16 reveals how strong the mutual interprotonic coupling is, and how it can lead to the formation of polarized chains comprising a number of H-bonds. The existence of these chains is reminiscent of the long-anticipated concerted Grotthuss mechanism in water, which up to now has never been revealed in extended H-bonded media. These chains are terminated by the $H_2PO_4^-$ and $H_4PO_4^+$ species.

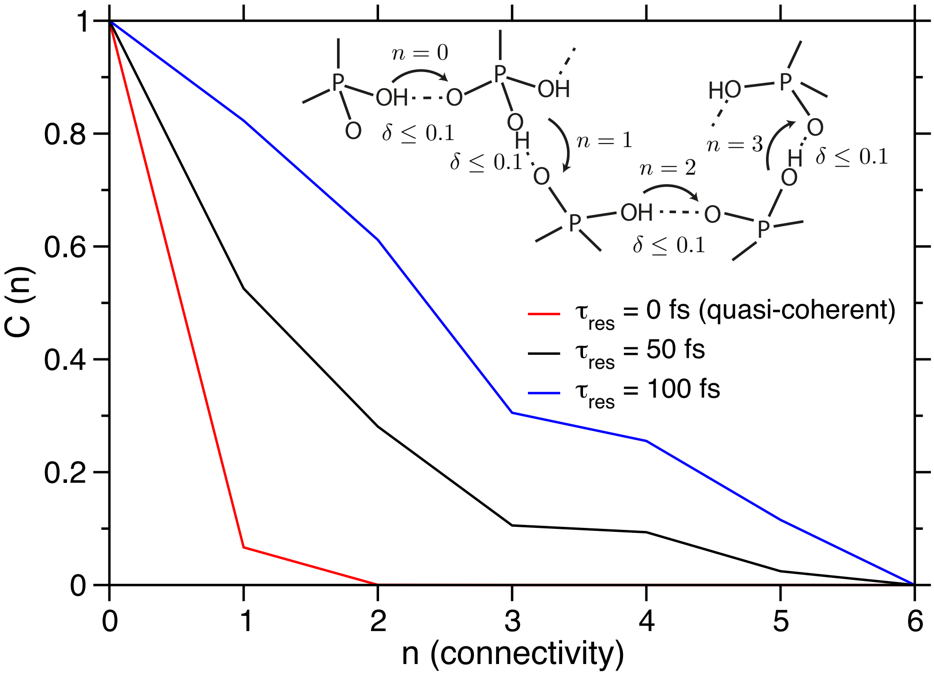

Figure 4.16: Proton coupling correlation function $C_{pc}(n)$ as a function of connectivity n. Specific values include $n = 0$, (single H-bond), 1 (adjacent H-bonds), and 6 (longest non-cyclic path in the H-bond network). Only the H-bonds with $\delta \leq 0.1$ Å (only $\sim$ 1.5% of the total number) are considered as undergoing PT. The time increment τ_{res} sets the finite relay time for the system to respond to correlated PTs.[171]

As mentioned previously, the formation of an extended polarized chain is limited by the increase of the electrostatic energy, essentially determined by the dipolar moment of the chain and the dielectric constant of the unrelaxed environment. As a result of the short H-bonds in phosphoric acid, the dipolar moment resulting from one PT event is small (small displacement in an almost barrierless H-bond) and the coupling to the dielectric environment is probably of a different nature.[171] Although, the dielectric response of H-bonded systems still needs to be better understood on the molecular level,[173,174] we speculate that the fairly high dielectric constant of phosphoric acid ($\epsilon_0 \approx 61$[175]) has a significantly higher contribution from protonic polarizability than is the case for water.[82] As opposed to water, which has a significant dipolar moment as a single molecule (1.85 D), the H_3PO_4 molecule has a small dipolar moment (0.45 D), which leads us to speculate that the pronounced dielectric response of bulk phosphoric acid mainly originates from the protons involved in the intermolecular H-bonding.[171] This type of polarizability is expected to persist even at high frequencies, where the dielectric response of water is significantly reduced (in the 10^9-10^{10} s^{-1} range[176]). Therefore, we assume that the relatively low dipolar moment of extended Grotthuss chains in phosphoric acid and the rapid dielectric stabilization of such a chain through the protonic polarization of the solvent reduce the electrostatic energy penalty compared to the situation in water.[171]

4.10 On the Proton Transport Mechanism

As previously mentioned, systems with good proton conductivity should not only contain short, strong hydrogen bonds with low proton transfer barriers, but they must also allow for solvent reorientation and its dielectric relaxation. Normally, these require the breaking and forming of H-bonds within the solvation shells of the protonic defect. Having discussed the most important aspects of the proton transfer in phosphoric acid, at this stage a possible mechanism leading to fast long-range proton transport in H_3PO_4 is proposed. The general molecular picture of proton conduction involves the following steps, all of which are accompanied by solvent reorganization: (1) formation of a contact ion pair; (2) solvation and separation of the charge carriers; (3) migration; and (4) subsequent neutralization. It is assumed that the proposed model for the proton transfer and solvent reorganization is consistent for the extraordinary high proton conductivity of phosphoric acid. The most important steps of the proposed mechanism are schematically shown in Fig. 4.17. The figure shows snapshots with molecular configurations directly extracted from the AIMD trajectory. Each configuration shows four H_3PO_4 molecules forming a polarized Grotthuss-like chain and several molecules representing the solvent response during the successful proton transfer events. The schematic pictures below the molecular structures show a generalized view of the ion pair (red and blue circles) and the orientation of interchain dipoles (red-blue arrows), forming upon the PT and polarization of the H-bonds, as well as their reorientation due to the solvent response, which is represented by a generalized solvent coordinate $\vec{S}$.

Generally, the process is initiated by an occasional fast PT ($\tau \sim 0.15$ ps) between the two neutral molecules, leading to the formation of a contact ion pair ($H_4PO_4^+/H_2PO_4^-$) and starting a self-dissociation step. Due to the high inter-protonic coupling and an easy formation of a Grotthuss chain, this pair is separated over several molecules via correlated PTs within the hydrogen bonded chain (Fig. 4.17 (a) and (b)). This process of low activation energy is highly reversible ($\tau \sim 1.1$ ps). In order to complete the charge separation/self-dissociation, the central part of the polarized H-bonded chain connecting both defects must be depolarized, as has been previously emphasized for the self-dissociation of water.[177] Without this depolarization, the charge separation can be easily reversed through the intact chain. The depolarization must take place in the center of the chain, since the terminal H-bonds already have the proper orientation with respect to the terminating charges.[171] At first glance, it might seem that the presence of only short, strong H-bonds in phosphoric acid would prevent rapid solvent reorientation processes. However, phosphoric acid has a very peculiar H-bond network topology – the imbalance in the numbers of potential proton donor and acceptor sites (three O–H donors and only one non-protonated oxygen) is anticipated to lead to configurational "frustration".[171] In crystalline H_3PO_4, this is clearly manifested by the presence of three types of H-bonds (two strong and one weak and distorted).[70] These frustrated sites facilitate the efficient step-wise mechanism of solvent reorientation, essentially playing a similar role as orientational defects in "proton wires" of water molecules.[61,64] Solvent relaxation (depolarization) is initiated when one of the solvent H_3PO_4 molecules forms a new H-bond by donating a proton to an oxygen atom in the chain (Fig. 4.17 (c)). This proton is transiently transferred to the new acceptor (Fig. 4.17 (d)), which causes a strong coupling to the original H-bond in the chain and gives rise to the small peak at at $r \approx 2.3$ Å in Fig. 4.12. In this way, the original H-bond is effectively weakened since the same oxygen atom must simultaneously be a proton donor and acceptor. This weakened H-bond can easily break and, through a rapid torsional rotation around the P–O bond axis, reorient, forming a new H-bond with a less acidic (protonated) oxygen in the surrounding solvent molecules (Fig. 4.17 (d)). This relaxation, having a much longer time scale ($\tau \sim 8$ ps), completes the charge separation, and subsequent PTs close to charged species (mostly $H_4PO_4^+$) can be considered already a part of the "independent" migration of these charged species (Fig. 4.17 (e) and (f)).[171] The latter process does not hinder the formation of new chains and reorientation of solvent molecules until the oppositely charged species meet, leading to a neutralization step. Mechanistically, this neutralization event is simply the complement of the self-dissociation process.[171]

Certainly, one can immediately argue that a system such as phosphonic acid, which has similarly strong hydrogen bonds but does not posses the same intrinsically frustrated hydrogen bond network as phosphoric acid, cannot allow for a solvent reorientation though the same mechanism and should not show good proton conductivity. However, as it happens, in phosphonic acid proton structural diffusion in phosphoric acid constitutes ~90 % of the total conductivity, which is only slightly lower than that of H_3PO_4.[65] This question will be addressed in the following chapter of this work.

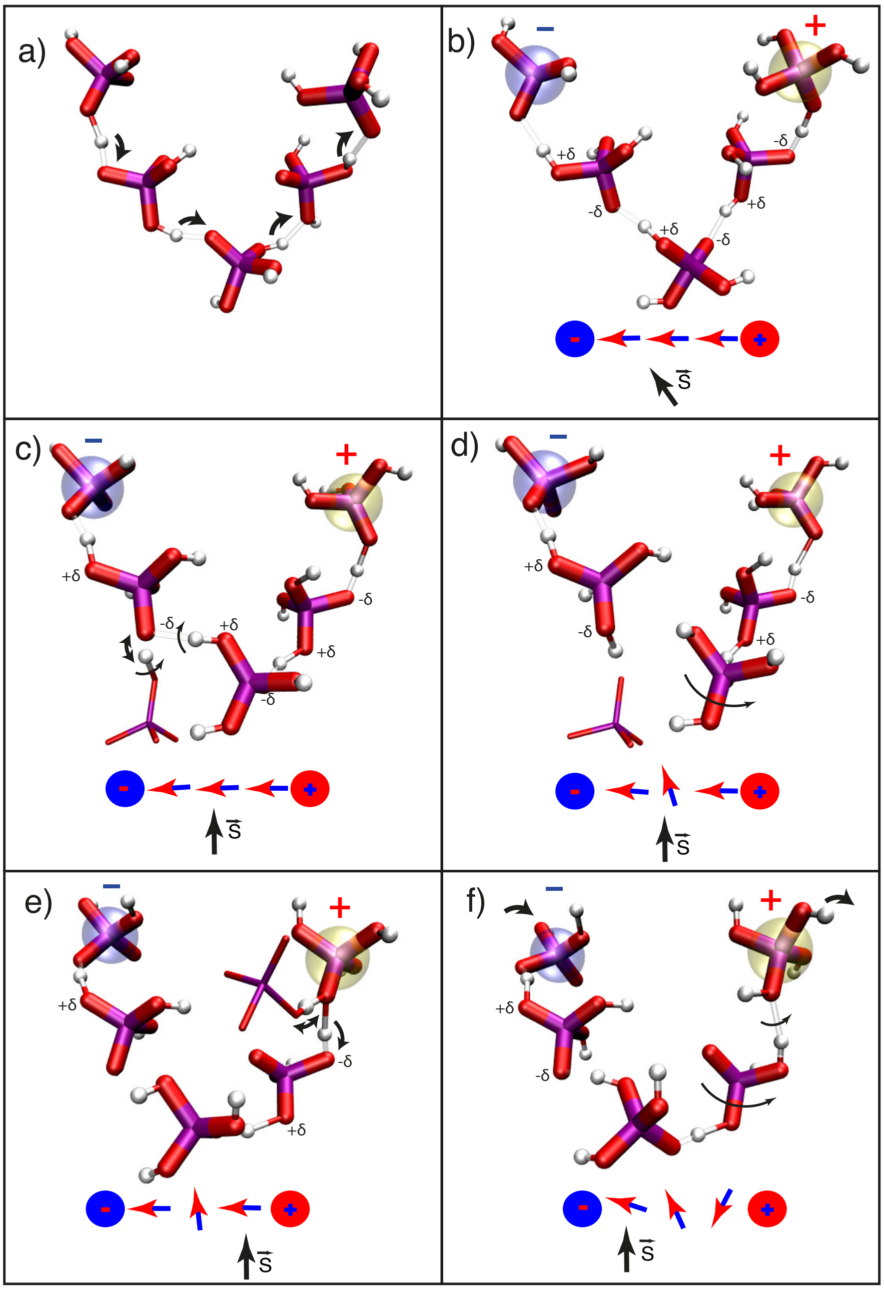

Figure 4.17: Snapshots of the elementary steps of the proton structural diffusion mechanism in H_3PO_4. This sample event shows five molecules extracted from the simulation box, which participate in the correlated PTs over four neighboring H-bonds and in the formation of a Grotthuss chain. The schemes below the molecular structures show the ions and the interchain dipoles, with the remaining solvent molecules represented by a generalized coordinate $\vec{S}$. The arrows denote the PTs and molecular reorientations for the important steps in the mechanism: (a) and (b) correlated PTs and formation of a Grotthuss chain; (c) and (d) reorientation of the solvent H_3PO_4 molecule induced by the formation and breaking of the 'frustrated' H-bond; (e) and (f) formation and breaking of the second 'frustrated' H-bond.[171]

5

Phosphonic and phosphinic acids

In this chapter the results of AIMD simulation on neat phosphonic and phosphinic acids are presented. These systems represent the other two members of the phosphorus oxoacid family. The AIMD production runs of at least 50 ps for each system were obtained. The directly accessible properties such as structure, diffusivities etc. are compared to the available experimental data. Afterwards the attention is turned towards the discussion of the proton transport mechanisms and their dependence of molecular structure and the topology of the H-bond network. Two snapshots of typical configurations representing the H_3PO_3 and H_3PO_2 simulation boxes are shown in Fig. 5.1.

5.1 Structural Properties

Identically to the case of neat phopshoric acid, the discussion of the properties of phosphonic and phosphinic acids is started by the analysis of the structural properties. The radial pair distribution functions are evaluated for all atom pairs and the comparison of all three oxoacid systems is presented in Fig. 5.3. The structure of liquid H_3PO_3 was studied at different levels of hydration by neutron scattering.[95] In Fig. 5.2, the Fourier transform of the obtained full structure factor $S_{XX}(k)$ is compared to the simulated g_{XX}. The resolution of the experiment was rather low, what complicates the analysis and comparison of the fine structural details. However, the general trends of the bonding strengths can be

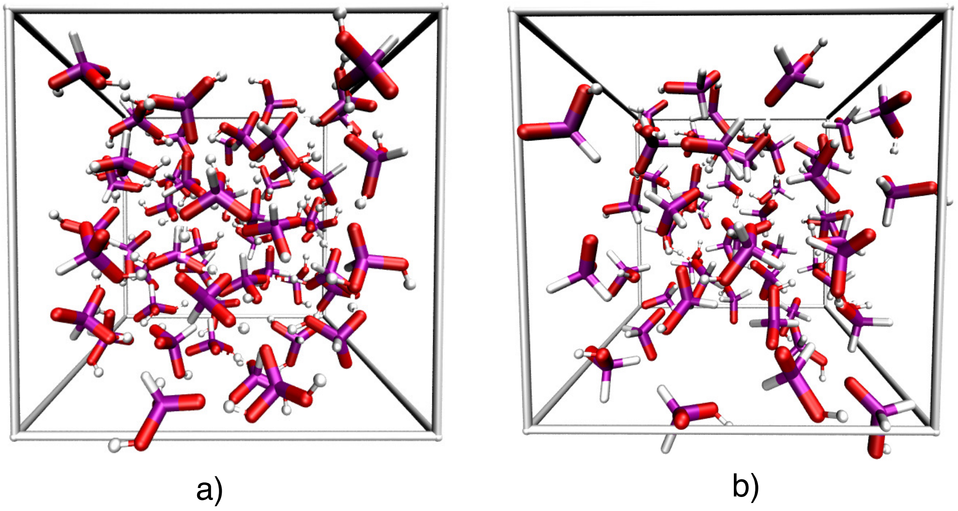

Figure 5.1: Snapshots representing the typical configurations from an equilibrated simulation boxes containing (a) 54 H_3PO_3 and (b) 54 H_3PO_2 molecules.

easily comparied and verified. The positions of all the important contributions agree very well between the simulation and experiment (Fig. 5.2), whereas the structure is significantly sharper similarly to the case of H_3PO_4.

As it comes to the structural comparison of the three systems: H_3PO_4, H_3PO_3 and H_3PO_2, it is clear that the $g_{H_OH_O}$ (for acidic protons only) show similar features for all three systems (Fig. 5.2 (top)). The intramolecular H–H correlation at ∼2.3 Å is the most pronounced in H_3PO_3 and only slightly visible in the case of H_3PO_2. The positions of the main peak as well as the overall structure of g_{HH} indicates that interprotonic distribution is virtually identical for the H_3PO_4 and H_3PO_3, whereas H_3PO_2 shows slightly different pattern. The g_{OH_O} RDFs also show similar patterns for all three acids (Fig. 5.2 (middle)). However, one can immediately see that the covalent O–H bond (first peak in Fig. 5.2 (middle)) and especially the H-bonds $r_{O\cdots H}$ (second peak in Fig. 5.2 (top)) are getting stronger and stiffer in phosphonic and phosphinic acids. Fig. 5.2 (bottom) depicts the various contributions to the total heavy atom RDF – g_{XX} (X = P and O). The P–P correlations are almost identical in H_3PO_4 and H_3PO_3, whereas in H_3PO_2 they shift towards smaller values. This probably indicates that the network of PO_2 units, despite of lower dimensionality is much tighter and tends for the formation

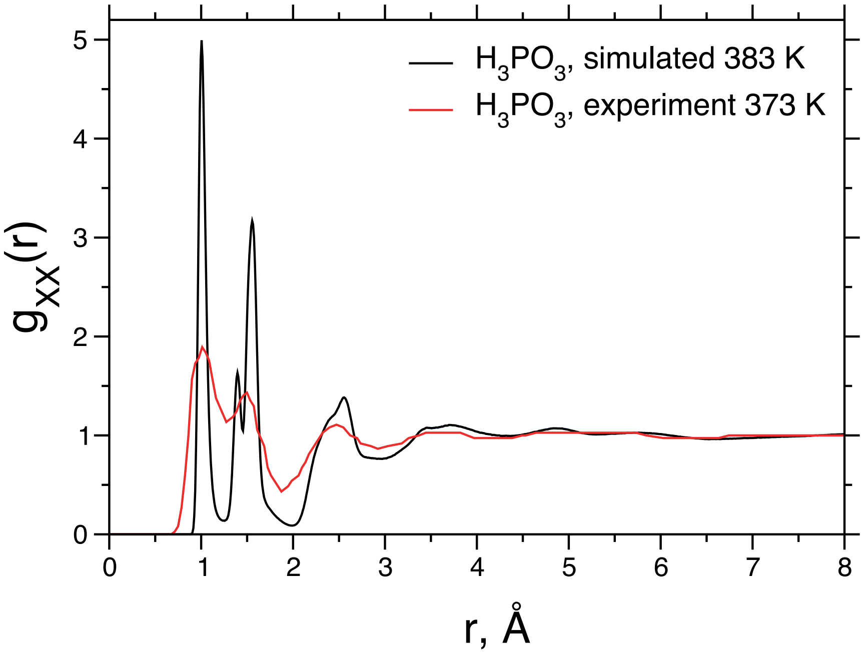

Figure 5.2: The full simulated radial pair distribution function g_{XX} (where X = P, O and H) and g_{XX} from the neutron scattering study.[95]

of linear chains, as was also anticipated from the study of the crystalline structure of H_3PO_2.[72] Surprisingly, the intramolecular structure (P–O bonds; Fig. 5.2 (bottom)) does not show any pronounced changes between the three systems. The g_{OO} peak, which contains both the intramolecular and intermolecular contributions slightly shifts in H_3PO_2 and suggests that the internal structure of hypophosphite anion is more rigid than that of phosphite or phosphate anions, whereas the covalent O-H strengths show an opposite trend.

Fig. 5.4 depicts the distribution of the H-bond geometries (lengths and angles) for all three acid systems. The H-bond length markedly decreases in the series: $r_{\mathrm{OO}} \approx (H_3PO_4)$ 2.60 Å > $r_{\mathrm{OO}} \approx (H_3PO_3)$ 2.57 Å > $r_{\mathrm{OO}} \approx (H_3PO_2)$ 2.52 Å. This increase in the H-bond strength is also pronounced in the distribution of the donor–acceptor–proton angles. The extremely short H-bond in H_3PO_2 is associated with a very low PT barrier and an appropriate account of the nuclear quantum effects would probably make the bond symmetrical with respect to the position of the proton.

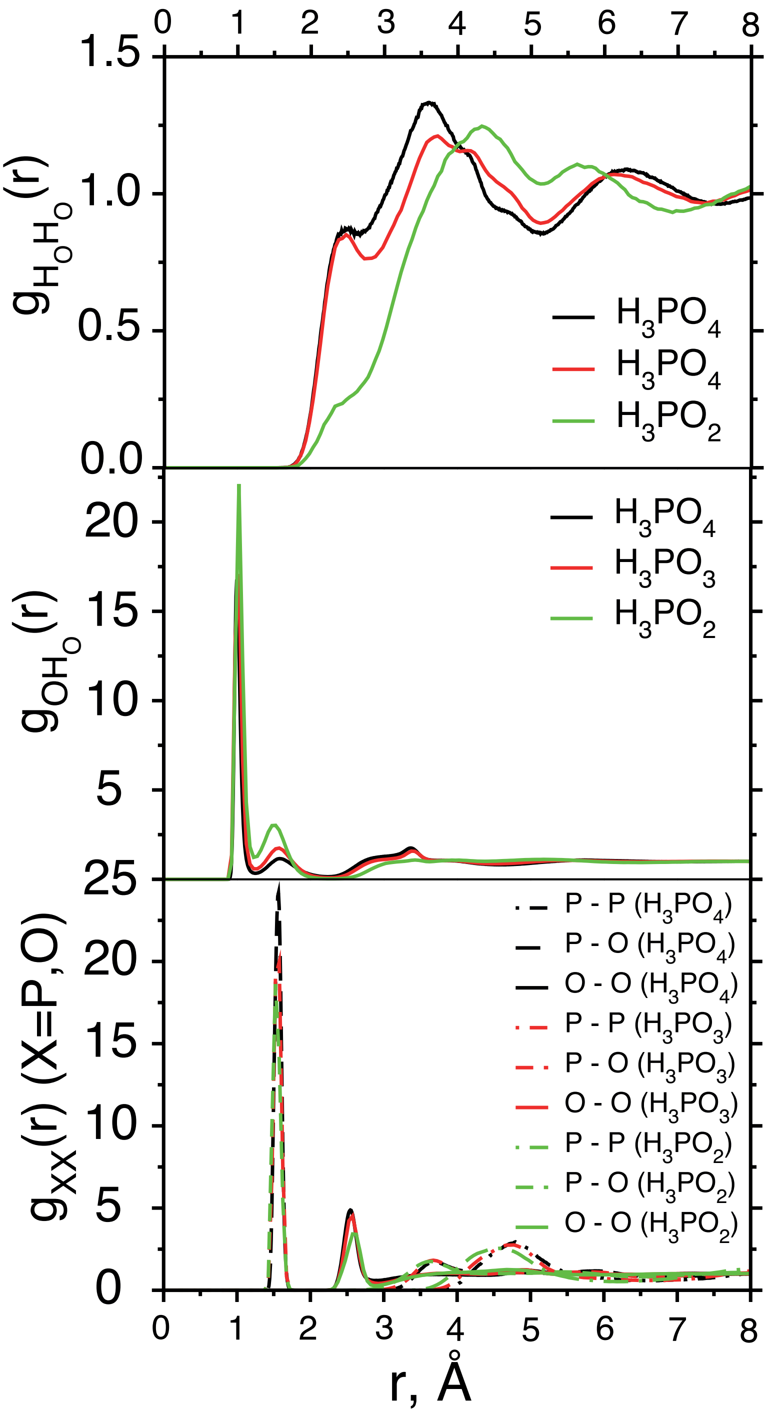

Figure 5.3: Radial pair distribution functions for the liquid H_3PO_4, H_3PO_3 and H_3PO_2. (top) $g_{H_OH_O}$ only for the acidic protons (excluding the hydrogens covalently bonded to phosphorus). (middle) g_{OH_O} for the acidic protons and oxygen atoms, the first peak comes form the covalent O–H bond and the second due to the H-bonding ($H\cdots O$). (bottom) g_{XX}, where X = P or O, shows the different heavy atom pair contributions.

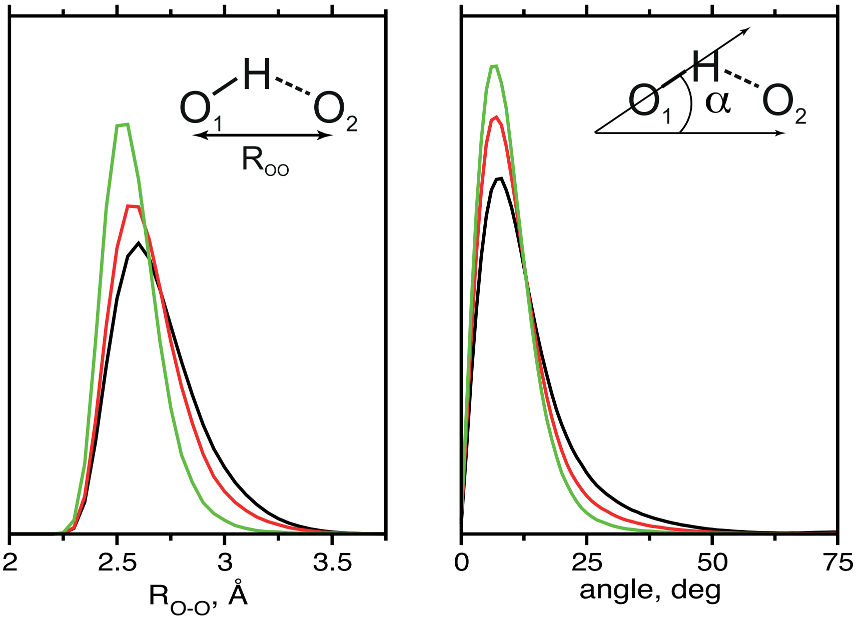

Figure 5.4: H-bond geometries for H_3PO_4 (black), H_3PO_3 (red) and H_3PO_2 (green): probability distributions for (left) $R_{O...O}$ distances, and $\alpha_{O-H...O}$ angles.

5.2 Dynamical Properties

Similarly to the previous discussion on phosphoric acid, the next step in the elucidation of the properties of the other two phosphorus oxoacids is the evaluation of proton and molecular diffusion coefficients. Although, the proton conducting properties of H_3PO_4 and H_3PO_3 have already been experimentally established,[65,68] up to now little was known about the proton transport in H_3PO_2. For this reason, a number of experiments were carried out on phosphinic acid and the results are used to supplement the modeling work.[66]

The crystals of nominally dry phosphinic acid were obtained by vacuum drying ($P=10^{-5}$ mbar) the aqueous solution (Sigma-Aldrich ~50% aq.) using the procedure described by Jenkins et al.[178] Before the conductivity and self-diffusion measurements, the acid crystals were additionally dried on a filter paper and afterwards transferred into gas-tight glass sample holders in an argon filled glove box. The crystals were subsequently melted and a number of conductivity and PFG-NMR measurements were performed at different temperatures on the liquid sample.[66] The experimental results for all three acids are presented in Fig. 5.5

and 5.6.

The experimentally measured conductivities together with the tracer diffusion coefficients in phosphinic acid allow for the general picture of proton conduction mechanism to be drawn. Although the conductivity of H_3PO_2 is significantly lower than that of other acids (Fig. 5.6), it is still relatively high compared to a wider class of H-bonded liquids. Moreover, there still exists an approximately 10% difference between proton and phosphorus diffusion coefficients, indicating a contribution from structural diffusion to proton conductivity. Although, the precise determination of this contribution is complicated without experimental input for the degree of self-dissociation, one can still try to systematically include the correlations in proton transport (Haven ratio (H)) from the knowledge of H_3PO_4 and H_3PO_3. Two different limiting situations concerning the mechanism of proton conduction in phosphinic acid can be assumed: first all the current is carried out via structural diffusion with perfectly random motion of protonic defects (H = 1) and second a completely vehicular nature of proton transport (H = ∞). One can estimate the structural diffusion contribution from the Nernst-Einstein relation using the difference of the two self-diffusion coefficients rather than separately estimating the mobilities and concentrations of protonic defects:[66]

$$\sigma_D^{structure} \approx \frac{F^2}{RT} c(H_{OH})(D(H_{OH}) - D(H_{PH})) \tag{5.1}$$

where $\sigma_D^{structure}$ is the conductivity contribution of structural diffusion, $D(H_{OH})$ and $D(H_{PH})$ the average self-diffusion coefficients obtained from ^{1}H PFG-NMR and $c(H_{OH})$ the concentration of all acidic (H_{OH}) protons. The advantage of this procedure is the possibility to obtain the proton conductivities from tracer diffusion coefficients without precise knowledge of the charge carrier concentrations, assuming that the mobility of protonic defects and proton diffusion are completely random (Haven ratio is unity) processes. For the case of completely vehicular transport, one has to assume equal proton and molecular diffusion coefficients and by using the Nernst-Einstein equation:[66]

$$\begin{aligned}\sigma_D^{vehicle} &= \frac{F^2}{RT}(c(H_4PO_2^+)D(H_4PO_2^+) + c(H_2PO_2^-)D(H_2PO_2^-)) \\ &\approx \frac{F^2}{RT}2\alpha c(H_{PH})D(H_{PH})\end{aligned} \tag{5.2}$$

where $c(H_{PH})$ is the phosphonic acid concentration ($c(H_{PH}) = \rho/M_W$; ρ is the density and M_W the molecular weight of the phosphonic acid). Taking $D(H_{PH})$ as being identical with the $H_4PO_2^+$ and $H_2PO_2^-$ self-diffusion coefficients, one obtains the degree of self-dissociation (α) in H_3PO_2 to be ~5.6%. This α would explain the experimentally measured total conductivity (σ_{exp}^{tot}) by a completely vehicular proton transport mechanism. However, this is not the case, since as mentioned before, there is an approximately 10% difference between the experimentally obtained $D(H_{OH})$ and $D(H_{PH})$ (Fig. 5.5). In the case of entirely structural diffusion proton transport, the calculated $\sigma_D^{structure}$ only accounts for approximately 60% of the σ_{exp}^{tot}, suggesting that in contrary to the other two acids, there is a substantial vehicular contribution to proton conductivity in phosphinic acid. In this mechanism, we assumed that the Haven ratio is equal to 1, which is only the case of perfectly random processes but deviates once the different correlations between mobility of protonic charge carriers and proton diffusion appear. These deviations are known to occur in various proton conductors.[179] Knowing that Haven ratios for phosphorus oxoacids are higher than unity and that the degree of correlations increases from phosphoric ($H \approx 1.5$) to phosphonic ($H \approx 2.5$) acid, this most probably must also hold for phosphinic acid. We believe that an assumption of linearly increasing Haven ratio for all three acids would provide a reasonable approximation, which could help to reveal the principle proton transport mechanism in phosphinic acid. Taking $H(H_3PO_2) \approx 3.5$, one can self-consistently solve for α by estimating the total conductivity ($\sigma_D^{structure} + \sigma_D^{vehicle}$) and comparing it to the experimental σ_{exp}^{tot} until the two are equal:[66]

$$\begin{aligned}\sigma_{exp}^{tot} &\approx \sigma_D^{vehicle} + \sigma_D^{structure} \\ &\approx \frac{F^2}{RT}(2\alpha c(H_{PH})D(H_{PH}) + \frac{1}{H}c(H_{OH})(D(H_{OH}) - D(H_{PH})))\end{aligned} \tag{5.3}$$

Using this approximation, one obtains the degree of self-dissociation $\alpha \approx 4.5\%$ which results in $\sim$21% of the current in phosphinic acid carried by proton structural diffusion (Fig. 5.6).[66]

As in any intrinsic proton conductor, self-dissociation is initiated by a PT in an intermolecular H-bond and leading to the formation of a contact ion pair. Before this pair is separated there is a high probability for the reverse process to occur in strong low-barrier bonds. If a backward transfer occurs, the whole process contributes neither to proton diffusion nor conduction. But if before the proton is transferred back, the H-bond is broken through reorientation of the newly formed defect and another exchangeable proton of the same species forms a H-bond with the initial proton acceptor, this different proton may be transferred. The latter process does then not lead to charge separation and hence conductivity, but since the protons exchange their identity, it contributes to proton diffusion. It is clear that the corresponding Haven ratio depends on the lifetime of the H-bond, the probability for proton backward transfer and the number of exchangeable protons of the protonic defect. In the case of e.g. $H_4PO_2^+$ the latter is only two, and if the process, as described above, involves two neighboring molecules only, the maximum Haven ratio expected for very short H-bond life times should not exceed a value of 2. Although, out of the three phosphorus oxoacids, H_3PO_2 has the strongest H-bonds and the lowest hydrogen bond concentration, which leads to the lowest viscosity, highest molecular diffusion and probably also the lowest hydrogen bond lifetime. From this consideration a Haven ratio of $\sim$2 is feasible, but if more than just two molecules (contact ion pair) were involved in cooperative PTs, the Haven ratio may also be higher.[66] Since at this stage it is difficult to conclusively decide on this issue, without an independent determination of the exact degree of self-dissociation, the transport data for $H = 2$ corresponding to a degree of self dissociation of $\alpha \approx 3.5$ % and $\sim$38 % of the current carried via proton structural diffusion mechanism are included in (Fig. 5.6).[66]

The evaluation of diffusion coefficients from the AIMD simulation is based on the same procedure as in Eq. 4.1. The obtained mean square displacement dependence versus time as well as calculated diffusion coefficients are presented in Fig. 5.7. The estimated and experimental values are summarized and compared in Table 5.1. In the case of phosphonic acid the AIMD calcu-

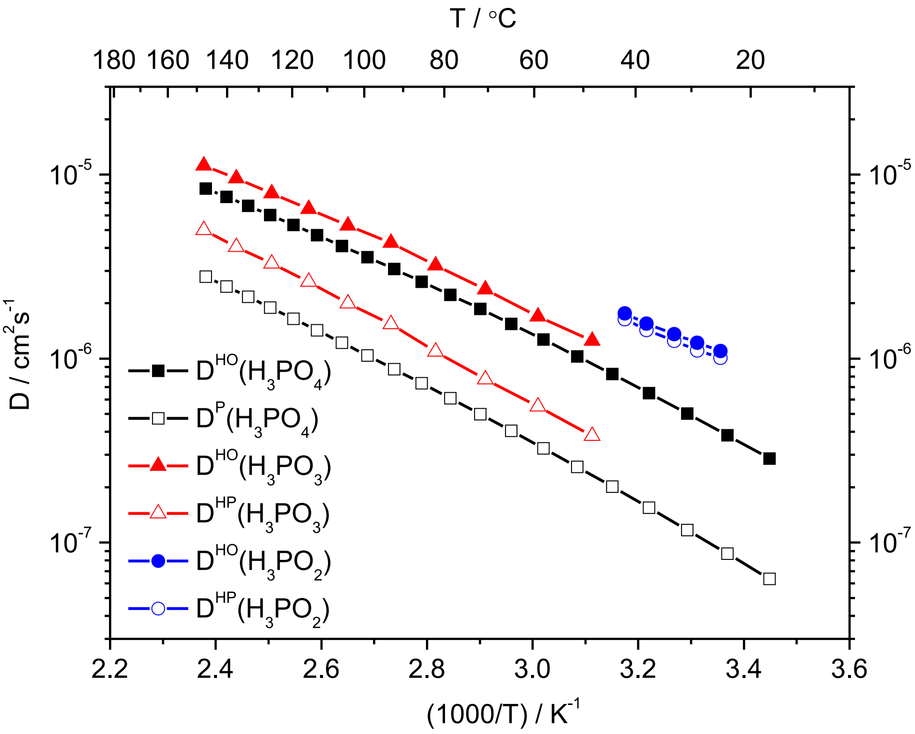

Figure 5.5: Proton and molecular diffusion coefficients determined by the PFG-NMR with respect to temperature.[66]

lated diffusion coefficients show a reasonably good agreement to the experimental ones obtained from the PFG-NMR. Surprisingly, $D^{2\mathrm{H}}_{\mathrm{CPMD}}(\mathrm{H_3PO_3})$ is slightly lower than $D^{2\mathrm{H}}_{\mathrm{CPMD}}(\mathrm{H_3PO_4})$ and contradicts the experimental finding, whereas $D^{\mathrm{mol}}_{\mathrm{CPMD}}(\mathrm{H_3PO_3})$ is higher than $D^{\mathrm{mol}}_{\mathrm{CPMD}}(\mathrm{H_3PO_4})$ (Fig. 5.7; Table 5.1) and complies with the experimental results. This observation might indicate an artefact of the simulation, which could possibly arise from different equilibration histories of two different simulations, since the same kinetic temperature was used in both systems with different melting points (315 K ($\mathrm{H_3PO_4}$) vs. 346 K ($\mathrm{H_3PO_3}$). Nevertheless, the expected decrease in the ratio of proton versus molecular diffusion rates in the simulation of $\mathrm{H_3PO_3}$ is observed: $D^{2\mathrm{H}}_{\mathrm{CPMD}}/D^{\mathrm{P}}_{\mathrm{CPMD}}$ ($\mathrm{H_3PO_4}$) $\approx$ 5.4 vs. $D^{2\mathrm{H}}_{\mathrm{CPMD}}/D^{\mathrm{P}}_{\mathrm{CPMD}}$ ($\mathrm{H_3PO_3}$) ≈ 3.7. The simulated diffusion coefficients for phosphinic acid confirm the experimental prediction of even higher proton diffusion rate than in the case of other acids, as well as much higher hydrody-

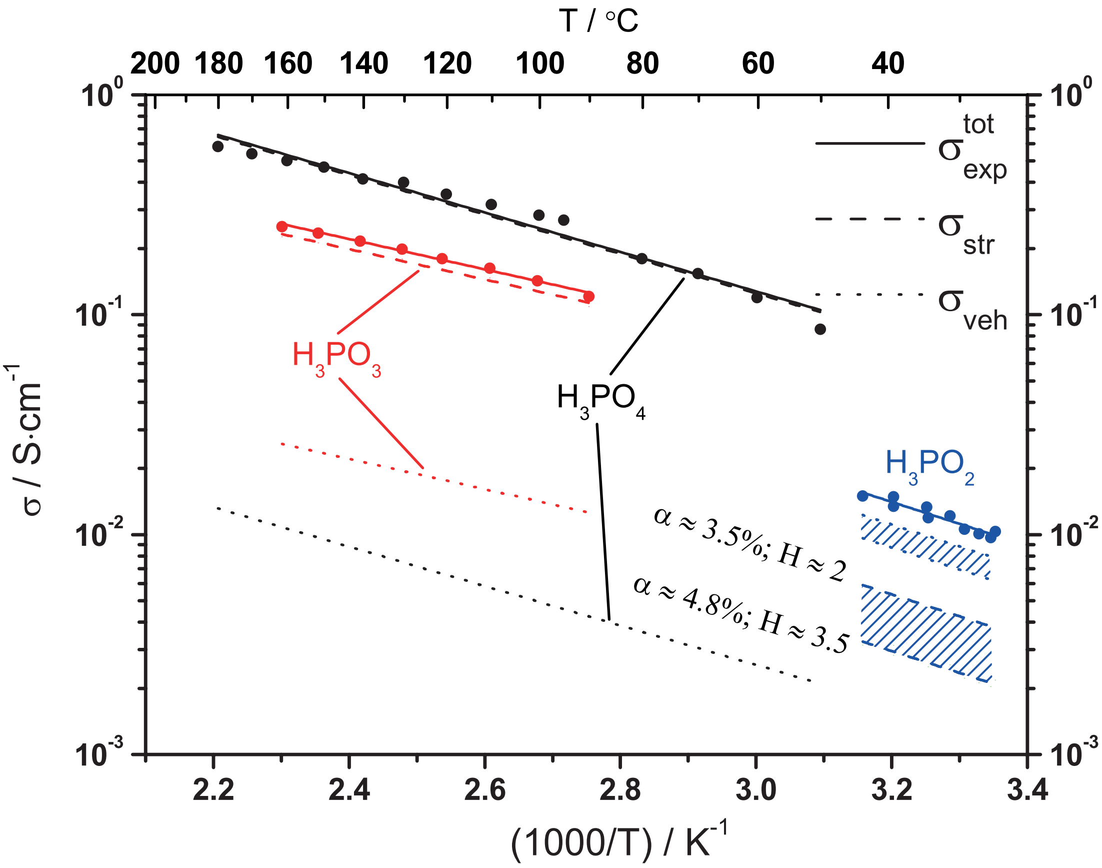

Figure 5.6: Conductivities and the respective contributions due to structural diffusion in H_3PO_4, H_3PO_3 and H_3PO_2.[66]

namic background due to the molecular diffusion of PO_2 species. Although the estimated $D^{2\mathrm{H}}_{\mathrm{CPMD}}$ and $D^{\mathrm{P}}_{\mathrm{CPMD}}$ show reasonably good agreement, similar to the other two cases, their ratio is significantly deviating from the experimental ratio ($D^{2\mathrm{H}}_{\mathrm{CPMD}}/D^{\mathrm{P}}_{\mathrm{CPMD}}$ (H_3PO_2) ≈ 1.56 vs. $D^{2\mathrm{H}}_{\mathrm{CPMD}}/D^{\mathrm{P}}_{\mathrm{CPMD}}$ (H_3PO_2) ≈ 1.1). This probably indicates the fact that even though the proton dynamics is rather well described within this AIMD scheme, the treatment of the hydrodynamic motion of the molecules is still incomplete due to the short simulation time, limited system size, periodic boundary conditions or absence of the van der Waals interactions.

As was already discussed in the previous part on phosphoric acid, within the Debye diffusive model, a rotational diffusion constant D_{rot} can be evaluated from the angular mean square displacement via the relation in Eq. 4.3. The resulting mean angular displacements and the calculated D_{rot} values are presented

System	D^{2H}_{CPMD}	D^{31P}_{CPMD}	$D^{1H}_{PFG-NMR}$	$D^{mol(H-P)}_{PFG-NMR}$
H_3PO_4	$4.03 \cdot 10^{-6}$	$0.75 \cdot 10^{-6}$	$5.40 \cdot 10^{-6}$	$1.15 \cdot 10^{-6}$
H_3PO_3	$3.67 \cdot 10^{-6}$	$0.99 \cdot 10^{-7}$	$5.98 \cdot 10^{-6}$	$2.30 \cdot 10^{-6}$
H_3PO_2	$6.27 \cdot 10^{-6}$	$4.03 \cdot 10^{-6}$	$7.63 \cdot 10^{-6}$	$7.48 \cdot 10^{-6}$

Table 5.1: Calculated and experimental diffusion coefficients at 383 K for phosphonic and phosphinic acids.

in Fig. 5.8. The results are consistent with the notions already applied when discussing the structure of H-bond networks and diffusion coefficients. The calculated rotational diffusion coefficients are very similar for H_3PO_4 and H_3PO_3, reflecting the similar finding for the molecular diffusion coefficients (Fig. 5.5). The $D_{\mathrm{rot}}(H_3PO_4) \approx 0.00775$ rad^2·ps^{-1} and $D_{\mathrm{rot}}(H_3PO_3) \approx 0.0081$ rad^2·ps^{-1} are ∼2.5 times lower than $D_{\mathrm{rot}}(H_3PO_2) \approx 0.0207$ rad^2·ps^{-1}, indicating a much more pronounced rotational freedom in the latter system. Nevertheless, despite the fact that phosphinic acid molecule, on average forms only two H-bonds, its molecular rotational dynamics is still much slower (about one order of magnitude) than that of water.[159,160] This indicates that the very strong H-bonds present in H_3PO_2 are strongly hindering the reorientation of molecules and their rotational freedom.

5.3 Vibrational spectra

In molecular dynamics simulations, the vibrational power spectrum of a classical fluid can be estimated from the Fourier transformed ensemble averaged particle velocity autocorrelation function:

$$C_{vv}(t) = \langle \mathbf{v}(t) \cdot \mathbf{v}(0) \rangle \tag{5.4}$$

$$\tilde{C}_{vv}(\omega) = \frac{1}{2\pi} \int_{-\infty}^{+\infty} dt \exp^{-i\omega t} C_{vv}(t). \tag{5.5}$$

At this point it is important to note that the power spectrum obtained from Eq. 5.5 carries no information about the IR or Raman activities or absorption intensities and only gives the vibrational modes (including the anharmonic contributions) of the system.

The vibrational spectra of all three acid systems are presented in Fig. 5.9.

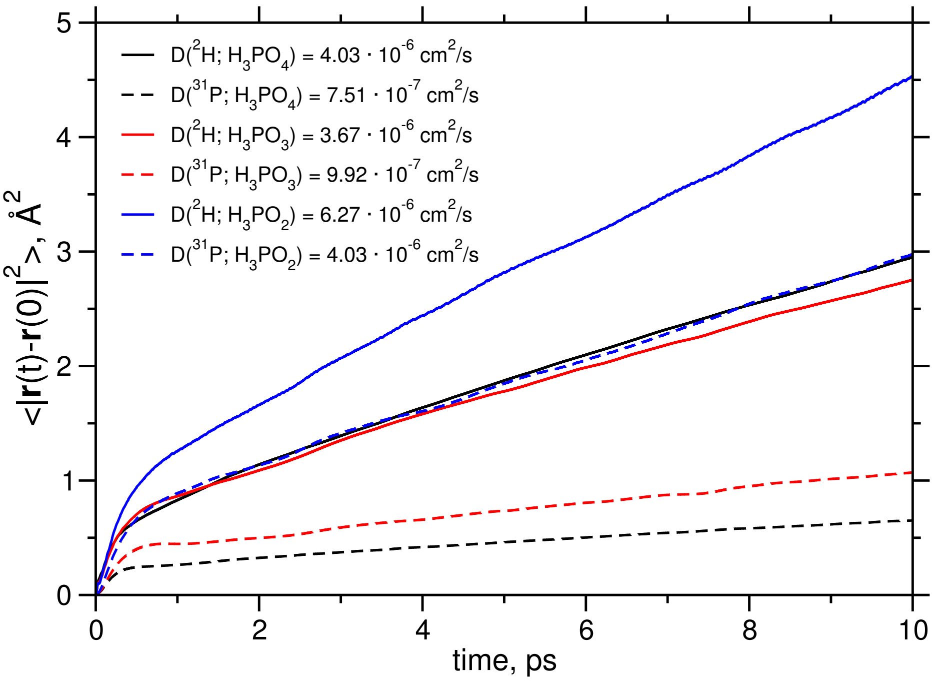

Figure 5.7: The average angular displacement of the P–O bond with respect to time and the corresponding rotational diffusion constants for H_3PO_4, H_3PO_3 and H_3PO_2 at 383 K.

As one can see from Fig. 5.9, the frequency of the O–H stretching frequency is significantly red-shifted as compared to its typical value in liquid water. This shift is primarily due to the deuteration of the system (in comparison $\nu OH \approx$ 3500 cm^{-1} in H_2O vs. $\nu OD \approx 2500$ cm^{-1} in D_2O) as well as the much stronger H-bonding present in phosphorus oxoacids. The effect of the increasing strength of the H-bonds is clearly manifested in the red-shift of the νOH vibration going from D_3PO_4 ($\nu OD \approx 2450$ cm^{-1}) to D_3PO_3 ($\nu OD \approx 2200$ cm^{-1}) and D_3PO_2 ($\nu OD \approx$ 2000 cm^{-1}). An identical trend was found by Leuchs and Zundel[82] from the IR spectra of the non-deuterated acids : $\nu OH \approx 3000$ cm^{-1} (H_3PO_4), $\nu OH \approx 2900$ cm^{-1} (H_3PO_3) and $\nu OH \approx 2650$ cm^{-1} (H_3PO_2). The vibrations at 1750 cm^{-1} and 1700 cm^{-1} for H_3PO_3 and H_3PO_2 respectively, are the corresponding νPD stretching modes and which are absent in the H_3PO_4 spectrum. In the Raman and IR spectra,[180,181] the peaks at ~1100 cm^{-1} were identified as $\nu P = O$, symmetric and asymmetric $\nu_{s,as}PO_n^-$ stretch frequencies. The peaks at ~950 cm^{-1} (D_3PO_4), ~940 cm^{-1} (D_3PO_3) and ~880 cm^{-1} (D_3PO_2) correspond to $\nu_{s,as}POD$ stretching

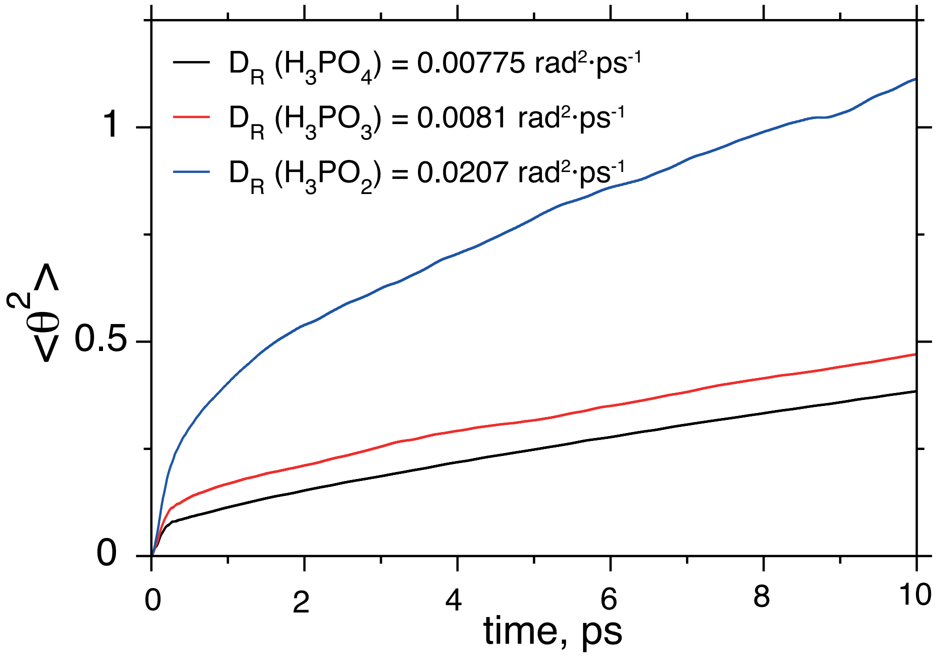

Figure 5.8: Average mean square displacements and corresponding diffusion constants as obtained from the Einstein relation for hydrogen and phosphorus atoms in H_3PO_4 at 383 K.

and δPOD bending modes. The rest of the modes at lower frequencies arise from the O–P–O bending vibrations.

5.4 Proton Transfer Kinetics

In this section, the important time scales for the proton transfer and solvent reorientation are extracted using the same population correlation function (PCF) approach as described in Section 4.4. The obtained PCFs for H_3PO_3 and H_3PO_2 and their triexponential fits are shown in Figs. 5.10 and 5.11. In the case of phosphonic acid, the obtained decay constants for the PCF including all proton transfers (including rattling) are: $\tau_1 = 0.275$ ps, $\tau_2 = 1.78$ ps and $\tau_3 = 7.37$ ps. In the case of phosphinic acid, the obtained decay constants for the PCF including all proton transfers are: $\tau_1 = 0.492$ ps, $\tau_2 = 2.32$ ps and $\tau_3 = 9.32$ ps. Generally, the three constants and especially their ratios for H_3PO_3 and H_3PO_2 are reminiscent of the ones obtained for H_3PO_4, indicating that probably very similar mechanisms

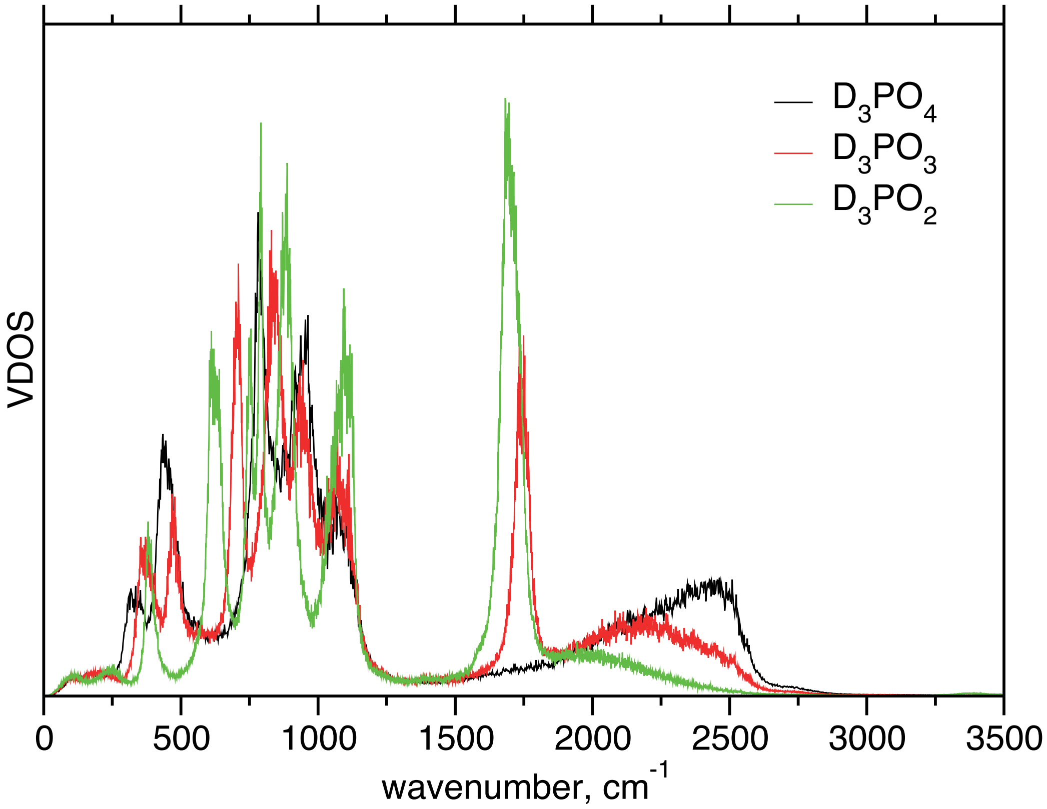

Figure 5.9: Comparison of the vibrational power spectra for H_3PO_4, H_3PO_3 and H_3PO_2.

are governing the proton dynamics in all three acids. Identically to the case of phosphoric acid the fast time constant represents the fast proton rattling, the second τ_2 corresponds to the fast response of the solvent (interprotonic coupling and formation of Grotthuss chains) and the third, slowest to the complete H-bond network reorganization. The results indicate that the time scales of the PT reactions are not only strongly affected by the H-bond strength, but also by the rotational and hydrodynamic background of the molecular system. Although the overall process ($\int C_c(t)dt$) is becoming faster from phosphoric to phosphinic acid, the individual constants corresponding to the build-up (τ_2) and depolarization of polarized chains (τ_3) are slower in less tightly bound H-bond networks.

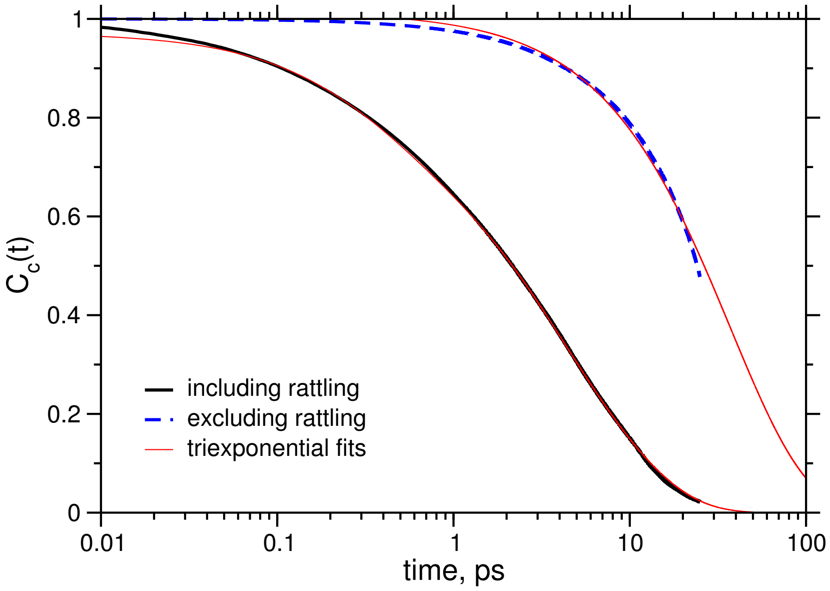

Figure 5.10: Proton transfer population correlation functions (including and excluding proton rattling) and their triexponential fits for H_3PO_3.

5.5 Proton Transfer Energetics

In Fig. 5.12 the free energy profiles along the asymmetric stretch coordinate δ are presented. All the calculated $\Delta A[\delta]$ show distinct double well character. As mentioned in the previous chapter, the PT barriers are predominantly affected by the most probable proton donor–acceptor separation, which is decreasing in a row from phosphoric to phosphinic acid: $r_{OO}(H_3PO_4) > r_{OO}(H_3PO_3) > r_{OO}(H_3PO_2)$. This trend is clearly reflected in the reduction of the PT barrier: $\sim$62 meV (H_3PO_2) $<$ $\sim$71 meV (H_3PO_3) $<$ $\sim$80 meV (H_3PO_4). Nuclear quantum effects might lower these barriers slightly, but as already noted, the effects are expected to be small and the protons are undergoing transfer close to the full adiabatic limit.[182,183]

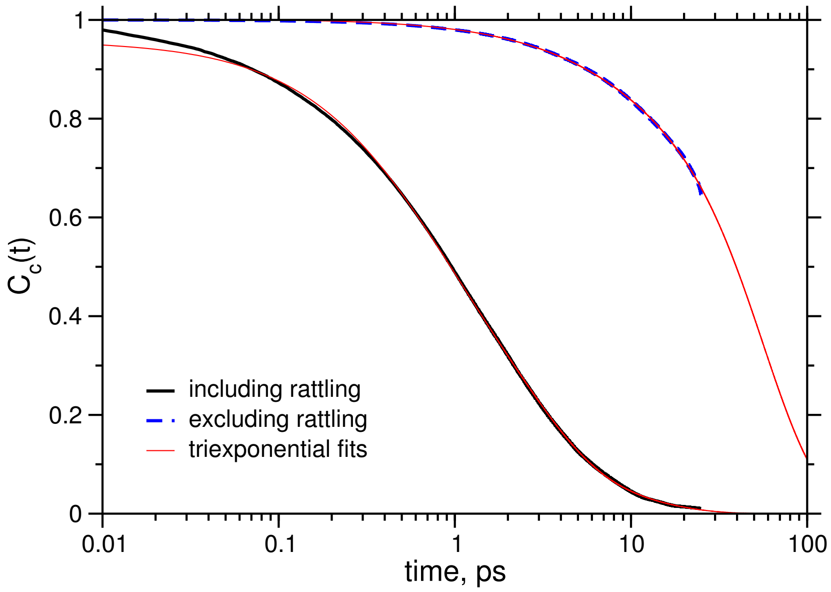

Figure 5.11: Proton transfer population correlation functions (including and excluding proton rattling) and their triexponential fits for H_3PO_2.

5.6 The Structure and Energetics of Charged Species

In this section the structure and energetics of protonic defects (species with carrying excess and deficient protons) are analyzed. Identically to the analyses carried out on phosphoric acid, each proton is formally assigned to its nearest neighbor oxygen atom and subsequently to a particular PO_3 or PO_2 unit. After this assignment, one can even formally define the 'degree of self-dissociation' in each acid. However, this kind of definition still includes all the transiently transferring protons, which do not contribute to the actual charge separation and self-dissociation. One way to exclude these events and get a better estimate for the degree of self-dissociation is to select a certain δ cut-off value and only count those protons which are truly associated with a certain phosphate species, excluding those transiently shared by two species. Protons with δ approaching 0 are being transferred, therefore one can select a certain value for $|\delta_{\text{cut-off}}|$ which selects only those protons which are far from the PT transition state and can be unambiguously assigned to a particular PO_4 unit. The results for two different $\delta_{\text{cut-off}}$

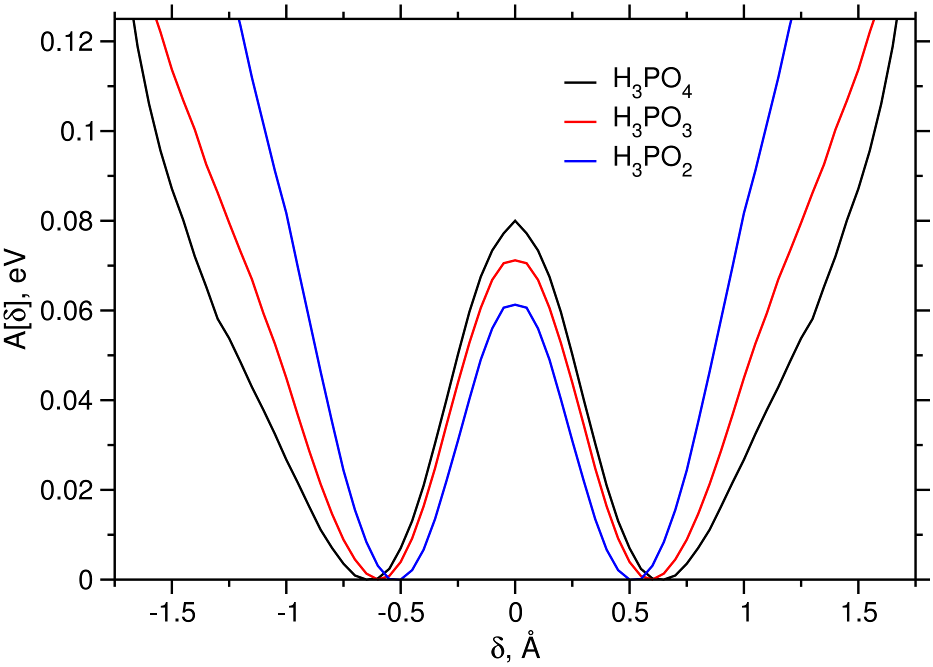

Figure 5.12: Free energy profiles $A(\delta)$ along the proton transfer coordinate δ for H_3PO_4, H_3PO_3 and H_3PO_2.

values: 0.0 Å (all protons are unambiguously assigned to phosphate species) and 0.3 Å (protons close to the PT transition state are excluded), are presented in Table. 5.2. These values correspond to the fractions of $H_nPO_x^y$ species having uncompensated protonic charge (excess or deficient protons). Although, this approach to estimate the charge carrier concentration is rather crude, it still shows some interesting features, which can be compared to the available experimental data. The only available experimental value of this property is that for phosphoric acid: ~7.4%. From Table. 5.2, one can see that the charge carrier concentration is systematically decreasing from H_3PO_4 to H_3PO_2. This reflect the previously, discussed finding that even though the proton mobility is increasing from H_3PO_4 to H_3PO_2, the measured conductivities show an opposite trend and suggest that the effective charge carrier concentration is significantly reduced. Nevertheless, the simulated values are still in a reasonably well agreement, especially if the transiently shared protons are excluded from the analysis.

The next question addressed in this section is: what is the extent of the H-bond network contraction around the regions carrying excess protonic charge in

$\delta_{\mathrm{cut-off}}$, Å	H_3PO_4	H_3PO_3	H_3PO_2
0.0 Å	25.6 %	20.1 %	8.1 %
0.3 Å	11.3 %	7.5 %	1.9 %

Table 5.2: Calculated fractions of molecules with uncompensated protonic charge (having excess or deficient protons) for H_3PO_4, H_3PO_3 and H_3PO_2 systems and different proton assignment criteria $\delta_{\mathrm{cut-off}}$.

H_3PO_3 and H_3PO_2? The calculated $g_{\mathrm{OO}}(r)$ RDFs for phosphonic and phosphinic acids with respect to the protonation of PO_x species are presented in Figs. 5.13 and 5.14. Identically to the case of phosphoric acid, the other two acids also feature a marked contraction of the H-bond network around the positive defects. In H_3PO_3 for instance: $r_{\mathrm{OO}}(H_4PO_3^+) \approx 2.47$ Å $< r_{\mathrm{OO}}(H_2PO_3^-) \approx 2.53$ Å $< r_{\mathrm{OO}}(H_3PO_3) \approx 2.55$ Å (Fig. 5.13) and the running coordination numbers of the first solvation shell of each species: $n_{\mathrm{OO}}(H_4PO_3^+) \approx 3.2 < n_{\mathrm{OO}}(H_3PO_3) \approx 4.0 < n_{\mathrm{OO}}(H_2PO_3^-) \approx 5.1$ (Fig. 5.13). In the case of H_3PO_2: $r_{\mathrm{OO}}(H_4PO_2^+) \approx 2.44$ Å $< r_{\mathrm{OO}}(H_2PO_2^-) \approx 2.46$ Å $< r_{\mathrm{OO}}(H_3PO_4) \approx 2.51$ Å and the running coordination numbers: $n_{\mathrm{OO}}(H_4PO_2^+) \approx 2.0 < n_{\mathrm{OO}}(H_3PO_2) \approx 2.0 < n_{\mathrm{OO}}(H_2PO_2^-) \approx 2.6$ (Fig. 5.14). The results show that all three acid systems show a similar shortening of H-bonds in the vicinity of charged species, the most severe being around the region having an excess number of protons. Phosphoric and phosphonic acids show an equivalent asymmetry of their solvation shells, with $H_4PO_x^+$ displaying undercoordination and $H_2PO_x^-$ a noticeable overcoordination. Although, H_3PO_2 features the same trend in the H-bonding strength (just the least pronounced), its solvation asymmetry is not visible anymore. This could be explained by the fact that contrary to phosphoric and phosphonic acids or even water, phosphinic acid, already, has an excess number of proton acceptor sites and even nominally neutral species are on average undercoordinated (only one acceptor site occupied).

It is also interesting to look at the PT energetics around the $H_4PO_x^+$ and $H_2PO_x^-$ species. The PT free energy profiles calculated using the same procedure as in Eq. 4.8 taking into account only those protons belonging to the charged defects are shown in the Fig. 5.15 and 5.16. In both cases, the computed free energy profiles show very similar trends as those of H_3PO_4: the PT barrier around the positive ion is the lowest and the one for the protons in the vicinity of a negative site in between the 'positive' and 'overall' PT barrier heights. The PT barriers for $H_4PO_x^+ \cdot (H_3PO_4)_n$ in phosphonic and phosphinic acid systems are significantly below the average thermal energy of the simulation with H_3PO_2 showing an almost single well PT potential (Fig. 5.16) for protons bound by $H_4PO_2^+$. The latter behavior in the case of aqueous protonic defect simulations becomes apparent only after introducing appropriate treatment of nuclear quantum effects.[9,167]

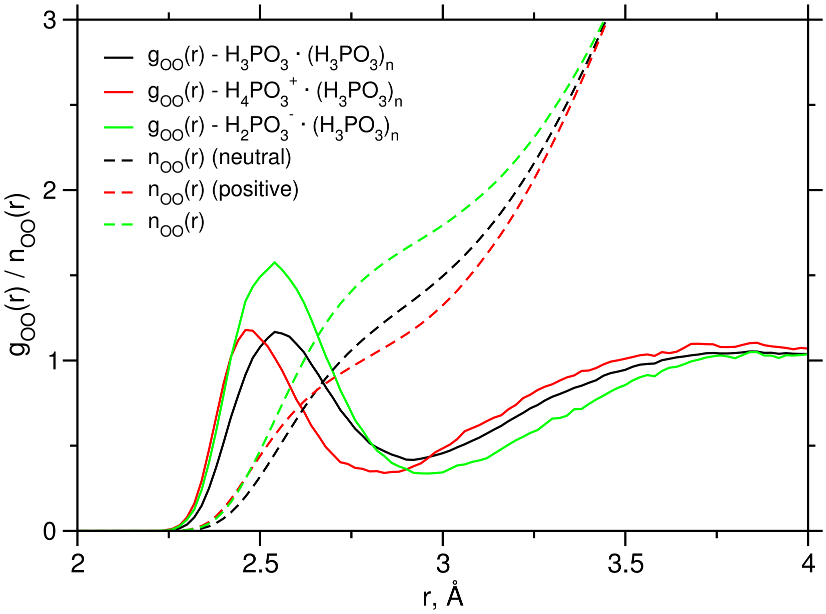

Figure 5.13: g_{OO} and running coordination numbers (n_{OO}) of oxygen atoms for H_3PO_3 in its various states of protonation.

5.7 On the Degree of Protonation

In this section the properties of the H-bond networks of phosphonic and phosphinic acids are discussed. As already mentioned in the previous chapter, it is only the phosphoric acid, which has an excess ratio of proton donor versus acceptor sites resulting in frustrated H-bond network. The importance of this property for the overall proton transport mechanism was underlined in the discussion of proton transport mechanism in H_3PO_4. The approach involved here is identical to the one used in Section 4.7. The parameters in Eq. 4.9 were fine-tuned in the

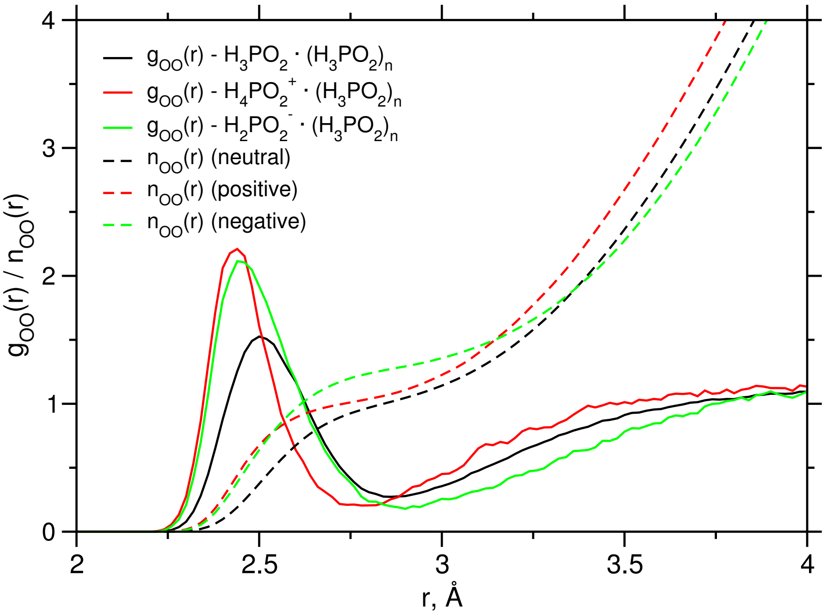

Figure 5.14: g_{OO} and running coordination numbers (n_{OO}) of oxygen atoms for H_3PO_2 in its various states of protonation.

same way as in the case of phosphoric acid in order to reproduce the average oxygen protonations of 0.67 and 0.5 in phosphonic and phosphinic acids, respectively. From Fig. 5.17, one can immediately see that all oxygen atoms form a continuous population of various H-bond configurations with respect to their degree of protonation. The bond-order distribution curves for oxygen populations show very similar structure for all three acid systems (Fig. 5.17). The reduction of the fraction of proton donors in the H-bond networks is manifested by the shift of the first peak towards even lower oxygen protonations in phosphonic and phosphinic acids. The same trend is observed in the proton donating oxygen peaks as well. However, the profiles still indicate a significant presence of oxygens with a higher than unity protonation. The latter indicates that even in these “non intrinsically frustrated” H-bond networks, the situations where an already proton donating oxygen accepts another H-bond are forming due to the dynamic disorder. The latter was also anticipated by Leuchs and Zundel from the appearance of a shoulder in the νOH IR absorption band of liquid H_3PO_3 and H_3PO_2. Moreover, in the case of H_3PO_2 (Fig. 5.17 (blue line)) the presence of these sites even results in a finite concentration of non-protonated oxygen atoms (blue curve is not equal to

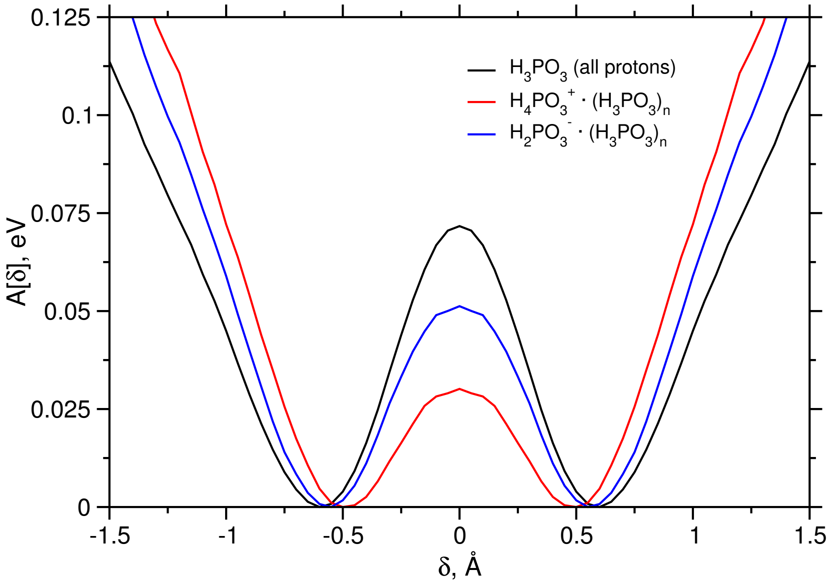

Figure 5.15: Free energy profiles $A(\delta)$ along the proton transfer coordinate δ for H_3PO_3, $H_4PO_3^+$ and $H_2PO_3^-$.

0 for $\sum n_i = 0$). In principle these frustrated configurations must play a similar role as in H_3PO_4 by facilitating the efficient solvent depolarization and dielectric relaxation and give rise to proton conductivity. The actual mechanisms are more thoroughly addressed in the following sections.

5.8 Interprotonic Coupling

The proton dynamics in phosphonic and phosphinic acid is characterized by an even more pronounced rattling of protons than in phosphoric acid, which mainly arises from the presence of stronger H-bonds (Sec. 5.4). For the case of phosphoric acid we already proved that a dynamical response mainly driven through the electrostatic proton-proton interaction accompanies the PT events, leading to correlated PTs and the formation of polarized chains spanning several molecular lengths. In this part, the same kind of methodology and line-of-thought is followed to address these questions for the other two acid systems.

Figs. 5.18 and 5.19 depict the g_{HH} RDFs resolved in r and δ, containing information about the spatial distribution of protons with respect to their position in

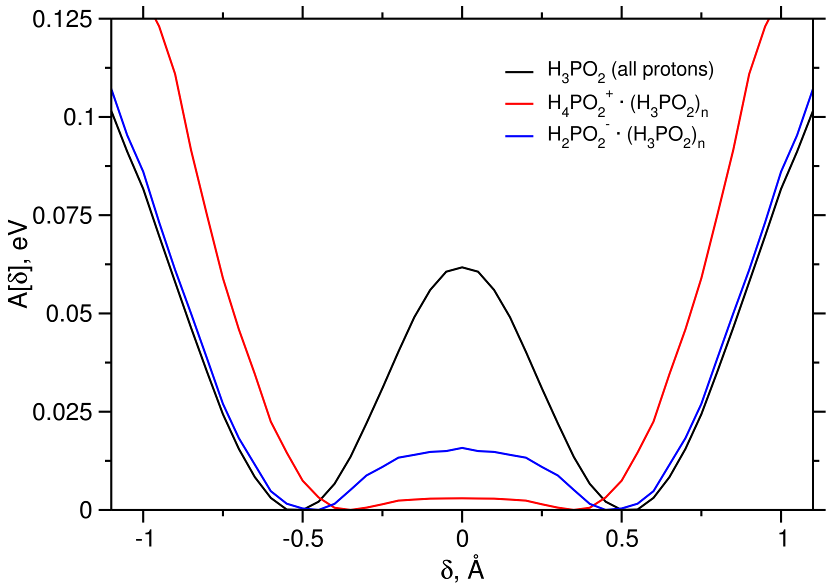

Figure 5.16: Free energy profiles $A(\delta)$ along the proton transfer coordinate δ for H_3PO_2, $H_4PO_2^+$ and $H_2PO_2^-$.

the H-bond (δ). As one can see, both systems feature a significant response of the protonic subsystems upon the PT process. The $g_{HH}(r, \delta)$ for the case of H_3PO_3 clearly resembles the one calculated for H_3PO_4 (Fig. 4.13). In phosphonic acid, only the position of the main peak is slightly shifted towards larger separations (3.5 Å vs. 3.9 Å), reflecting the lower average density of protons. Nevertheless, the main peak at ∼3.9 Å in H_3PO_3 increases for $\delta \to 0$ in a similar fashion as in H_3PO_4. The calculated $g_{HH}(r, \delta)$ for phosphinic acid, clearly exhibits a different pattern from those found for the other two systems. In this case, the main peak is much more diffuse and does not show a significant variation in height with respect to δ. However, the position of the main peak is significantly shifted towards shorter proton-proton separations (onset shifts from ∼4.0 to ∼3.7 for $\delta \to 0$). This shift most probably, can be explained by stronger contraction of the H-bonds around the species carrying excess protonic charges in H_3PO_2 (Fig. 5.14), as well as the fact that the overall density of protons is significantly lower (there is on average only one proton per PO_2 species).

In principle, these results suggest that PTs are obviously strongly correlated to the dynamics of surrounding protons these two acids (especially in H_3PO_3) as well.

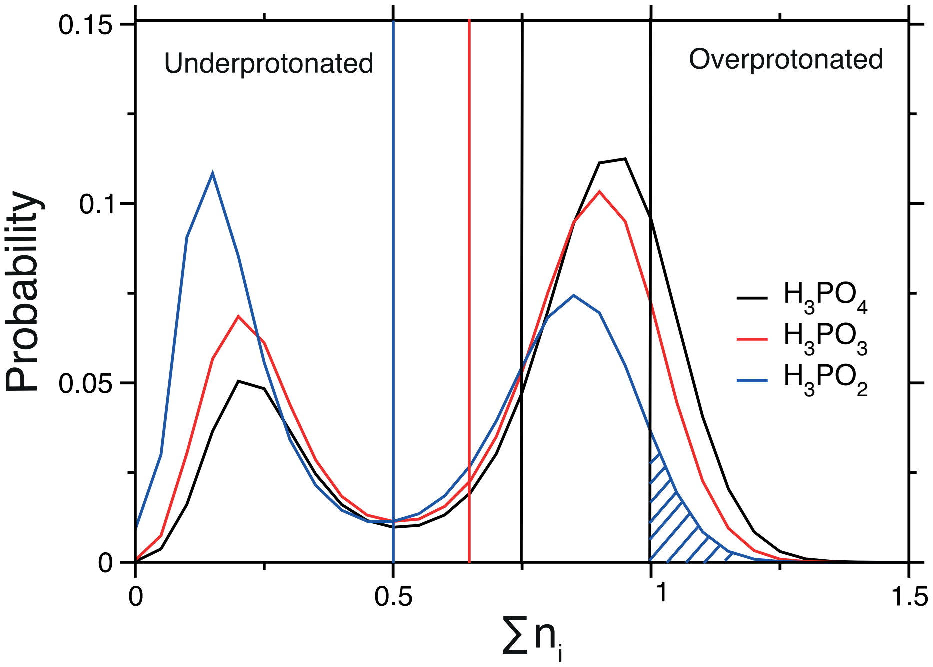

Figure 5.17: The probability distribution of various oxygen protonation states defined as the sum of individual bond-orders due to surrounding protons ($\sum n_i$).

In the following section, the questions whether this behavior can lead to several correlated PTs and the formation of extended polarized chains is addressed.

5.9 On the Formation of Grotthuss Chains and Proton Conduction Mechanisms

It was previously described that *special* configurations forming in phopshoric acid due to interprotonic coupling could seed up the formation of extended Grotthuss chains without a significant solvent reorganization at *slow* dipolar level. Concerning this process in H_3PO_3 and H_3PO_2 on a qualitative level, there are obviously two effects competing for and against the formation of extended polarized chains: stronger and shorter H-bonds should result in an even more pronounced protonic polarization, whereas stronger dynamical background and dipolar nature of the medium ($\mu_{\text{gas}}H_3PO_3 \approx 1.5$ D and $\mu_{\text{gas}}H_3PO_2 \approx 2.5$ D) should disrupt this process. The possibility of mutual protonic polarizability and correlated motion in

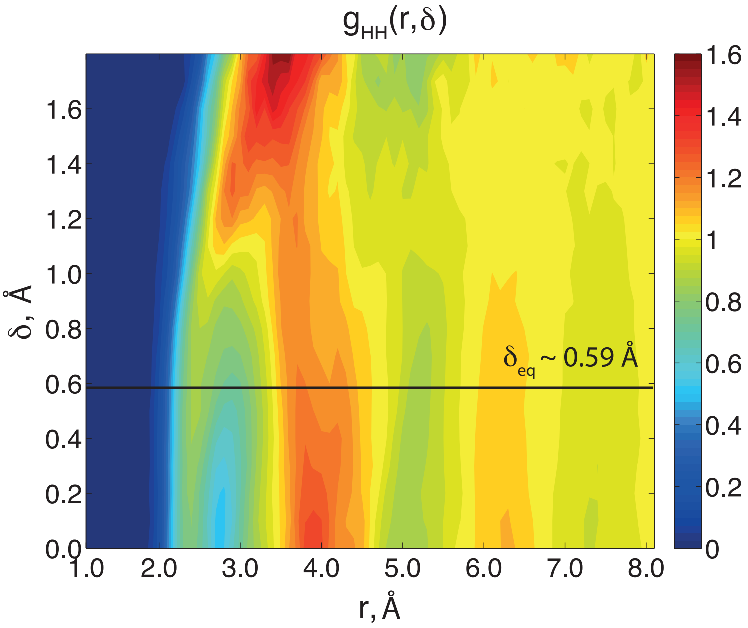

Figure 5.18: $g_{HH}(r, \delta; H_3PO_3)$ radial distribution function resolved in r and δ, containing information about the spatial distribution of protons with respect to δ (δ_{eq} is the equilibrium value in the simulation).

extended molecular aggregates in these two acid systems was also suggested by Leuchs and Zundel in their IR study.[82]

AIMD simulations enable the determination of existence and average length of extended Grotthuss chains. In order to extract these quantities for phosphonic and phosphinic acid systems the same correlation function approach developed in Sec. 4.9 is employed. The calculated proton coupling correlation functions $C(n)(H_3PO_3)$ and $C(n)(H_3PO_2)$ are presented in Fig. 5.20. The probability of forming extended Grotthuss chains in phosphonic and phosphinic acids increases with time; for an increment of $\tau_{res} = 50$ fs, Fig. 5.20 indicates ~10% probability for forming a Grotthuss chain of four phosphite or hypophosphite species connected by three H-bonds (see also Fig. 5.21 (a)). Clearly, the degree of coupling between the protons within the neighboring H-bonds is significantly reduced, despite the stronger H-bonds and lower concentration of frustrated sites which also contribute to the destructive solvent response on the formation of chains comprising polarized H-bonds. Interestingly, both H_3PO_3 and H_3PO_2 show an almost identical decay of $C(n)$ for protons n H-bonds away from each other, with H_3PO_3

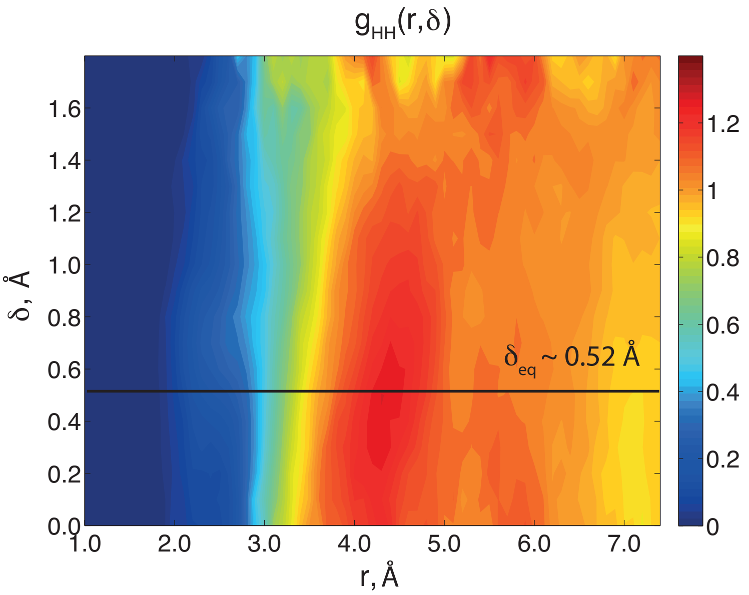

Figure 5.19: $g_{\mathrm{HH}}(r, \delta; \mathrm{H_3PO_2})$ radial distribution function resolved in r and δ, containing information about the spatial distribution of protons with respect to δ (δ_{eq} is the equilibrium value in the simulation).

showing slightly higher probability for forming chains of three H-bonds and faster decay in the probability to form longer ones. The important point is that the probabilities for Grotthuss chain formation in H_3PO_3 and H_3PO_2 beyond three H-bonds are significantly lower than in H_3PO_4 and their slight variations can be attributed to the statistical noise present in the simulations.

Identically to the case of phosphoric acid, these chains are terminated by the $H_2PO_{3-2}^-$ and $H_4PO_{3-2}^+$ species. The latter can more easily propagate through the H-bond network (Figs. 5.15 and 5.16; Fig. 5.21 (a) and (b)), while the former are less mobile. In order to complete the charge separation/self-dissociation, the central part of the polarized H-bonded chain connecting both defects must be depolarized, as has been previously emphasized for the self-dissociation of phosphoric acid (Sec. 4.10) or water.[177] Without this depolarization, the charge separation can be easily reversed through the intact chain. The depolarization must take place in the center of the chain, since the terminal H-bonds already have the proper orientation with respect to the terminating charges. At first glance, it might seem that the presence of even stronger H-bonds in these systems would

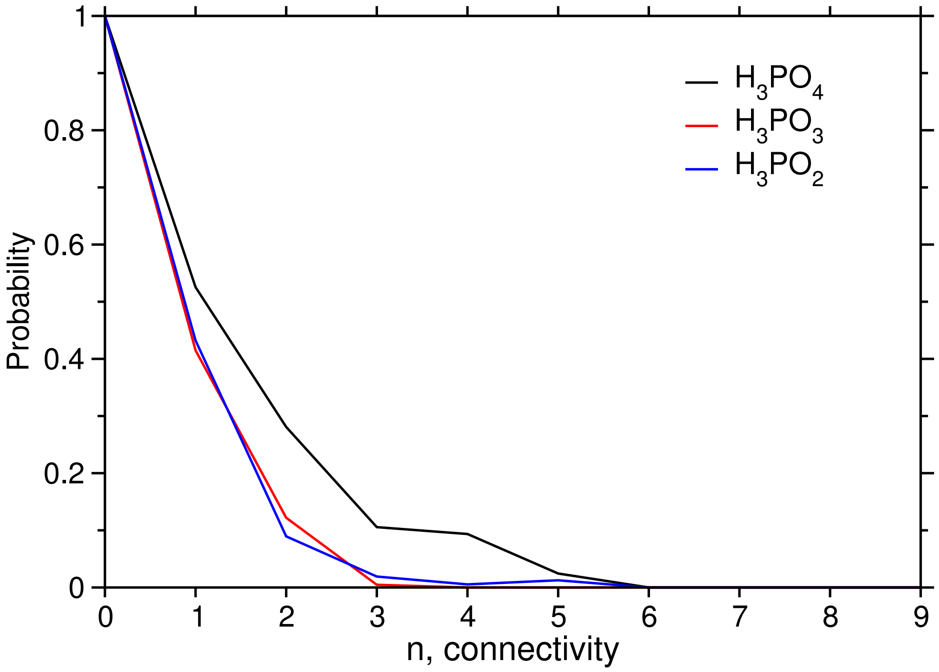

Figure 5.20: Proton coupling correlation function $C_{pc}(n)$ as a function of connectivity n. Only the H-bonds with $\delta \leq 0.1$ Å ($\sim 2.0\%$ of the total number for H_3PO_3 and $\sim 3.5\%$ for H_3PO_2) are considered as undergoing PT. The time increment τ_{res} sets the finite relay time for the system to respond to correlated PTs ($\tau_{res} = 50$ fs).

prevent efficient solvent reorientation processes. In the case of H_3PO_4, which has a very peculiar H-bond network topology, the solvent reorganization is facilitated by the intrinsic presence of frustrated sites. However, as is shown later and was already predicted by Leuchs and Zundel in their IR study, the "less strongly bound OH groups" are able to form transiently due to the liquid disorder and their concentration increases from phosphinic to phosphoric acid (see also Sec. 5.7). As is shown later, the formation of 'frustrated' sites, where the same oxygen atom simultaneously acts as a donor and an acceptor, in H_3PO_3 and H_3PO_2 essentially plays the same role in the solvent reorientation process as in H_3PO_4 (Fig. 5.21).

Solvent relaxation (depolarization) is initiated when one of the solvent H_3PO_{3-2} molecules forms a new H-bond by donating a proton to an oxygen atom in the chain (Fig. 5.21 (c)). This proton is transiently transferred to the new acceptor (Fig. 4.17 (c)), which causes a strong coupling to the original H-bond in the chain. In this way, the original H-bond is effectively weakened since the same oxygen atom must simultaneously be a proton donor and acceptor. This weakened H-bond can easily break and, through a rapid torsional rotation around the P–O bond axis, reorient, forming a new H-bond with a less acidic (protonated) oxygen in the surrounding solvent molecules (Fig. 5.21 (d)). This relaxation completes the charge separation, and subsequent PTs close to charged species (mostly $H_4PO_{3-2}^+$) can be considered already a part of the "independent"migration of these charged species. The latter process does not hinder the formation of new chains and reorientation of solvent molecules until the oppositely charged species meet, leading to a neutralization step. Mechanistically, this neutralization event is again simply the complement of the self-dissociation process.

Obviously, the main features of the proton transport mechanism in phosphonic and phosphinic acids are similar to those already described for phosphoric acid. Nevertheless, the systematic changes in molecular properties of these systems also result in pronounced differences at the macroscopic level. The increasingly stronger H-bonds and protonic polarizabilities in H_3PO_3 and H_3PO_2 compensate for the stronger dynamical background and dipolar coupling resulting in formation of extended Grotthuss chains, which are only slightly shorter than those in the case of H_3PO_4. Although, H_3PO_3 and H_3PO_2 do not posses the intrinsically frustrated H-bond networks, the situations where the same oxygen atoms must act as proton donors and acceptors, form due to the disorder in protonic and molecular subsystems. The importance for these sites for the solvent depolarization and in turn for the overall stability and mobility of protonic defects was emphasized for all three acid systems. Their concentration decreases in a row from phosphoric to phosphonic to phosphinic acid and follows the trend observed for the proton conductivities. This means that although the correlated proton transfers and formation of polarized chains are essential ingredients for the emergence of intrinsic transport of protonic defects, the efficient solvent reorientation is no less important.

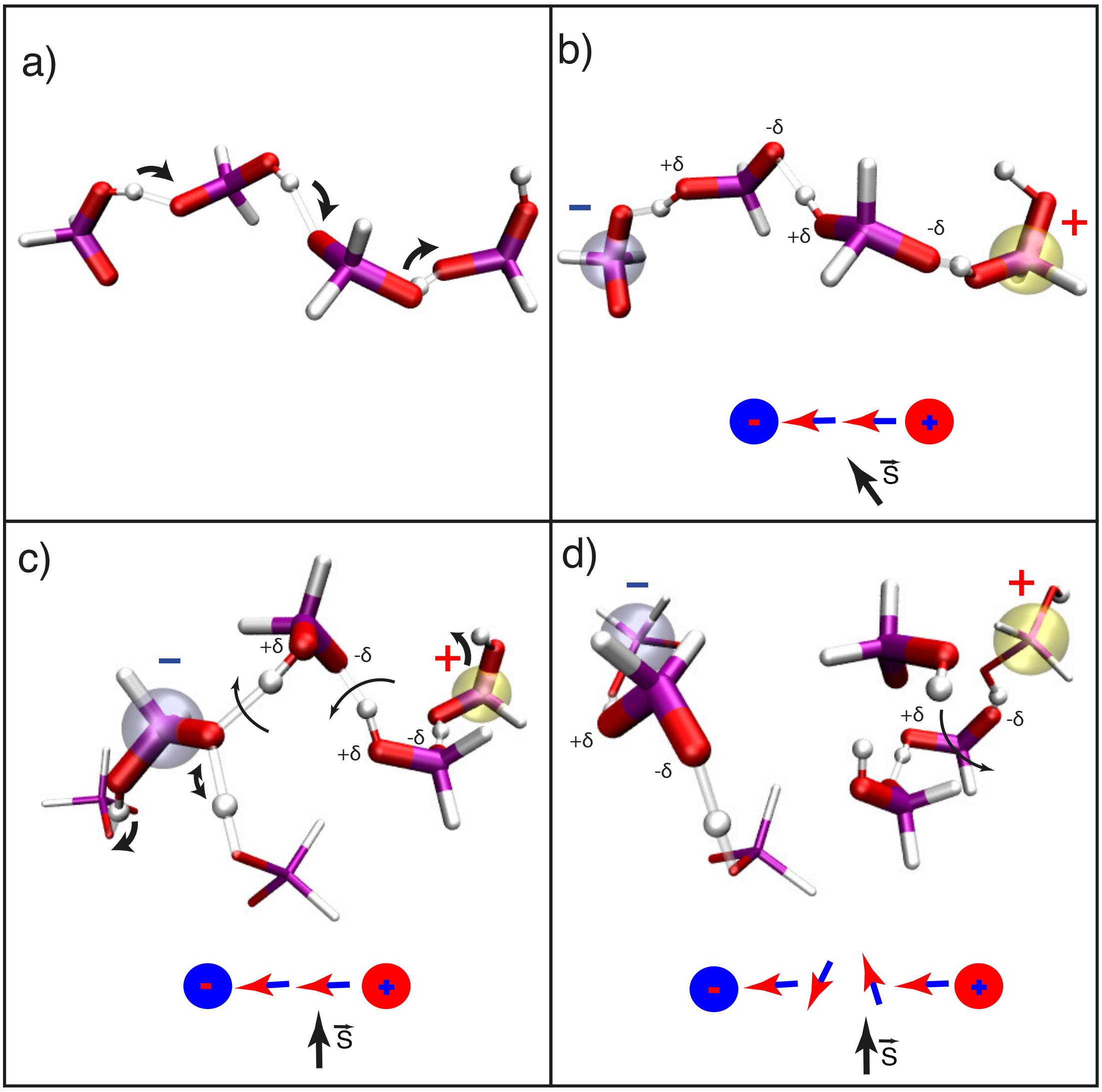

Figure 5.21: Snapshots of the elementary the proton structural diffusion steps in H_3PO_2. The schemes bellow the molecular structures show the ions and interchain dipole orientations, with the solvent being represented by a generalized coordinate $\vec{S}$. The charged ion pair is indicated with (+) and (-), the partial charges on the oxygen atoms are marked by $+\delta$ and $-\delta$. The arrows denote the proton hops and molecular reorientations.

6

Phosphoric acid and water mixtures

In this chapter the results of AIMD simulations on phosphoric acid and water mixtures are presented. Two systems corresponding to different phosphoric acid – water ratios were chosen: the first one represents the intrinsic condensation equilibrium existing in neat phosphoric acid (50 H_3PO_4 molecules + 2 $H_4P_2O_7$ molecules + 2 H_2O, System I), the second one – 85% wt. commercially available phosphoric acid electrolyte (36 H_3PO_4 molecules + 36 H_2O molecules, System II). Two microcanonical runs of 25 and 50 ps were obtained for System I and System II, respectively. The structure and dynamics of water in mixtures with phosphoric acid is an intriguing problem since water is the only “dopant” which does not disrupt the H-bond network of phosphoric acid and does not destroy its ability to transport protonic charge carriers. System I was selected in order to investigate the very low concentration of water molecules and their acid-base equilibria, present in nominally dry phosphoric acid. The H_3PO_4 and water mixtures are not only interesting from a fundamental point of view, but are also relevant for understanding the biological role of phosphates, which are always in equilibrium with surrounding water,[184] or even the proton transport mechanisms on the surface of phospholipid bilayers.[185–188] The discussion in this chapter is started by evaluating the structural and dynamical properties from the simulations and comparing them to the experimental data available in the literature.

Afterwards, a number of experimentally unavailable properties are estimated. Finally the discussion is turned towards the structure and transport mechanisms of protonic defects. A snapshot from an equilibrated simulation of System II is presented in Fig. 6.1.

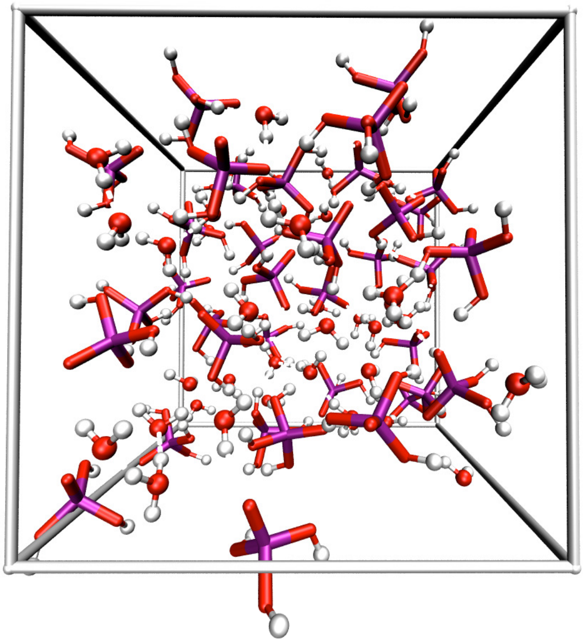

Figure 6.1: A snapshot of a typical configuration from an equilibrated simulation box containing 36 H_3PO_4 and 36 H_2O molecules.

6.1 Structural Properties

The discussion of the phosphoric acid – water mixtures is commenced by evaluating the radial pair distribution functions and comparing them to the experimental data, available in the literature.[189] The simulated and experimental total RDFs (g_{XX}) for System II are presented in Fig. 6.2. The general shape of the two curves agrees very well, however the two RDFs are shifted with respect to each other, the experimental g_{XX} indicates slightly weaker bonds. Surprisingly, all bonds lengths obtained from the simulation show a systematic, equally strong, deviation from the experimental data. Since, the systems described in the previous chapters of this work, show a much better agreement to the neutron scattering data, it is possible that this shift could be an artifact of the post-experimental data treatment procedures.[189] Moreover, the structure factors obtained by X-ray and neutron scattering experiments in the same study also show significant discrepancies.[189]

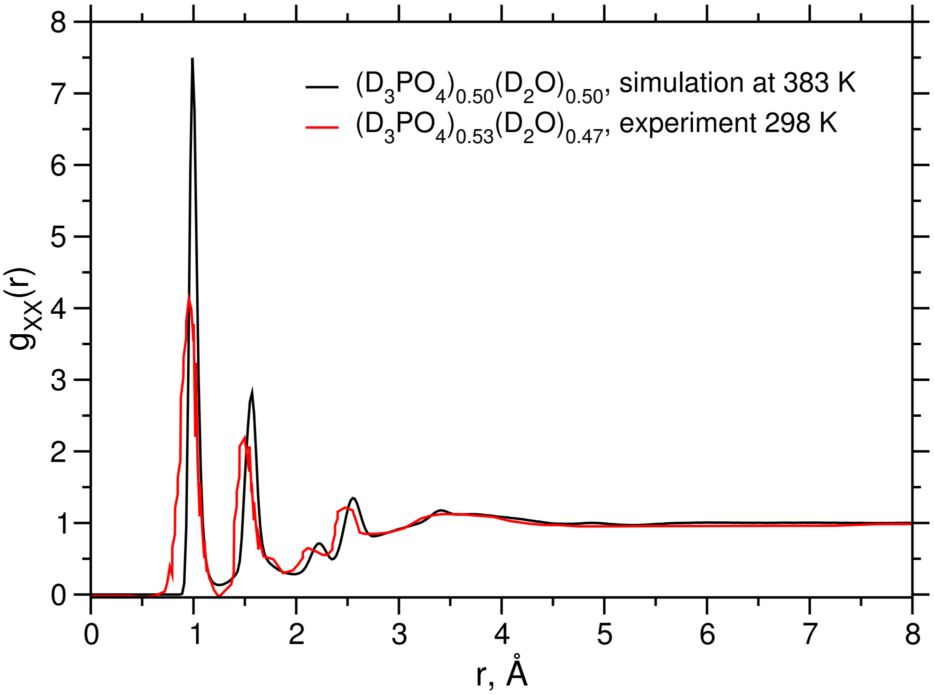

Figure 6.2: The total simulated radial pair distribution function g_{XX} (black) (where X = P, O and H) and g_{XX} (red) from the neutron scattering study of Kameda et al.[189]

Fig. 6.3 shows the contributions of various atom pairs to the total RDF. Most of the results correspond to System II, and only the important features of System I, e.g. representing the coordination of water molecules, are depicted. Fig. 6.3 (top) shows the g_{HH}(System II) superimposed with $g_{\mathrm{HH}}(H_2O)$ and $g_{\mathrm{HH}}(H_3PO_4)$. The first peak at 1.55 Å is a contribution from the intramolecular H–H of water molecules, the second one at ∼2.2 Å comes from the two hydrogen atoms forming two H-bonds with the same acceptor oxygen atom of the phosphate, and the third one at ∼3.65 Å is due to the hydrogen atom located on the same phosphate unit. An important feature of the g_{HH}(System II) (Fig. 6.3 (top)) is the shifting and lowering of the second peak as compared to pure water, indicating that, on average, the H-bonds are stronger in System II and water molecules are accepting fewer H-bonds (a significant fraction of H_2O molecules are in H_3O^+ state). The g_{OH} (Fig. 6.3 (middle)) reveals an even more interesting feature of the H-bonding in H_3PO_4–H_2O systems: the overall structure of g_{OH}(System II) is virtually identical to $g_{\mathrm{OH}}(H_3PO_4)$ ($g_{\mathrm{HH}}(H_2O)$ is given for comparison). This indicates that H-bonds (the second peak in g_{OH}) in System II are much stronger than those of water and essentially as strong as those of phosphoric acid, although if one tries to evaluate the volume contraction by comparing the experimental densities of System II ($\rho = 1.680 g/cm^3$) and pure H_3PO_4 ($\rho = 1.885 g/cm^3$), there is only a ~2% deviation from the ideal mixing. These features and especially the H-bond strength suggest that general proton dynamics as well as proton transport mechanisms in these systems should be much more similar to those in phosphoric acid than to those in water. The origin for this observation must lie in the electrostatics of the system: although the acidities of the systems are not so different, a significant fraction of water molecules must be in hydronium state and contract the H-bond networks in their vicinity. The same trends are visible in the heavy atom correlation functions g_{XX} (Fig. 6.3 (bottom)). The P–O, $O_{\mathrm{P,W}}$–$O_{\mathrm{P,W}}$ (H-bonds) are identical in System II and neat H_3PO_4 and different from the pure water peaks. The individual contributions to g_{OO} show pronounced differences between System II and water as well, e.g. $g_{\mathrm{O_wO_w}}$(System II) is shifted towards lower values whereas $g_{\mathrm{O_PO_W}}$ (System II) and $g_{\mathrm{O_PO_P}}$ (System II) show similar bonding strengths as $g_{\mathrm{OO}}(H_3PO_4)$. Furthermore, only a very slight difference is seen between the average phosphate separation between System II and phosphoric acid (g_{PP} in Fig. 6.3 (bottom)). All these observations suggest that the molecular and especially the H-bond structure of phosphoric acid solution, even at the 50% mol. water concentration, is virtually unperturbed by the presence of water molecules. This strongly implies that the analysis of the molecular details of proton transport mechanisms in these systems must follow the same line of thought as previously developed for three neat phosphorus oxoacids.

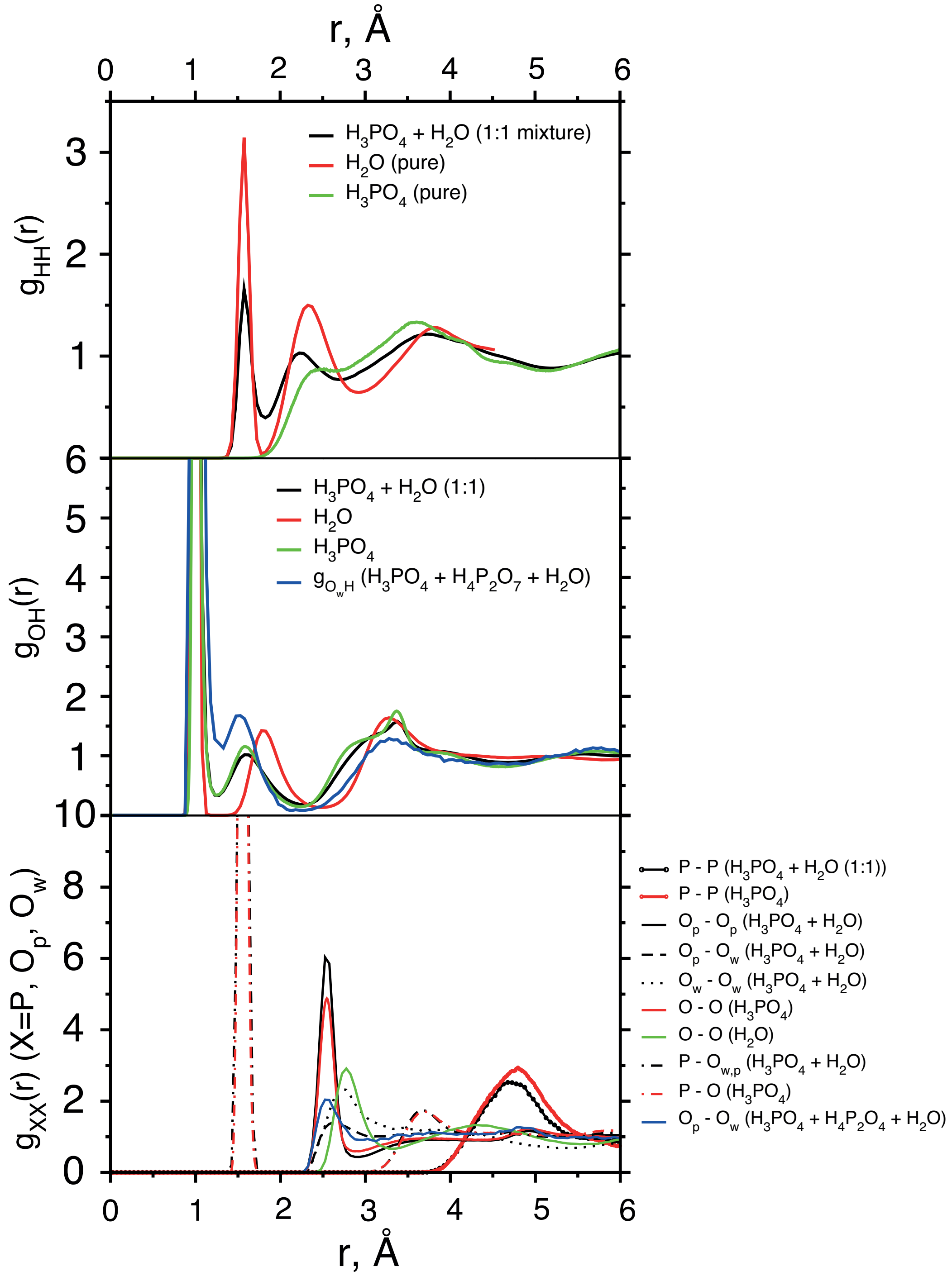

Figure 6.3: Radial pair distribution functions of the H_3PO_4 water solutions. The structure of neat H_3PO_4 and H_2O are given for comparison. (top) g_{HH} for System II, H_3PO_4 and H_2O. (middle) g_{OH} for for System I, System II, H_3PO_4 and H_2O; the first peak comes form the covalent O–H bond and the second due to the H-bonding (H. . . O). (bottom) g_{XX}, where X = P or O, shows the different contributions from heavy atom pairs to the total RDF.

6.2 Dynamical Properties

Now that the main structural properties of phosphoric acid – water system have been established, this section deals with the dynamical properties of these systems. The proton diffusion and conductivity of phosphoric acid – water system in a broad concentration range has already been addressed in a number of experimental studies.[69,79,190] The AIMD simulated diffusion coefficients in System II were evaluated by Eq. 4.1. The calculated time dependence of the mean square displacements for phosphorus, hydrogen and oxygen (in H_2O) atoms are presented in Fig. 6.4. Before starting the discussion of the results, it is important to mention that all of the experimental studies in these systems so far, only measured the $D(^1H)$ and $D(^{31}P)$ diffusion coefficients and the separate measurement of $D(^{17}O)$, which could rigorously establish the relation between the vehicular and structural contributions to diffusion processes, is not yet available for any phosphoric acid based proton conducting system. As indicated in Fig. 6.4, the CPMD calculated proton diffusion constant ($D^{2\mathrm{H}}_{\mathrm{CPMD}} = 4.22 \cdot 10^{-6}$ cm^2/s) is in a relatively good agreement to the experimental value ($D^{2\mathrm{H}}_{\mathrm{exp}}$ (383 K) $\approx 7.5 \cdot 10^{-6}$ cm^2/s). A similar agreement is found for phosphorus diffusion coefficient ($D^{31\mathrm{P}}_{\mathrm{CPMD}}$ (383 K) $= 1.2 \cdot 10^{-6}$ cm^2/s vs. $D^{31\mathrm{P}}_{\mathrm{exp}}$ (383 K) $\approx 4.0 \cdot 10^{-6}$ cm^2/s),[79,190] despite very limited statistics and finite size effects.

A simple way for estimating the contribution due to structural diffusion in System II, can be achieved by taking the proton diffusion coefficient ($D(H)$(System II)) and subtracting the contributions from the individual vehicles (in this case the diffusion coefficients of water $D^{\mathrm{H_2O}}(O)$ and phosphorus $D^{\mathrm{H_3PO_4}}(P)$):

$$D^{str}(H) = D(H) - xD^{\mathrm{H_2O}}(O) - (1-x)D^{\mathrm{H_3PO_4}}(P) \tag{6.1}$$

where x represents the fraction of protons attached to water. In the case of System II $x = 2/5$ (two out of five protons are located on the water molecule). For System II, $D^{str}(H) = 0.021$ Å^2/ps, whereas in the case of neat phosphoric acid ($x = 0$) $D^{str}(H) = 0.032$ Å^2/ps (assuming that H_3PO_4 is a system with 100% structural diffusion). In 50% mol. phosphoric acid solution, this results in ~66% of the proton diffusion coming from structural diffusion.

As previously mentioned, the experimental confirmation for this fact can not be fully confirmed without the ^{17}O tracer diffusion experiments. Nevertheless, one can roughly try to estimate whether the substantial increase in the conductivity of phosphoric acid upon dilution can be explained by simple hydrodynamic arguments. One way of calculating whether this contribution can account for the ~2-2.5 times increase in conductivity (System II: $\sigma(333K) \approx 0.25$ S/cm; H_3PO_4: $\sigma(333K) \approx 0.1$ S/cm) is to assume a completely vehicular contribution of water to the proton transport (protons are carried as part of H_3O^+ species and do not undergo any intermolecular PT). The viscosity of the 85% wt. phosphoric acid solution shows a ~5 fold decrease compared to 100% neat phosphoric acid. At first, let's assume that the diffusivity of H_3O^+ is approximately twice as large as the one of the phosphate (species size consideration): $D(O) = 2 \cdot D(P)$. The second necessary assumption is that of the fraction of molecules in H_3O^+ state, if one considers that ~50% of the water molecules are hydronium ions, the theoretical (Nernst-Einstein) contribution to conductivity would be ~0.024 S/cm. Even with these severe assumptions, implying very different acidities of water and phosphoric acid, the increase in conductivity can not be explained by purely vehicular arguments, suggesting that proton structural diffusion still plays an important role in the conduction mechanism of these systems. The microscopic details of the structural diffusion in System II, as obtained from the AIMD simulations, are discussed in the following sections.

The computed vibrational spectrum of System II only confirms the general picture of H-bonding, suggested by the analysis of the RDFs. The main features in the vibrational power spectra of System II are virtually identical to those obtained for neat H_3PO_4 (Fig. 6.5). The frequencies of the principal vibrational modes in the two systems are only slightly shifted with respect to each other. Only the $\nu(OD)$ is slightly broadened and shifted to higher frequencies, mainly due to the presence of more diverse and weaker $D_2O - D_2O$ H-bonds.

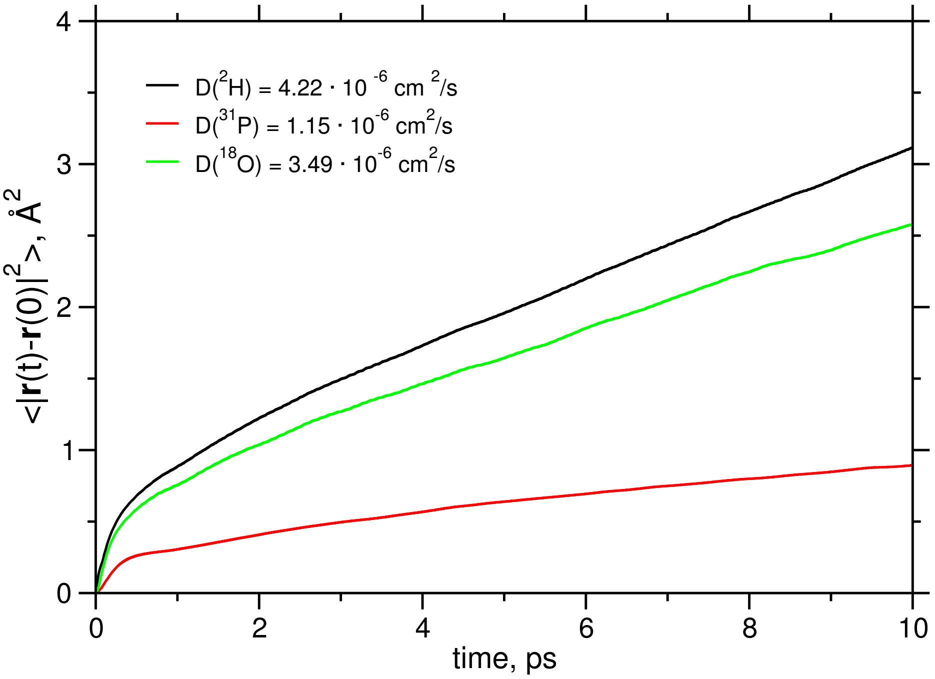

Figure 6.4: Average mean square displacements and corresponding diffusion constants as obtained from the Einstein relation for hydrogen, oxygen and phosphorus atoms in System II at 383 K.

6.3 Proton Transfer Energetics and the State of Charged Species

Having established the observation that neither the H-bonding nor the vibrational properties of phosphoric acid substantially change upon the addition of water, the next question to address is: how does the local energetics of PT look like and how are the charges separated in these systems? Similarly to the previous procedure (Table 5.2), the individual protons are assigned as belonging to a particular oxygen atom or being transiently shared between the two. The presence of short H-bonds between H_3PO_4 and H_2O molecules must also result in low PT barriers and formation of a plethora of species with uncompensated protonic charges. The experiments suggest that on the phosphoric acid rich side of the H_3PO_4–H_2O mixtures the proton affinities of both species should be very similar, otherwise the water would trap protons and assume a hydronium state, therefore hindering the proton structural diffusion. The results for different values of $\delta_{\text{cut-off}}$ used

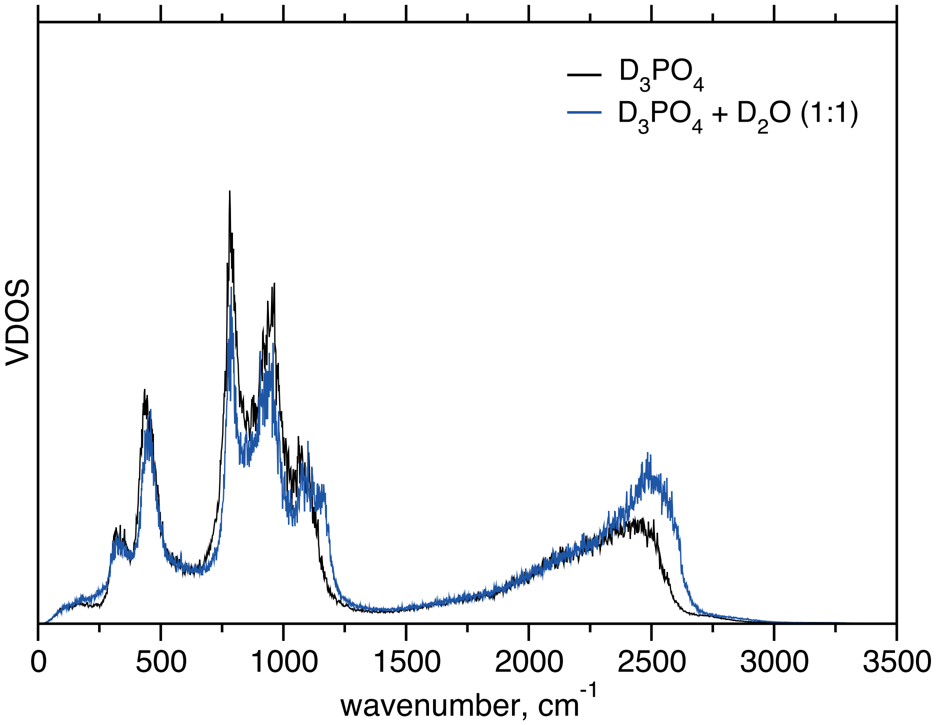

Figure 6.5: Vibrational spectrum for System II ($H_3PO_4 + H_2O$ (1:1)) (blue) and H_3PO_4 (black).

to count or exclude the transiently shared protons in System II are presented in Table 6.1. The data summarizes the fractions of H_3PO_4 and H_2O molecules with respect to their state of protonation. Using the strict $\delta_{\text{cut-off}} = 0$ Å criterion, one can immediately see that the degree of self-dissociation of the phosphoric acid molecules is reduced in System II (see Table 5.2 for comparison), however approximately 12% of the water molecules are in the Eigen-like ion form. Basically, this shows that the overall charge carrier concentration is very close to that of pure H_3PO_4. If one assumes a stricter $\delta_{\text{cut-off}}$ criterion (e.g. $\delta_{\text{cut-off}} = 0.3$ Å), the concentration of positively charged species is decreased, whereas the concentration of negatively charged species increases. This indicates that a significant fraction of the protons also are in Zundel-like forms, i.e. transiently shared between water and phosphoric acid molecules and suggesting that PT barriers in acid-water H-bonds are very low. In the case of similar proton affinities of the two species, another important aspect of this analysis is the possibility of phosphoric

$\delta_{\mathrm{cut-off}}$	$H_4PO_4^+$	$H_2PO_4^-$	H_3O^+	OH^-
0.0 Å	7.5 %	19.0 %	12.0 %	0.0026 %
0.3 Å	2.5 %	34.1 %	5.2 %	7.1 %

Table 6.1: Calculated fractions of water and phosphoric acid molecules in their different states of protonation in System II, with different proton assignment criterion $\delta_{\mathrm{cut-off}}$.

acid abstracting a proton from water and forming a hydroxide ion. However, the results (Table 6.1) show that with $\delta_{\mathrm{cut-off}} = 0$ Åonly a very tiny fraction of water molecules are in a probably, short-lived Zundel-like OH^- form. Nevertheless, if the $\delta_{\mathrm{cut-off}}$ value is increased up to 0.3 Å a significant fraction of the protons assigned to water molecules tend to be localized close to the centre of H-bonds (this includes phosphoric acid – water adducts ($OH^- - H^+ - H_3PO_4$ or $OH^- - H^+ - H_2PO_4^-$).

The local proton transfer energetics for different situations is estimated by calculating the free energy profiles along the δ coordinate (Eq. 4.8). The results for System I and System II are presented in Figs. 6.7 and 6.6. It is important to note that in all cases, the calculated free energy profiles show a distinct double well character. The overall proton averaged PT barrier in System II (Fig. 6.7 (black)) is comparable to that obtained for pure H_3PO_4 (Fig. 4.8 (b)). Furthermore, the overall PT barrier and the barrier heights for PT between H_3PO_4 – H_3PO_4 (Fig. 6.7 (red)) and H_3PO_4 – H_2O (Fig. 6.7 (green)), regardless of their protonation state, are virtually identical (∼75 meV) and only the PT barrier for protons between H_2O – H_2O is significantly higher (∼90 meV). In a similar manner to the previous discussion on other phosphorus oxoacid systems it is also interesting to resolve the overall PT barrier into various contributions with respect to the excess protonic charge particular species is carrying. The different contribution are presented in Fig. 6.7. The computed free energy profiles obviously share similarities with those of other investigated systems, as well as those obtained for protonic defects in water: the PT barriers around the positive defects are the lowest (∼40 meV), of the same order as the thermal kinetic energy in this simulation (∼35 meV), whereas PT barriers involving $H_2PO_4^-$ species show an intermediate barrier height (∼55 meV), in agreement to equivalent findings in other investigated systems.

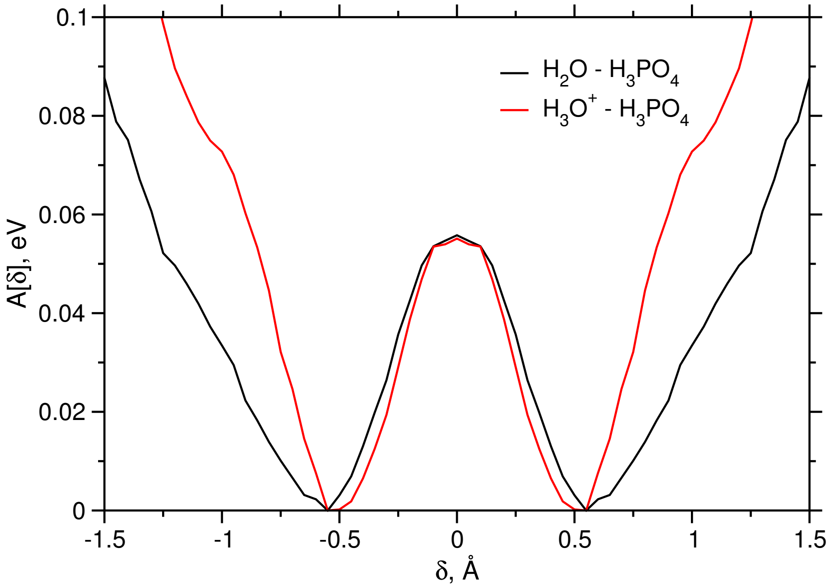

Figure 6.6: Free energy profiles $\Delta A(\delta)$ along the proton transfer coordinate δ for PT between phosphoric acid and water for System I.

6.4 Interprotonic Coupling

Already understanding that the main features of the proton dynamics in phosphoric acid – water system are very similar to neat phosphoric acid, it is instructive to ask whether a similar picture of proton-proton coupling is at play here as well. Furthermore, is the formation of Grotthuss chains only limited to homogeneous acid systems or is it possible in mixtures as well?

Fig. 6.8 depicts the hydrogen-hydrogen g_{HH} RDF resolved in r and δ, which contains the complete information of the spatial distribution of protons (both associated with water and H_3PO_4 molecules) with respect to how close the protons are to the transition state of PT reaction. Obviously, System II also features a significant response of the protonic subsystem upon the PT. Interestingly, a small peak at >2.0 Å present in H_3PO_4 and H_3PO_3, which comes from the configurations where the same oxygen atoms must simultaneously act as proton donor and acceptor, is much more intense in System II (∼1.8 Å for $\delta \to 0$). This feature most

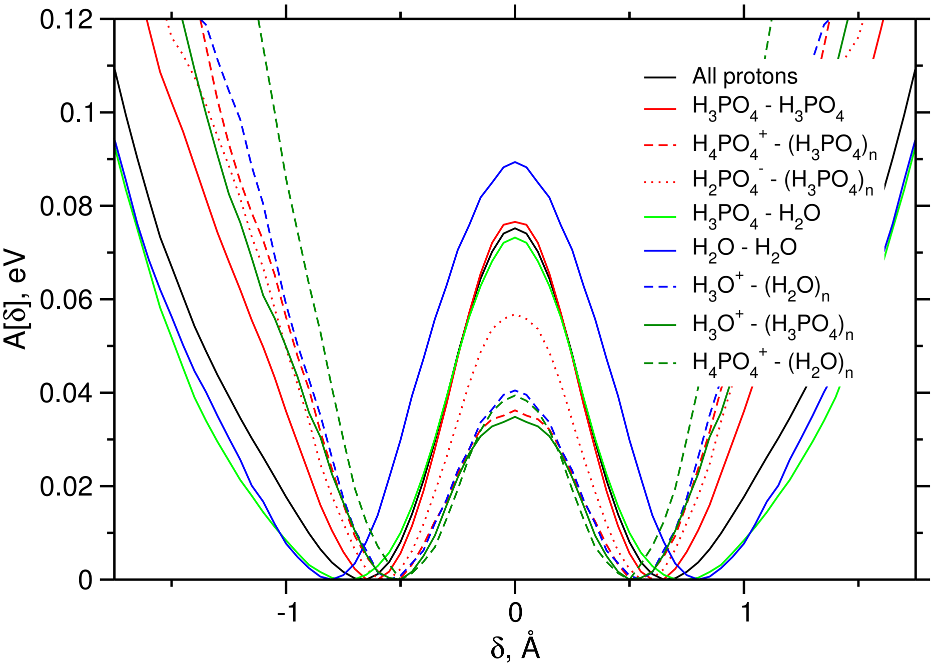

Figure 6.7: Free energy profiles $\Delta A(\delta)$ along the proton transfer coordinate δ for all protons and different proton donor/acceptor pairs in System II.

probably arises from a strong proton-proton coupling around the positive core of the H_3O^+ ion. In general, the addition of water increases the H/O ratio and overall proton concentration, leading to stronger electrostatic coupling between the protons. Moreover, the main peak at ∼3.9 Å also shows a marked increase for $\delta \to 0$, in a similar fashion as the $g_{HH}(\delta, r)$ of neat acid systems. Fig. 6.8 suggests that qualitatively very similar mechanism governing proton dynamics and transport are at play in phosphoric acid – water mixtures as that previously described for neat systems. The H-bonds in System II are on average very similar in strength and hence highly polarizable. The PT events are obviously strongly correlated to the dynamics of surrounding protonic subsystem opening a possibility for strong mutual protonic polarization and the build up of extended polarized chains. In the next section, the question whether this behavior could also lead to the formation of extended Grotthuss chains is addressed.

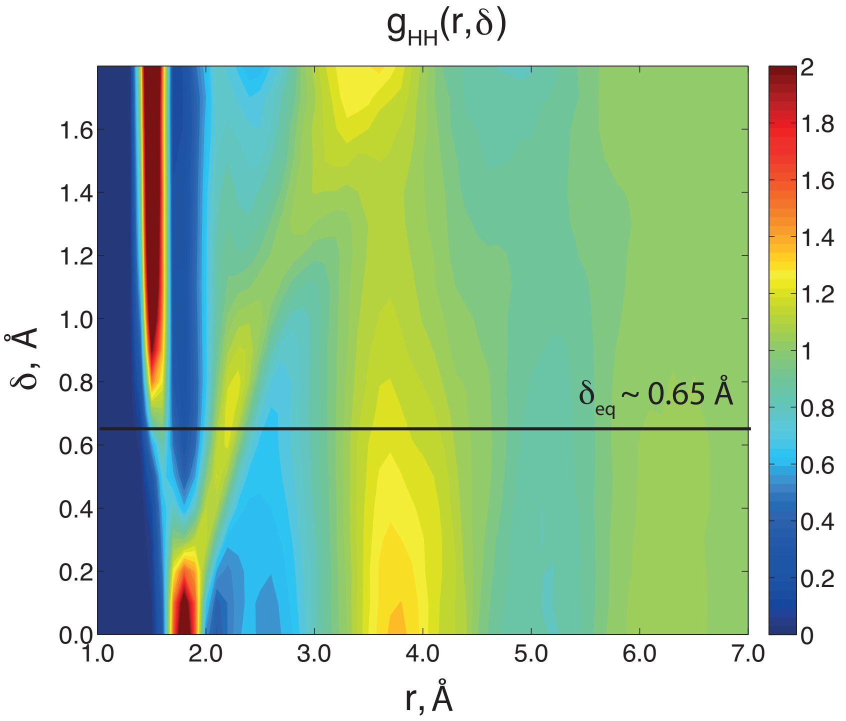

Figure 6.8: $g_{\mathrm{HH}}(SystemII)$ radial distribution function resolved in r and δ, containing information about the spatial distribution of protons with respect to δ (δ_{eq} is the equilibrium value in the simulation).

6.5 On the Formation of Grotthuss Chains and Proton Transport Mechanism

In the first part of this chapter we established that the properties of H-bonding, molecular vibrations and proton transfer in phosphoric acid – water mixtures, even at 1:1 molar ratio, are surprisingly similar to those of pure phosphoric acid. Moreover, there is a similarly strong correlation between the PT events and the dynamics of surrounding protons. Can this coupling lead to chains of correlated PTs, which in this case would involve not only phosphoric acid, but also water molecules and would be terminated by $H_4PO_4^+$ or H_3O^+ and $H_2PO_4^-$ species. In order to prove this hypothesis, we make use of the same proton coupling correlation function, initially developed for phosphoric acid (Eq. 4.10 in Sec. 4.9). In the calculation of the $C(n)$, the phosphate tetrahedra and the water's oxygen atoms are treated as equivalent vertices in the graph-theoretical framework, used in Eq. 4.10 ($N = N_{\mathrm{PO}_4} + N_{O_\mathrm{W}}$). The calculated $C(n)$ for System II is presented in Fig. 6.9 ($C(n)$ for phosphoric acid (Fig. 4.16) is used for comparison). The results indicate that the probability of two quasi-coherent PT events ($\tau_\mathrm{res} = 0$) within two neighboring H-bonds in System II is ∼4%, which is about two times lower than in neat H_3PO_4. Upon the increase of relay time parameter, allowing for the relaxation of H-bond network around the displaced proton, the probabilities of forming extended polarized chains start to increase. At $\tau_\mathrm{res} = 50$ fs, the probabilities to form chains of three and four consecutive H-bonds are ∼18% and ∼2%, respectively. Evidently, these values are significantly lower than in the case of neat phosphoric acid (∼30% and ∼10%), indicating that the presence of water tends to oppose the formation of Grotthuss chains. The representative snapshots of the self-dissociation/neutralization and polarized chain formation processes in System II showing this coupling, as extracted from the AIMD trajectory, are presented in Fig. 6.10. The entire sequence features several interconversion events between various charged species, including H_3O^+ (both Zundel- and Eigen-like forms), $H_4PO_4^+$ and $H_2PO_4^-$. The sequence starts with one of the water molecules already having an excess proton (Eigen-like) and one dihydrogen phosphate species (Fig. 6.10 (a)). Then, one of the protons is transferred through a Zundel-like state to another water molecule (Fig. 6.10 (b) and (c)). It is important to note that both water molecules share one H-bond but, in principle, are solvated by phosphate species (two are depicted), which in turn are bound by a common H-bond. As previously shown, all H-bonds in this complex are of very similar strength, therefore the mutual proton motion is strongly coupled and a more distant proton can be further transferred to the phosphate (Fig. 6.10 (d) and (e)). The latter process can be formally seen as a neutralization reaction between two species carrying excess charges (H_3O^+ and $H_2PO_4^-$). Furthermore, the H-bond between the two water molecules is weakened and easily breaks, since none of the molecules has an excess proton thus more resembling the H-bonds in ‘normal’ liquid water. The breakage of this bond, allows the second water molecule to easily reorient (Fig. 6.10 (e) and (f)) and start the solvent depolarization process. This event certainly creates a new termination and shortens the initial Grotthuss chain. Fig. 6.10 (f), (g) and (h) depict a formally new self-dissociative event between two H_3PO_4 molecules and a Grotthuss chain of three H-bonds forming between three phosphate species and one water molecule.

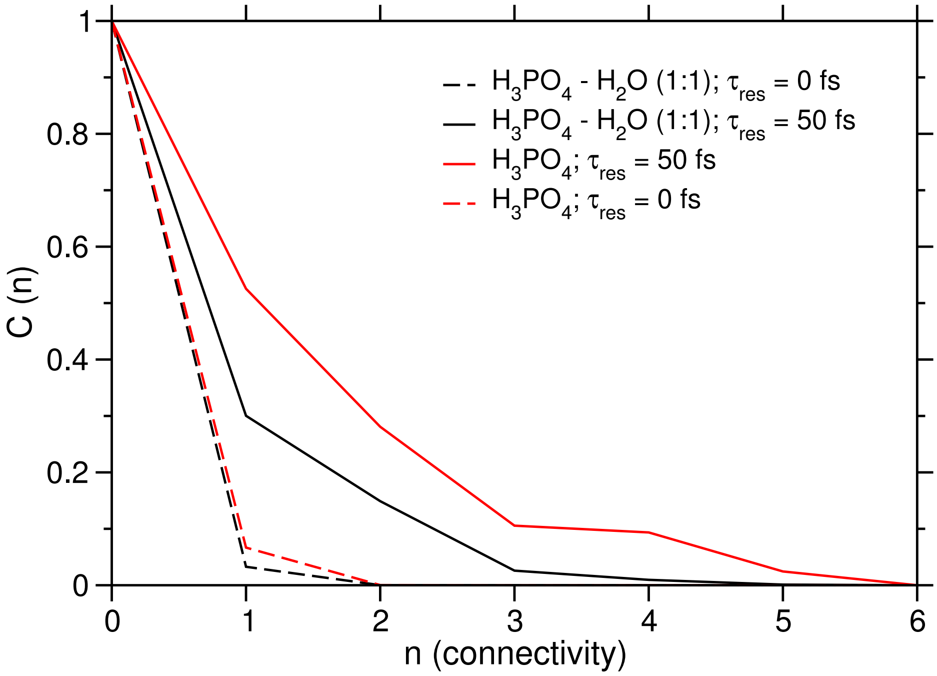

Figure 6.9: Proton coupling correlation function $C_{pc}(n)$ as a function of connectivity n for pure H_3PO_4 and System II. $\delta_{cut} \leq 0.1$ Å and $\tau_{res} = 0$ and 50 fs.

Fig. 6.10 depicts some representative snapshots of the self-dissociation/neutralization and polarized chain formation processes in System II. The entire sequence features several interconversion events between various charged species, including H_3O^+ (both Zundel- and Eigen-like forms), $H_4PO_4^+$ and $H_2PO_4^-$. The sequence is started with one of the water molecules having an excess proton and one dihydrogen phosphate (Fig. 6.10 (a)). Then one of the protons is transferred though a Zundel-like state to another water molecule (Fig. 6.10 (b) and (c)). It is important to note that both water molecules share one H-bond, but are at the ends solvated by two phosphate species, which in turn have a common H-bond. All the H-bonds in this complex are of very similar strength, therefore the proton can be further transferred to the phosphate due to the mutual interprotonic coupling (Fig. 6.10 (d) and (e)). The latter process can be seen as a neutralization reaction between two species carrying excess charge (H_3O^+ and $H_2PO_4^-$). Moreover, the H-bond joining two water molecules is weakened (none of the molecules have an excess proton) and breaks, letting the second water molecule reorient (Fig. 6.10 (e) and (f)). This event creates a new termination of Grotthuss chain. (f), (g) and (h) in Fig. 6.10 depict a self-dissociative event between two H_3PO_4 molecules and a Grotthuss chain of three H-bond forming between three phosphate species and one water molecule.

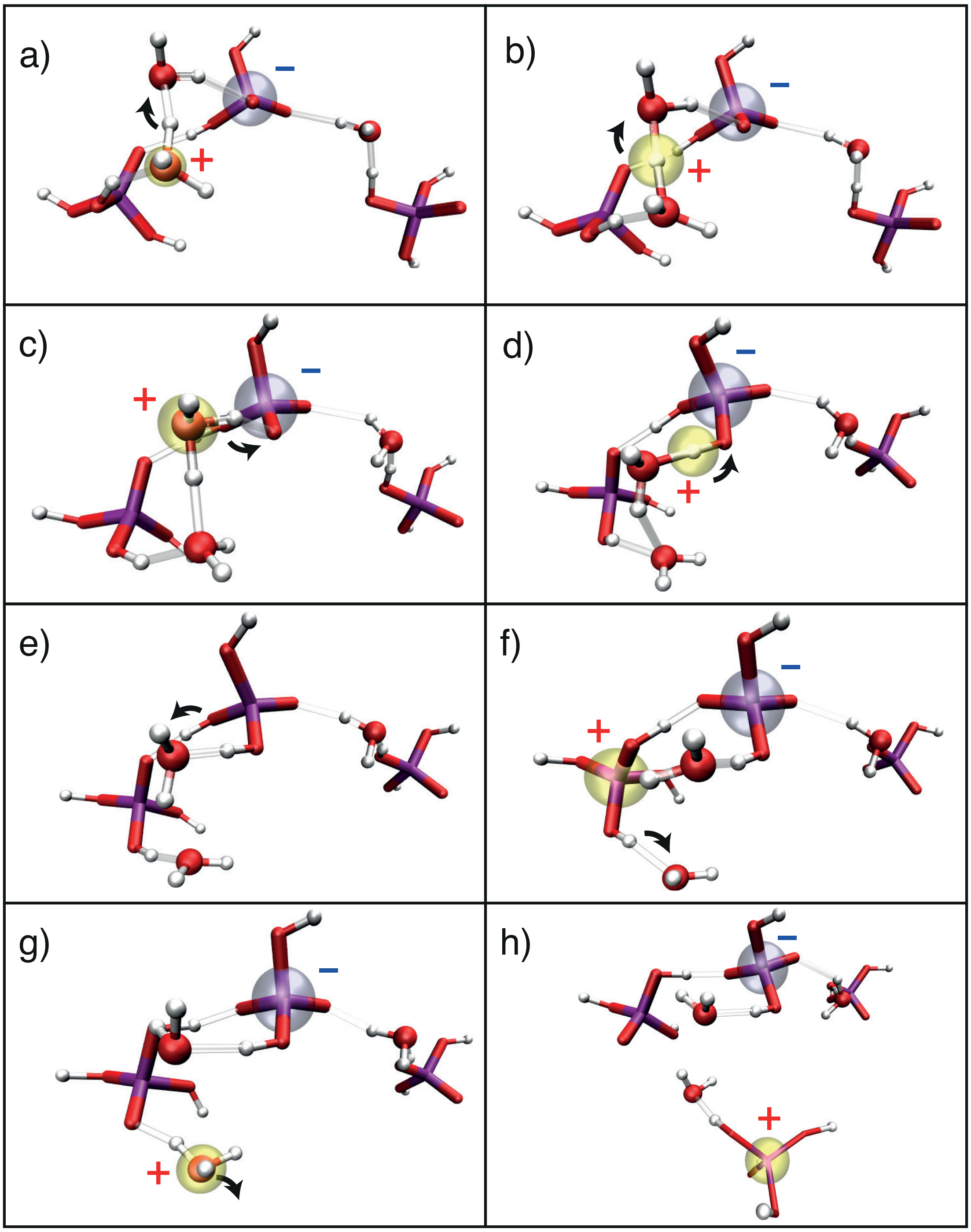

Figure 6.10: Snapshots of the elementary proton structural diffusion steps in System II. The charged ion pair is indicated with (+) and (-). The arrows denote the proton hops and molecular reorientations.

7

Conclusions

Understanding proton transport in hydrogen bonded systems on the molecular level remains a fundamental problem in many areas of science ranging from biological processes to electrochemical energy conversion. In this work, the molecular details of proton transport mechanisms in a number of phosphorus oxoacid systems are addressed. Currently, the experimental probes able to resolve the time and length scales of these mechanisms are still lacking. Therefore, molecular simulation techniques prove to be indispensable for the study of proton transport processes. Proton transfer is essentially a chemical reaction, which requires a dynamical self-consistent description of bond breaking and forming at the quantum mechanical level. In a large part thanks to *ab initio* molecular dynamics simulations, water became the first and remains the only bulk H-bonded network for which at least the mobility mechanism of protonic defects has been envisioned in great detail. In this work, a number of systems showing the highest known proton conductivities are studied. Five different systems based on phosphorus oxoanions: phosphoric, phosphonic and phosphinic acids and phosphoric acid – water mixtures are investigated with the help of *ab initio* molecular dynamics simulations.

For the first time, the microscopic mechanism of proton conduction in phosphoric acid, the central compound of this study, is revealed. We find that the high density of strong, polarizable H-bonds are involved in coupled proton motion and a pronounced protic dielectric response of the H_3PO_4 medium, thus forming *extended*, polarized (Grotthuss) chains up to six molecules, in the close sense to the earlier notions of aqueous proton transport but never truly observed in H-bonded systems. It is commonly understood that the presence of only short, strong H-bonds would lead to protonic ordering and slow dynamics, preventing rapid solvent reorientation (depolarization) processes and fast charge transport, however, phosphoric acid has a very peculiar H-bond network topology: an imbalance in the numbers of potential proton donor and acceptor sites (three OH donors and only one non-protonated oxygen) is anticipated to lead to configurational *frustration* and disorder. In the mechanism proposed in this work, it is the interplay between these chains and a frustrated H-bond network, which is found to lead to extremely high proton conductivity in phosphoric acid. This mechanism is in stark contrast to that of water, which has negligible intrinsic proton conductivity, but can transport the excess protonic charges at anomalously high rates, occurring not through extended chains but rather through *local* H-bond rearrangements that drive individual proton transfer reactions.

The next part of this work addresses an immediately arising question: why does phosphonic acid, which has even stronger H-bonds but does not posses the same frustrated hydrogen bond network as phosphoric acid (donor/ac-ceptor ratio 2:2), still shows good proton conductivity. The experimentally measured proton structural diffusion in phosphonic acid constitutes ∼90% of the total conductivity, which is only slightly lower than that of H_3PO_4. Moreover, in phosphinic acid, which has an even lower proton donor versus acceptor ratio (1:2), ∼20% of the reasonably good proton conductivity comes from structural diffusion. The presence of very strong H-bonds in H_3PO_3 and H_3PO_2 allow for a mutual proton-proton coupling and formation of polarized H-bonded chains, however, on the other hand, this process is counteracted by a much stronger hydrodynamic and dipolar background existing in these systems. Therefore, the average length of Grotthuss chains building up in phosphonic and phosphinic acid systems is significantly shorter than in the case of phosphoric acid. Furthermore, the results show that weak H-bond configurations, although not an property of the H-bond network, are still forming in a dynamical sense due to liquid disorder, essentially playing the same role in the solvent reorientation process as in H_3PO_4.

Nearly all types of chemical perturbations destroy the proton conducting properties of phosphoric acid, apart from the severe conductivity reduction caused by the addition of bases, even the addition of acids leads to some decrease in conductivity. Apparently, the only dopant that increases the conductivity of H_3PO_4 is water. The question of whether the excess water simply accelerates the intrinsic proton conduction process already operating in H_3PO_4 or the entire proton conduction mechanism changes, has not been clear yet and was therefore, addressed in the last chapter of this work. The results show than neither at the very low nor at 50% mol. concentration, water acts as classical Brønsted base, abstracting protons from phosphoric acid molecules and only contributing to the proton conductivity through the vehicular diffusion of H_3O^+ species. From the comparison of the simulated proton diffusion coefficients in 1:1 $H_3PO_4 - H_2O$ system, the contribution due to structural diffusion is as high as 70%. Moreover, the H-bond structure and vibrational properties of this system are virtually identical to those of neat phosphoric acid and unlike those of water. This leads to similarly strong proton-proton interaction and mutual protonic polarizability and the formation of extended Grotthuss chains of up to three H-bonds. Although the dielectric and hydrodynamic properties of water in these systems are significantly reduced, it still increases the electrostatic penalty for the formation of polarized chains. On the other hand, the nature of water increases the configurational entropy of the system, providing new possibilities for efficient solvent reorganization, which, in addition to the vehicular contribution to the proton transport lead to very high proton conductivities.

The understanding of the molecular details of proton transport in phosphorus oxoacid systems has relevance for many fields of science such as chemistry, engineering and biophysics. Our findings show the limits of proton transport at the fundamental level – strong hydrogen bonding does not necessarily lead to protonic ordering and slow dynamics. The proposed mechanisms show how weak solvent coupling and sufficient degree of configurational disorder can lead to fast proton transport. These systems can be regarded as a prototype models for understanding molecular proton transport mechanisms in many other proton conductors. This could serve as the first step in overcoming many technical hurdles concerning the use of phosphate based materials as electrolytes in e.g. fuel cells. Moreover, the abundance and crucial role of phosphates in the chemistry of life are relevant in the light of our findings. The recent view of chemiosmotic theory of ATP synthesis suggest that the protons building up the gradient are transported near the surface region of the phospholipid membrane rather than quickly equilibrating with the bulk aqueous phase. Although, the active role of the phospholipid membrane for the proton transport has been firmly established, a complete molecular scale understanding of this process has not yet been achieved. The molecular understanding of proton transport mechanism in neat phosphorus oxoacids could serve as the next step towards the further elucidation of one of the most important biological processes occurring at the phosphate/water interface.

References

[1] K. D. Kreuer. *Chem. Mat.*, **8**, 610–641, 1996.

[2] K. D. Kreuer, S. J. Paddison, E. Spohr and M. Schuster. *Chem. Rev.*, **104**, 4637–4678, 2004.

[3] D. Marx. *ChemPhysChem*, **7(9)**, 1848–1870, 2006.

[4] T. E. DeCoursey. *Physiol. Rev.*, **83**, 475–579, 2003.

[5] C. A. Wraight. *Biochim. Biophys. Acta.*, **1757(8)**, 886–912, 2006.

[6] K. D. Kreuer. *Solid State Ionics*, **136**, 149–160, 2000.

[7] N. Agmon. *Chem. Phys. Lett.*, **244**, 456–462, 1995.

[8] N. Agmon. *Chem. Phys. Lett.*, **319(3-4)**, 247–252, 2000.

[9] M. E. Tuckerman, D. Marx, M. L. Klein and M. Parrinello. *Science*, **275(5301)**, 817–820, 1997.

[10] D. Marx, M. E. Tuckerman, J. Hutter and M. Parrinello. *Nature*, **397(6720)**, 601–604, 1999.

[11] M. E. Tuckerman, D. Marx and M. Parrinello. *Nature*, **417(6892)**, 925–929, 2002.

[12] R. Vuilleumier and D. Borgis. *J. Phys. Chem. B*, **102(22)**, 4261–4264, 1998.

[13] R. Vuilleumier and D. Borgis. *J. Chem. Phys.*, **111(9)**, 4251–4266, 1999.

[14] U. W. Schmitt and G. A. Voth. *J. Chem. Phys.*, **111(20)**, 9361–9381, 1999.

[15] J. Lobaugh and G. A. Voth. *J. Chem. Phys.*, **104(5)**, 2056–2069, 1996.

[16] T. J. F. Day, U. W. Schmitt and G. A. Voth. *J. Am. Chem. Soc.*, **122(48)**, 12027–12028, 2000.

[17] O. Markovitch, H. Chen, S. Izvekov, F. Paesani, G. A. Voth and N. Agmon. *J. Phys. Chem. B*, **112(31)**, 9456–9466, 2008.

[18] T. C. Berkelbach, H.-S. Lee and M. E. Tuckerman. *Phys. Rev. Lett.*, **103(23)**, 238302, 2009.

[19] D. Marx, A. Chandra and M. E. Tuckerman. *Chem. Rev.*, **110(4)**, 2174–2216, 2010.

[20] A. Botti, F. Bruni, S. Imberti, M. A. Ricci and A. K. Soper. *J. Chem. Phys.*, **119(10)**, 5001–5004, 2003.

[21] S. Woutersen and H. J. Bakker. *Phys. Rev. Lett.*, **96(13)**, 138305, 2006.

[22] C. D. Cappa, J. D. Smith, B. M. Messer, R. C. Cohen and R. J. Saykally. *J. Phys. Chem. A*, **111(22)**, 4776–4785, 2007.

[23] E. F. Aziz, N. Ottosson, M. Faubel, I. V. Hertel and B. Winter. *Nature*, **455(7209)**, 89–91, 2008.

[24] K. J. Tielrooij, R. L. A. Timmer, H. J. Bakker and M. Bonn. *Phys. Rev. Lett.*, **102(19)**, 198303, 2009.

[25] S. T. Roberts, P. B. Petersen, K. Ramasheshа, A. Tokmakoff, I. S. Ufimtsev and T. J. Martinez. *Proc. Natl. Acad. Sci.*, **106(36)**, 15154–15159, 2009.

[26] K. D. Kreuer. *J. Membr. Sci.*, **185**, 29–39, 2001.

[27] K. Mauritz and R. Moore. *Chem. Rev.*, **104(10)**, 4535–4585, 2004.

[28] S. Paddison. *Ann. Rev. Mater. Res.*, **33**, 289–319, 2003.

[29] J. Wainright, J. Wang, D. Weng, R. Savinell and M. Litt. *J. Electrochem. Soc.*, **142(7)**, L121–L123, 1995.

[30] M. Schuster and W. Meyer. *Annu. Rev. Mater. Res.*, **33**, 233–261, 2003.

[31] Y. Ma, J. Wainright, M. Litt and R. Savinell. *J. Electrochem. Soc.*, **151(1)**, A8–A16, 2004.

[32] H. Steininger, M. Schuster, K. D. Kreuer, A. Kaltbeitzel, B. Bingoel, W. H. Meyer, S. Schauff, G. Brunklaus, J. Maier and H. W. Spiess. *Phys. Chem. Chem. Phys.*, **9(15)**, 1764–1773, 2007.

[33] M. B. Herath, S. E. Creager, A. Kitaygorodskiy and D. D. DesMarteau. *ChemPhysChem*, **11(13)**, 2871–2878, 2010.

[34] F. H. Westheimer. *Science*, **235(4793)**, 1173–1178, 1987.

[35] K. D. Kreuer, A. Rabenau and W. Weppner. *Angew. Chem. Int. Ed.*, **21(3)**, 208–209, 1982.

[36] C. J. T. de Grotthuss. *Ann. Chim. (Paris)*, **LVIII**, 54–74, 1806.

[37] J. N. Collie and T. Tickle. *J. Chem. Soc.*, **75**, 710, 1899.

[38] C. Dempwolff. *Phys. Z.*, **5**, 637, 1904.

[39] S. Tijmstra. *Z. Elektrochem.*, **11**, 249, 1905.

[40] H. Danneel. *Z. Elektrochem.*, **11**, 249, 1905.

[41] E. Hückel. *Z. Elektrochem.*, **34**, 546, 1928.

[42] J. D. Bernal and R. H. Fowler. *J. Chem. Phys.*, **1(8)**, 515–548, 1933.

[43] G. Wannier. *Ann. Phys. (Leipzig)*, **24(6)**, 545–568, 1935.

[44] A. Gierer. *Z. Naturforsch.*, **5a**, 581, 1950.

[45] B. E. Conway, J. O. Bockris and H. Linton. *J. Chem. Phys.*, **24(4)**, 834–850, 1956.

[46] M. Eigen and L. D. Mayer. *Proc. R. Soc. Lon. Ser. A*, **247(1251)**, 505–533, 1958.

[47] G. Halle, B.; Karlström. *J. Chem. Soc. Far. Trans.*, **79**, 1047, 1983.

[48] H. G. Hertz, B. M. Braun, K. J. Muller and R. Maurer. *J. Chem. Educ*, **64(9)**, 777–784, 1987.

[49] M. E. Tuckerman, K. Laasonen, M. Sprik and M. Parrinello. *J. Phys.-Cond. Mat.*, **6**, A93–A100, 1994.

[50] M. E. Tuckerman, K. Laasonen, M. Sprik and M. Parrinello. *J. Phys. Chem.*, **99(16)**, 5749–5752, 1995.

[51] M. E. Tuckerman, K. Laasonen, M. Sprik and M. Parrinello. *J. Chem. Phys.*, **103(1)**, 150–161, 1995.

[52] S. Izvekov and G. A. Voth. *J. Chem. Phys.*, **123**, 044505, 2005.

[53] A. Chandra, M. E. Tuckerman and D. Marx. *Phys. Rev. Lett.*, **99(14)**, 145901, 2007.

[54] E. T. J. Nibbering and T. Elsaesser. *Chem. Rev.*, **104(4)**, 1887–1914, 2004.

[55] H. J. Bakker and J. L. Skinner. *Chem. Rev.*, **110(3)**, 1498–1517, 2010.

[56] R. A. Marcus. *J. Chem. Phys.*, **24(5)**, 966–978, 1956.

[57] R. A. Marcus. *Rev. Mod. Phys.*, **65(3)**, 599–610, 1993.

[58] N. Agmon. *Isr. J. Chem.*, **39(3-4)**, 493–502, 1999.

[59] G. Zundel. *Adv. Chem. Phys.*, **111**, 1, 2000.

[60] T. Dippel and K. D. Kreuer. *Solid State Ionics*, **46(1-2)**, 3–9, 1991.

[61] C. Dellago, M. Naor and G. Hummer. *Phys. Rev. Lett.*, **90(10)**, 105902, 2003.

[62] C. Dellago and G. Hummer. *Phys. Rev. Lett.*, **97(24)**, 245901, 2006.

[63] Z. Cao, Y. Peng, T. Yan, S. Li, A. Li and G. A. Voth. *J. Am. Chem. Soc.*, **132(33)**, 11395–11397, 2010.

[64] R. Pomès and B. Roux. *Biophys. J.*, **82(5)**, 2304–2316, 2002.

[65] M. Schuster, K.-D. Kreuer, H. Steininger and J. Maier. *Solid State Ionics*, **179(15-16)**, 523–528, 2008.

[66] L. Vilčiauskas, C. C. de Araujo and K. D. Kreuer. *Solid State Ionics*, (accepted), 2012.

[67] R. A. Munson. *J. Phys. Chem.*, **68**, 3374–3377, 1964.

[68] T. Dippel, K. D. Kreuer, J. C. Lassègues and D. Rodriguez. *Solid State Ionics*, **61(1-3)**, 41–46, 1993.

[69] D. Chin and H. Chang. *J. Appl. Electrochem.*, **19**, 95–99, 1989.

[70] R. H. Blessing. *Acta Cryst. B*, **44**, 334–340, 1988.

[71] G. Becker, H. D. Hausen, O. Mundt, W. Schwarz, C. T. Wagner and T. Vogt. *Z. Anorg. Allg. Chem.*, **591(12)**, 17–31, 1990.

[72] J. M. Williams and S. W. Peterson. *Spectrosc. Inorg. Chem.*, **2**, 1–56, 1971.

[73] E. Tsuchida. *J. Phys. Soc. Japan*, **75(5)**, 054801, 2006.

[74] L. Vilciauskas, S. J. Paddison and K. D. Kreuer. *J. Phys. Chem. A*, **113(32)**, 9193–9201, 2009.

[75] N. Greenwood and A. Thompson. *Proc. Chem. Soc.*, **(12)**, 352–353, 1958.

[76] N. N. Greenwood and A. Thompson. *J. Chem. Soc.*, 3485–3492, 1959.

[77] N. Greenwood and A. Thompson. *J. Chem. Soc.*, 3864–3867, 1959.

[78] R. A. Munson and M. E. Lazarus. *J. Phys. Chem.*, **71(10)**, 3245–3248, 1967.

[79] Y. Aihara, A. Sonai, M. Hattori and K. Hayamizu. *J. Phys. Chem. B*, **110**, 24999–25006, 2006.

[80] T. Dippel, N. G. Hainovsky, K. D. Kreuer, W. Münch and J. Maier. *Ferroelectrics*, **167**, 59, 1995.

[81] R. Janoschek, E. G. Weidemann, G. Zundel and H. Pfeiffer. *J. Am. Chem. Soc.*, **94(7)**, 2387–2396, 1972.

[82] M. Leuchs and G. Zundel. *Can. J. Chem.*, **57(5)**, 487–493, 1979.

[83] A. Schechter and R. Savinell. *Solid State Ionics*, **147(1-2)**, 181–187, 2002.

[84] R. A. Munson. *J. Phys. Chem.*, **69**, 1761–1762, 1965.

[85] W. Munch, K. D. Kreuer, W. Silvestri, J. Maier and G. Seifert. *Solid State Ionics*, **145(1-4)**, 437–443, 2001.

[86] M. Iannuzzi and M. Parrinello. *Phys. Rev. Lett.*, **93(2)**, 025901, 2004.

[87] M. Iannuzzi. *J. Chem. Phys.*, **124(20)**, 204710, 2006.

[88] H. Hen, T. Yan and G. A. Voth. *J. Phys. Chem. A*, **113(16)**, 4507–4517, 2009.

[89] F. Shimojo, K. Hoshino and H. Okazaki. *Solid State Ionics*, **113**, 319–323, 1998.

[90] F. Shimojo and K. Hoshino. *Solid State Ionics*, **145(1-4)**, 421–427, 2001.

[91] W. Munch, K. D. Kreuer, G. Seifert and J. Maier. *Solid State Ionics*, **136**, 183–189, 2000.

[92] K. Kreuer. *Ann. Rev. Mater. Res.*, **33**, 333–359, 2003.

[93] Q. Zhang, G. Wahnström, M. Björketun, S. Gao and E. Wang. *Phys. Rev. Lett.*, **101(21)**, 215902, 2008.

[94] B. Frick and et al. *to be published.*

[95] Y. Iwadate, Y. Tani, K. Fukushima, M. Misawa, T. Fukunaga, K. Itoh and T. Nakazawa. *J. Neutron. Res.*, **13(1)**, 139–144, 2005.

[96] J.-O. Joswig and G. Seifert. *J. Phys. Chem. B*, **113(25)**, 8475–8480, 2009.

[97] C. M. Maupin, B. Aradi and G. A. Voth. *Journal Of Physical Chemistry B*, **114(20)**, 6922–6931, 2010.

[98] S. Detoni, D. Hadži and B. Orel. *J. Mol. Struc.*, **33**, 279–288, 1976.

[99] M. A. Vargas, R. A. Vargas and B. E. Mellander. *Electrochim. Acta*, **44(24)**, 4227–4232, 1999.

[100] M. A. Vargas, R. A. Vargas and B. E. Mellander. *Electrochim. Acta*, **45(8-9)**, 1399–1403, 2000.

[101] M. A. Vargas, R. A. Vargas and B. E. Mellander. *Phys. Stat. Sol. B*, **220(1)**, 615–624, 2000.

[102] R. Vargas, V. Zapata, E. Matallana and M. Vargas. *Electrochim. Acta*, **46(10-11)**, 1699–1702, 2001.

[103] N. Sammes, R. Bove and K. Stahl. *Curr. Opin. Solid. St. Mat. Sci.*, **8(5)**, 372–378, 2004.

[104] A. Bozkurt, M. Ise, K. D. Kreuer, W. H. Meyer and G. Wegner. *Solid State Ionics*, **125(1-4)**, 225–233, 1999.

[105] M. Schuster, T. Rager, A. Noda, K. D. Kreuer and J. Maier. *Fuel Cells*, **5**, 355–365, 2005.

[106] H. Steininger, M. Schuster, K. D. Kreuer and J. Maier. *Solid State Ionics*, **177(26-32)**, 2457–2462, 2006.

[107] J. P. Lassegues. *in P. Colomban Proton Conductors: Solids, membranes and gelss - materials and devices*, 311–326. Cambridge University Press, 1992.

[108] Q. Li, J. O. Jensen, R. F. Savinell and N. J. Bjerrum. *Prog. Polym. Sci.*, **34(5)**, 449–477, 2009.

[109] A. Kaltbeitzel, S. Schauff, H. Steininger, B. Bingoel, G. Brunklaus, W. H. Meyer and H. W. Spiess. *Solid State Ionics*, **178(7-10)**, 469–474, 2007.

[110] A. Warshel and R. M. Weiss. *J. Am. Chem. Soc.*, **102**, 6218, 1980.

[111] A. C. T. van Duin, S. Dasgupta, F. Lorant and W. A. Goddard. *J. Phys. Chem. A*, **105(41)**, 9396–9409, 2001.

[112] U. W. Schmitt and G. A. Voth. *J. Phys. Chem. B*, **102(29)**, 5547–5551, 1998.

[113] Y. Wu, H. Chen, F. Wang, F. Paesani and G. A. Voth. *J. Phys. Chem. B*, **112(2)**, 467–482, 2008.

[114] H. Chen, G. A. Voth and N. Agmon. *J. Phys. Chem. B*, **114(1)**, 333–339, 2010.

[115] D. Marx and J. Hutter. *Ab Initio Molecular Dynamics: Basic Theory and Advanced Methods.* Cambridge University Press, New York, 2009.

[116] P. Hohenberg and W. Kohn. *Phys. Rev.*, **136(3B)**, B864, 1964.

[117] W. Kohn and L. Sham. *Phys. Rev.*, **140(4A)**, 1133, 1965.

[118] R. Car and M. Parrinello. *Phys. Rev. Lett.*, **55(22)**, 2471–2474, 1985.

[119] J. Morrone and M. Tuckerman. *J. Chem. Phys.*, **117(9)**, 4403–4413, 2002.

[120] J. Morrone, K. Hasllinger and M. Tuckerman. *J. Phys. Chem. B*, **110(8)**, 3712–3720, 2006.

[121] M. Diraison, G. J. Martyna and M. E. Tuckerman. *J. Chem. Phys.*, **111(3)**, 1096–1103, 1999.

[122] Y. Liu and M. Tuckerman. *J. Phys. Chem. B*, **105(28)**, 6598–6610, 2001.

[123] U. Rothlisberger and M. Parrinello. *J. Chem. Phys.*, **106(11)**, 4658–4664, 1997.

[124] S. Raugei and M. L. Klein. *ChemPhysChem*, **5(10)**, 1569–1576, 2004.

[125] B. C. Wood and N. Marzari. *Phys. Rev. B*, **76(13)**, 134301, 2007.

[126] H.-S. Lee and M. E. Tuckerman. *J. Phys. Chem. C*, **112(26)**, 9917–9930, 2008.

[127] R. M. Martin. *Electronic Structure: Basic Theory and Practical Methods.* Cambridge University Press, Cambridge, 2004.

[128] J. Kohanoff. *Electronic Structure Calculations for Solids and Molecules: Theory and Computational Methods.* Cambridge University Press, New York, 2006.

[129] R. G. Parr and W. Yang. *Density-Functional Theory of Atoms and Molecules.* Oxford University Press, New York, 1994.

[130] W. Koch and M. C. Holthausen. *A Chemist's Guide to Density Functional Theory.* Wiley-VCH, Weinheim, 2001.

[131] R. M. Dreizler and E. K. U. Gross. *Density Functional Theory: An Approach to the Quantum Many-Body Problem.* Springer-Verlag, 1991.

[132] A. D. Becke. *J. Chem. Phys.*, **98**, 1372–1377, 1993.

[133] A. D. Becke. *J. Chem. Phys.*, **98**, 5648–5652, 1993.

[134] T. Todorova, A. P. Seitsonen, J. Hutter, I. F. W. Kuo and C. J. Mundy. *J. Phys. Chem. B*, **110(8)**, 3685–3691, 2006.

[135] M. Guidon, F. Schiffmann, J. Hutter and J. VandeVondele. *J. Chem. Phys.*, **128(21)**, 214104, 2008.

[136] C. Zhang, D. Donadio, F. Gygi and G. Galli. *J. Chem. Theory. Comput.*, **7(5)**, 1443–1449, 2011.

[137] J. M. Tao, J. P. Perdew, V. N. Staroverov and G. E. Scuseria. *Phys. Rev. Lett.*, **91(14)**, 146401, 2003.

[138] G. Lippert, J. Hutter and M. Parrinello. *Mol. Phys.*, **92(3)**, 477–487, 1997.

[139] G. Lippert, J. Hutter and M. Parrinello. *Theor. Chem. Acc.*, **103(2)**, 124–140, 1999.

[140] J. VandeVondele, M. Krack, F. Mohamed, M. Parrinello, T. Chassaing and J. Hutter. *Comp. Phys. Comm.*, **167(2)**, 103–128, 2005.

[141] D. R. Hamann, M. Schlüter and C. Chiang. *Phys. Rev. Lett.*, **43**, 1494–1497, 1979.

[142] S. Goedecker, M. Teter and J. Hutter. *Phys. Rev. B*, **54(3)**, 1703–1710, 1996.

[143] G. Martyna, M. Klein and M. Tuckerman. *J. Chem. Phys.*, **97(4)**, 2635–2643, 1992.

[144] M. E. Tuckerman, B. J. Berne, G. J. Martyna and M. L. Klein. *J. Chem. Phys.*, **99**, 2796, 1993.

[145] M. E. Tuckerman. *Statistical Mechanics: Theory and Molecular Simulation.* Oxford University Press, New York, 2010.

[146] Max-Planck-Institut für Festkörperforschung, Stuttgart and IBM Zurich Research Laboratory. *CPMD; ver. 3.13*, 1995-2010.

[147] A. D. Becke. *Phys. Rev. A*, **38**, 3098, 1988.

[148] C. Lee, W. Yang and R. Parr. *Phys. Rev. B*, **37(2)**, 785–789, 1988.

[149] N. Troullier and J. Martins. *Phys. Rev. B*, **43(3)**, 1993–2006, 1991.

[150] The cp2k developers group.

[151] J. VandeVondele and J. Hutter. *J. Chem. Phys.*, **127(11)**, 114105, 2007.

[152] J. Perdew, K. Burke and M. Ernzerhof. *Phys. Rev. Lett.*, **77(18)**, 3865–3868, 1996.

[153] M. Krack. *Theor. Chem. Acc.*, **114**, 145–152, 2005.

[154] S. A. H. Spieser, B. R. Leeflang, L. M. J. Kroon-Batenburg and J. Kroon. *J. Phys. Chem. A*, **104(31)**, 7333–7338, 2000.

[155] W. Humphrey, A. Dalke and K. Schulten. *J. Mol. Graph.*, **14**, 33–38, 1996.

[156] R. Tromp, S. Spieser and G. Neilson. *J. Chem. Phys.*, **110(4)**, 2145–2150, 1999.

[157] B. Dünweg and K. Kremer. *J. Chem. Phys.*, **99(9)**, 6983–6997, 1993.

[158] I. Yeh and G. Hummer. *J. Phys. Chem. B*, **108(40)**, 15873–15879, 2004.

[159] D. Laage and J. T. Hynes. *J. Phys. Chem. B*, **112(45)**, 14230–42, 2008.

[160] I. M. Svishchev and P. G. Kusalik. *J. Phys. Chem.*, **98**, 728–733, 1994.

[161] D. Laage and J. Hynes. *Science*, **311(5762)**, 832–835, 2006.

[162] F. H. Stillinger. *Adv. Chem. Phys.*, **31**, 1–101, 1975.

[163] D. C. Rapaport. *Mol. Phys.*, **50**, 1151, 1983.

[164] A. Luzar and D. Chandler. *Nature*, **379(6560)**, 55–57, 1996.

[165] A. Luzar. *J. Chem. Phys.*, **113(23)**, 10663–10675, 2000.

[166] M. E. Tuckerman, A. Chandra and D. Marx. *J. Chem. Phys.*, **133(12)**, 124108, 2010.

[167] D. Marx, M. Tuckerman, J. Hutter and M. Parrinello. *J. Phys.-Cond. Matt.*, **12**, A153, 2000.

[168] L. Pauling. *J. Am. Chem. Soc.*, **69(3)**, 542–553, 1947.

[169] N. Agmon. *J. Mol. Liq.*, **73-4**, 513–520, 1997.

[170] H. Lapid, N. Agmon, M. Petersen and G. Voth. *J. Chem. Phys.*, **122**, 014506, 2005.

[171] L. Vilčiauskas, M. E. Tuckerman, G. Bester, S. J. Paddison and K. D. Kreuer. *Nature Chemistry*, (accepted), 2012.

[172] R. L. Hayes, S. J. Paddison and M. E. Tuckerman. *J. Phys. Chem. B*, **113(52)**, 16574–16589, 2009.

[173] P. Silvestrelli and M. Parrinello. *Phys. Rev. Lett.*, **82(16)**, 3308–3311, 1999.

[174] M. Sharma, R. Resta and R. Car. *Phys. Rev. Lett.*, **98(24)**, 247401, 2007.

[175] R. A. Munson. *J. Chem. Phys.*, **40**, 2044, 1964.

[176] R. Buchner, J. Barthel and J. Stauber. *Chem. Phys. Lett.*, **306(1-2)**, 57–63, 1999.

[177] P. Geissler, C. Dellago, D. Chandler, J. Hutter and M. Parrinello. *Science*, **291(5511)**, 2121–2124, 2001.

[178] W. A. Jenkins and R. T. Jones. *J. Am. Chem. Soc.*, **74(5)**, 1353–1354, 1952.

[179] M. Spaeth, K. D. Kreuer, J. Maier and C. Cramer. *J. Sol. State Chem.*, **148(1)**, 169–177, 1999.

[180] A. C. Chapman and L. E. Thirlwell. *Spectrochim. Acta*, **20(6)**, 937–947, 1964.

[181] A. Simon, F. Fehér and G. Schulze. *Zeit. Anorg. Allg. Chem.*, **230(3)**, 289–307, 1937.

[182] P. M. Kiefer and J. T. Hynes. *J. Phys. Chem. A*, **106(9)**, 1834–1849, 2002.

[183] P. M. Kiefer and J. T. Hynes. *J. Phys. Chem. A*, **106(9)**, 1850–1861, 2002.

[184] E. Tang, D. D. Tommaso and N. H. de Leeuw. *J. Chem. Phys.*, **130(23)**, 234502, 2009.

[185] A. Smondyrev and G. Voth. *Biophys. J.*, **82(3)**, 1460–1468, 2002.

[186] H. L. Tepper and G. A. Voth. *Biophys. J.*, **88(5)**, 3095–3108, 2005.

[187] H. L. Tepper and G. A. Voth. *J. Phys. Chem. B*, **110(42)**, 21327–21337, 2006.

[188] T. Yamashita and G. A. Voth. *J. Phys. Chem. B*, **114(1)**, 592–603, 2010.

[189] Y. Kameda, K. Sugawara, T. Hosaka, T. Usuki and O. Uemura. *Bull. Chem. Soc. Japan*, **73(5)**, 1105–1112, 2000.

[190] S. Chung, S. Bajue and S. Greenbaum. *J. Chem. Phys.*, **112(19)**, 8515–8521, 2000.

Lebenslauf

Linas Vilčiauskas

NATIONALITÄT:	Litauisch
28. April 1983	geboren in Joniškis, Litauen.

BILDUNG:

Januar 2008 – Dezember 2011	Doktorarbeit zum Thema *Mechanismen des Protonentransports in Phosphorsäure und verwandten Systemen von Phosphor Oxosäuren: eine "ab initio" molekulardynamische Untersuchung* am Max-Planck-Institut für Festkörperforschung, Stuttgart.
April 2007 – Oktober 2007	Masterarbeit am Max-Planck-Institut für Festkörperforschung (Betreuer: Dr. K.-D. Kreuer) und an der Universität Alabama in Huntsville, USA (Betreuer: Prof. S. J. Paddison).
Oktober 2005 – April 2007	Masterstudium der Werkstoffwissenschaft (Nanomaterialien) an der Universität Ulm, Deutschland.
Januar 2005 – Mai 2005	Austauschsemester an der Universität Lettland, Riga.
September 2001 – Juli 2005	Bachelorstudium der Chemie an der Universität Vilnius, Litauen.
September 1994 – Juli 2001	Matas-Slančiauskas-Gymnasium Joniškis, Litauen. *Abiturabschluss mit Auszeichnung*
September 1989 – Juni 1994	Mittelschule Nr. 2, Joniškis, Litauen.

AUSZEICHNUNGEN

2005 – 2007	Stipendium des Deutschen akademischen Austauschdienstes (DAAD) für Mastertudium an der Universität Ulm.
2004	Stipendium der Litauischen Stiftung für Wissenschaft und Studium.